ANALYSIS OF THE LACUSTRINE SEDIMENTS OF THE CREEDE FORMATION, MINERAL COUNTY, COLORADO

by

Bruce L. Batory

Submitted in Partial Fulfillment
of the Requirements for the Degree of
Master of Science in Geochemistry

New Mexico Institute of Mining and Technology
Socorro, New Mexico

December, 1981

ACKNOWLEDGEMENTS

First of all, I would like to thank the National Science Foundation, whose funding made this project possible.

In addition to the help and suggestions from my committee members, Dr. Marc Bodine, Dr. David Norman, and Dr. Philip Bethke, I would like to thank Dr. Wayne Ohline for substituting for a committee member during my defense and the following people.

My sincere appreciation goes to the owners of Broadacre Ranch, Freemon Ranch, and Phipps Ranch in Creede, Colorado, for their warm friendliness and their permission to study the outcrops on their property. Their cooperation made my field studies not only possible, but enjoyable.

My thanks also go to the faculty at the New Mexico Institute of Mining and Technology and the staff at the New Mexico Bureau of Mines and Mineral Resources.

Thanks, also, to Dr. Richard Sheppard of the U.S. Geological Survey, Denver, Colorado, whose zeolite standards made possible my chemical analyses.

My final thanks goes to my wife, Renie, who typed and edited my thesis in its entirety.

ABSTRACT

The Tertiary lacustrine deposits of the Creede Formation are confined within the Creede caldera. The deposits are the results of Fisher Quartz Latite pyroclastics being deposited in a closed lake occupying a moat within the caldera. The moat, which follows the caldera margin for approximately 270 degrees of arc, formed as a result of resurgent doming within the caldera. The chief lithologic units are shale and siltstones with minor beds of arenite and tuff present. Virtually all sediments contain tuffaceous material, and this report summarizes the alteration the vitric material has undergone and the resulting authigenic silicate mineral distribution present.

Clinoptilolite, analcime, montmorillonite, and authigenic quartz are associated with relict glass. Thin-section study shows montmorillonite and clinoptilolite replacing the shards and analcime replacing clinoptilolite. Textural evidence suggests that the tuffs were water-laid and alteration of the glass occurred after burial.

Three diagenetic facies were recognized in the sediments and can be identified by unaltered glass, clinoptilolite and analcime. The facies distribution occurs laterally with the unaltered glass occurring at the outer margin of the lake, followed by clinoptilolite and then analcime as the lake's center is approached. This zonation

reflects the changing alkalinity and salinity of the lake water which was trapped as connate water.

The lacustrine facies display no presence of marker beds nor syngenetic mineral deposits. Tuff beds converted to near monomineralic deposits of clinoptilolite may be of economic importance.

PLATES AND FIGURES

TABLE OF CONTENTS

TABLES

I. INTRODUCTION

Purpose of Study

The purpose of this paper is to provide a complete analysis, chemically, stratigraphically, and mineralogically, of the lacustrine facies of the Creede Formation. By sampling several stratigraphic sections in detail and determining the authigenic minerals present, it can be determined if the formation's environment was indeed a saline, alkaline lake. This can also aid in the evaluation of Bethke and Rye's (1979) hypothesis that evaporation and diagenesis in a saline Lake Creede lead to the enrichment in both deuterium and ^{18}O in the residual lake water which was postulated to be responsible for the sphalerite deposition in Creede's ore vein fracture system.

Other aspects of this investigation are: 1) identification of any lateral stratigraphic or authigenic mineral variation, 2) determination of the existance of any marker beds in the formation, 3) evaluation of the Creede Formation as an economic deposit, and 4) location of occurrences of any other zeolite species present besides the clinoptilolite already present.

Scope of Investigation

The sections analyzed were located in the northwest portion of the Creede caldera and were chosen for the following reasons: 1) They had excellent vertical exposures,

2) The formation showed only slight deformation, and 3) There was a presence of zeolitized tuff.

Sampling was confined to surface outcrops, and all rock types were sufficiently sampled so as to obtain representative material. Weathered surface outcrops were avoided. No cores were available to this investigation.

II. GEOLOGIC SETTING

Location

The Creede Formation of late Oligocene age is chiefly a lacustrine deposit confined to a structural moat within the Creede caldera in northwest Mineral County, Colorado. Most of the formation is in T41N, R1W and R1E. The nearest town is Creede, located along Highway 149, and situated in the northernmost part of the Creede Formation. The area is best shown as a part of the 15-minute geologic maps of the Creede, Bristol Head, and Spar City quadrangles by the U.S. Geological Survey.

Geography

The Creede Formation is in the Colorado Plateau physiographic province, which is characterized by the occurrence of scattered igneous centers, the roots of extinct volcanoes. That part of the Colorado Plateau province in southwestern Colorado is known as the San Juan volcanic field. The Creede Formation occupies a structural moat within the Creede caldera and follows the caldera margin for approximately 270 degrees of arc from Lime Creek on the southern margin of the caldera, extending down the Rio Grande to Wagon Wheel Gap, and up Goose Creek for nearly 8 km (Fig. 1). Most of the peaks encompassing the caldera rise to elevations of 3110 to 3810 meters.

The Creede Formation has an arc length of approximately 26 km. Its exposed width averages 2.9 kilometers with the widest portion occurring as a tongue filling an old stream canyon up to the Amethyst fault near the center of the Creede mining district. The Rio Grande River flows within the entire extent of the moat, thereby incising the Creede Formation and forming several excellent vertical exposures of the Creede sediments. The highest exposures, at an elevation of about 2987 meters, are northwest of Creede in the northcentral portion of the formation.

Geologic History

The San Juan volcanic region began when intensive volcanism during Oligocene time occurred along the crest of the northwest-trending Bazos-Uncompahgre uplift. These mid-Tertiary eruptions were intermediate composition lavas and breccias from widely scattered volcanoes. As the volcanoes grew, volcaniclastic debris accumulated in the intervening basins to eventually produce a volcanic pile of which the San Juan segment covered more than 40,000 km^2.

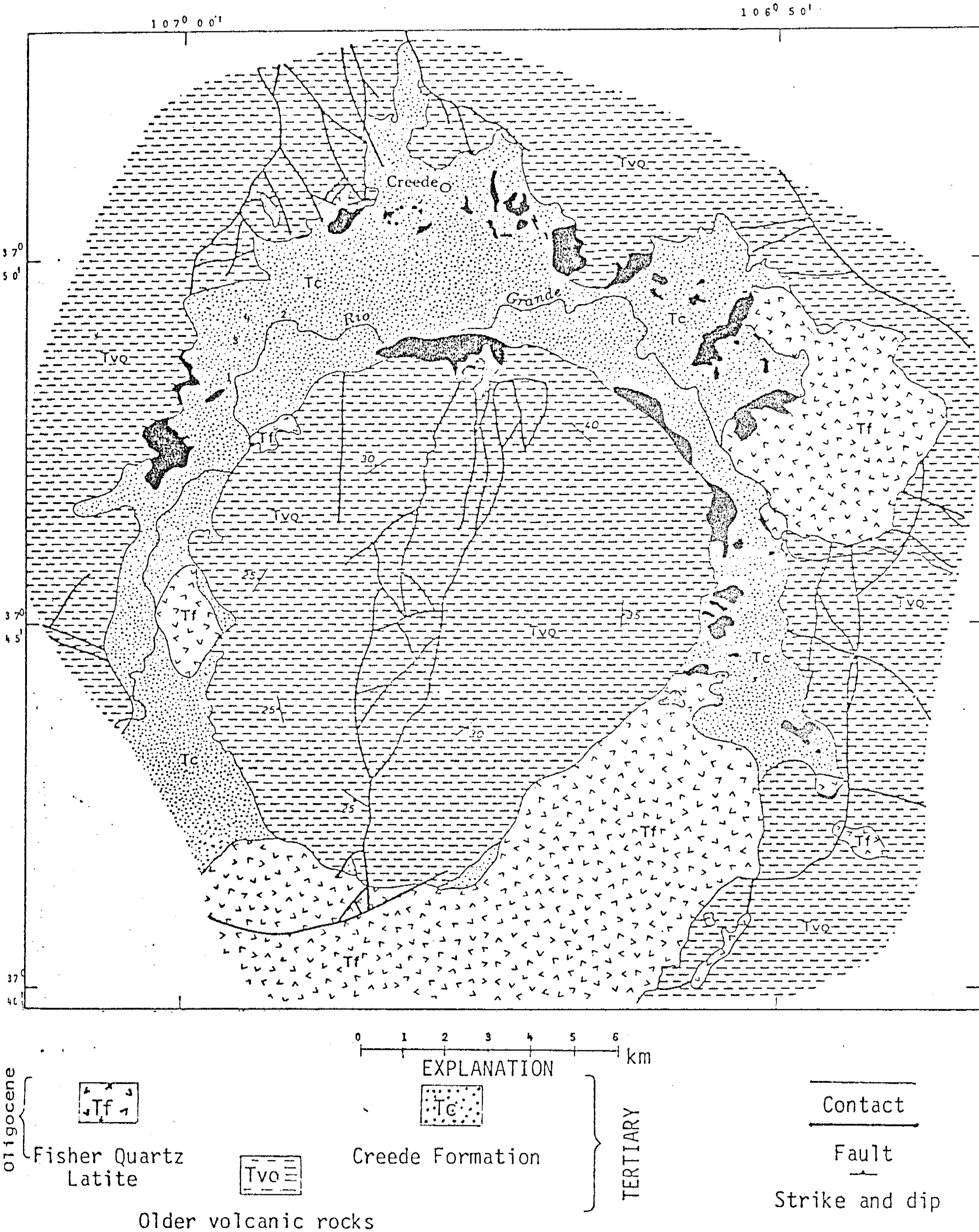

FIGURE 1. Geologic map of the Creede caldera showing location of Reference Sections 1-4. (Black areas indicate travertine bodies.)

Approximately 30 m.y. ago the eruptions became dominately ash flow tuff, and between 30 and 26.5 m.y. ago, ash flow sheets erupted from areally restricted sources marked by at least 15 large calderas (Lipman and others, 1978).

The youngest caldera in the central San Juan cluster was the Creede caldera. This formed near the end of Oligocene time 26.5 m.y. ago when immense amounts of Snowshoe Mountain tuff were erupted. Subsidence progressed concurrently with eruption, and the tuff accumulated within the subsiding area (Steven and Ratte, 1959).

The core of the caldera was strongly domed due to pressure from resurgent magma and caused a low-lying structural moat to be formed along the periphery (Steven and Eaton, 1975) and a deeply infaulted north-trending graben across the dome's top. Lavas and pyroclastics of the Fisher Quartz Latite, erupting from ring fractures, accumulated concurrently within the moat. Stream and lake-bed deposits, consisting of reworked ash supplied primarily by the erupting Fisher centers, were deposited in the moat to form the Creede Formation. Permeable talus-regolith and local fanglomeritic deposits formed along the outer caldera wall and the impermeable ashy sediments toward the basin's center. This distribution of facies is believed to have been a controlling factor in the hydrologic environment during mineralization in the Creede district (Fig. 2) (Steven and Eaton, 1975).

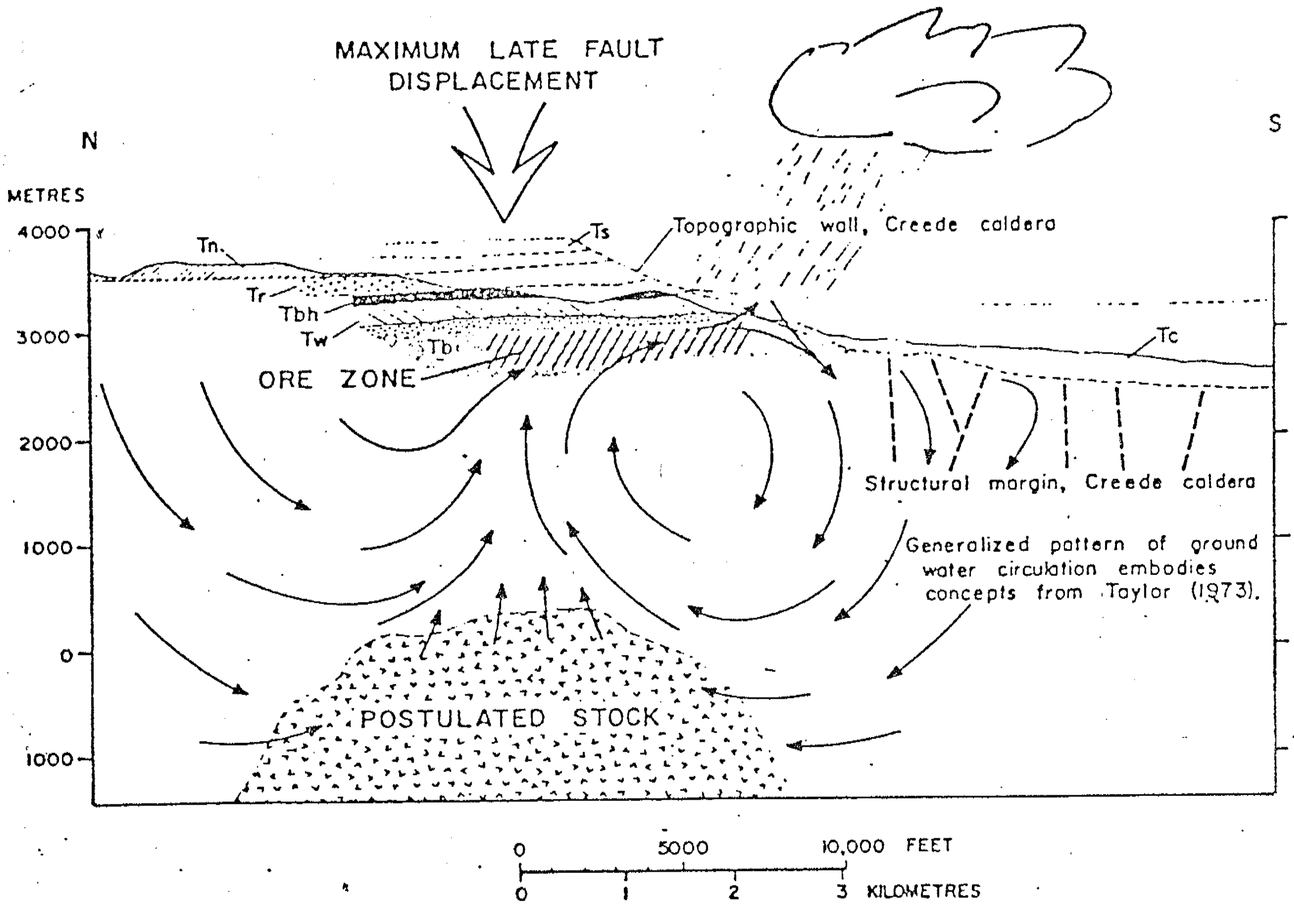

FIG. 2. Idealized north-south section through the Creede mining district. Existing rocks are patterned; restored rocks, open. Tc, Creede Formation; Ts, Snowshoe Mountain Tuff; Tn, Nelson Mountain Tuff; Tr, Rat Creek Tuff; Tbh, andesite of Bristol Head; Tw, Wason Park Tuff; Tb, Bachelor Mountain Member, Carpenter Ridge Tuff. Coarse stipple in the Rat Creek Tuff and at the top of the Bachelor Mountain Member indicates soft, relatively impermeable tuff.

After Fisher eruptions terminated and the trough was filled to overflowing with alluvium, the area of the Creede mining district was again faulted, and the resulting fractures mineralized. The faulting and mineralization are believed due to the intrusion of a magmatic body under the Creede district and occurred 24.6 ± 0.6 m.y. ago based on K-Ar dating of adularia.

Lake Creede and the Creede Formation

Lake Creede, which occupied the caldera moat during Fisher eruptions, was believed to be a shallow, moderately alkaline, saline lake (Bethke and Rye, 1979). This was based on the fact that the climate during deposition was similar to that of today (Steven and Eaton, 1975) favoring the evolution of the shallow closed basin lake to an alkaline,saline condition due to evaporation and diagenesis. Numerous mudcracks, excellently preserved plant fragments, and tuff beds converted to clinoptilolite (Steven and Van Loenen, 1971) reinforces this conclusion. Travertine accumulations were also scattered throughout the lake during pyroclastic deposition (Steven and Friedman, 1968).

The Creede Formation was mentioned as early as 1923 by Emmons and Larson who also formally named it. The formation has been divided into a lacustrine and fluviate facies (Steven and Ratte, 1965) with the latter composed primarily of sandstones and conglomerates. Common to buried tributary valleys, they constitute almost all of the tongue of the

Creede Formation that fills the old valley extending north across Bachelor Mountain to the Amethyst fault.

The lacustrine deposits are primarily thin-bedded tuffaceous shales and siltstones with some beds of tuffs and sandstones. The shales range from paper-thin laminations to beds several centimeters thick and locally grade into siltstones or mudstones with nearly all beds containing tuffaceous material.

The lacustrine facies also shows ripple marks and mud cracks. Cross-bedding, cut and fill relations, and soft sediment deformation (Fig. 3) are observable in several of the vertical exposures along the Rio Grande and road cuts.

Age of the Creede Formation

The lacustrine facies of the Creede Formation contains the most abundant and best preserved plant remains in the San Juan Mountain region. F.H. Knowlton (1923) studied the paleoflora within the Creede caldera. The fossils were collected from sec. 16, T41N, R1W, Creede quadrangle, with the fossil-bearing strata the same as those measured in Reference Section R1. He compared these fossils with those found in the Lake Florissant beds in the southern Front Range, Colorado, and assigned a Miocene age to both. MacGinitie (1953) showed that the Florissant Lake beds are Oligocene in age, and after examining Knowlton's collection, concluded that the Creede Formation was middle Pliocene in age. Larsen and Cross (1956) interpretted the age of the beds to be late Miocene or very early Pliocene.

In 1964 Steven and Ratte found that the Creede Formation was underlain, overlain, and intertongued with Fisher Quartz Latite confirming their earlier report (1959) that Creede sedimentation occurred concurrently with caldera subsidence and volcanic eruptions. The erupting Fisher Quartz Latite supplied the bulk of the material in the Creede sediments (Steven and Friedman, 1968) and is equivalent in age to the Creede Formation. Ratte and Steven (1967), and Steven and others (1967) gave K-Ar dates 26.5 m.y. and 26.4 m.y., respectively, for the latite. Armstrong (1969), and Lipman and others (1970) also dated the Fisher Quartz Latite which again yielded a date of 26.4 m.y. The age of the Fisher Quartz Latite is, therefore, probably the most firmly established of all units in the San Juan volcanic field and is also the accepted age of the Creede Formation.

Zeolite Prospect

The Creede Formation presents itself as an excellent prospect for zeolite formation since zeolites form as an alteration product of vitric tuffs in saline, alkaline lakes. The wide-spread occurrence of tuffaceous material in the formation; the presence of the zeolite, clinoptilolite; and the postulated alkaline, saline depositional environment reinforces this assumption.

Other factors influencing zeolite formation and speciation can be related to geologic age, burial depth, composition of host lithology, temperature, silica and water activity, and pH (Hay, 1965). As meteoric water descends through the formation and alters due to devitrification and argillization of tuffs, the variability of these parameters may cause diagenetic zeolitic facies distribution.

III. STRATIGRAPHY AND LITHOLOGY OF THE LACUSTRINE FACIES

The lacustrine facies extends over a vertical range of at least 732 meters. This is not the maximum thickness, however, as nowhere in the formation are the basal beds exposed and an unknown thickness of rocks have been eroded from the upper sections.

Very pale orange (10YR 8/2) to gray orange (10YR 7/4) shale or a silty to tuffaceous varient is the predominate lithology of the lacustrine facies. Altered tuff beds compose only a minor (less than 10%) part of the formation studied, and thin layers of limestone are very rare. The remainder of the formation is made up of siltstones, conglomerates, and arenites with all gradations existing between silty shales and silty sandstones. Interbedded within these lithologic units are beds of travertine, which were deposited by springs. Deposits of gypsum occur within the formation as both vertical fracture and joint fillings and horizontal, continuous beds of satin spar. The lacustrine sediments intertongue marginally with fluviate sandstones and conglomeritic beds in the vicinity of old

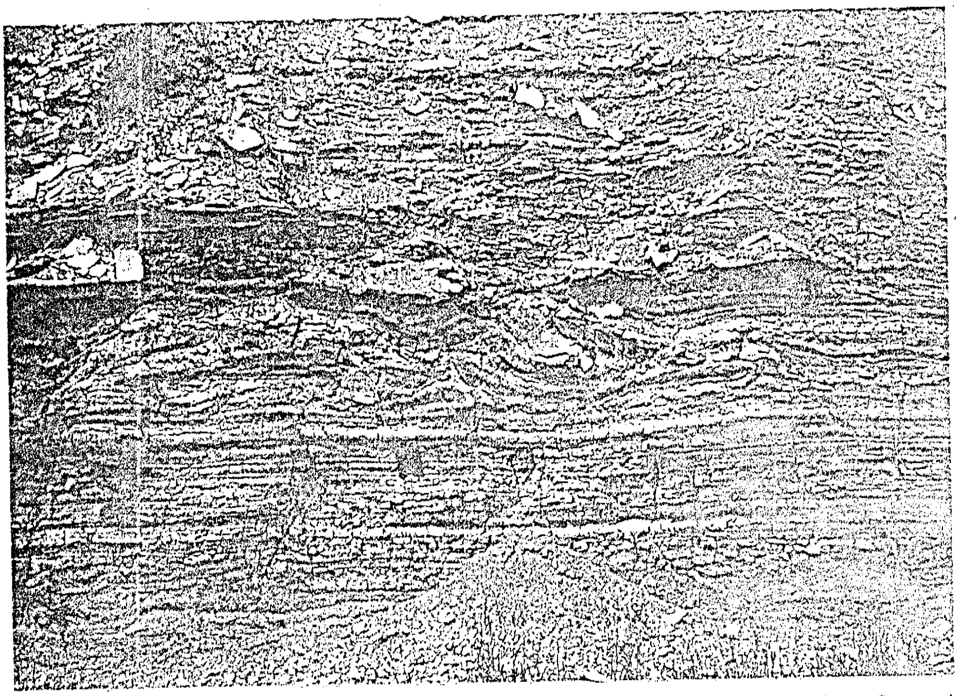

Figure 3. Typical soft sediment deformation of Lake Creede sediments.

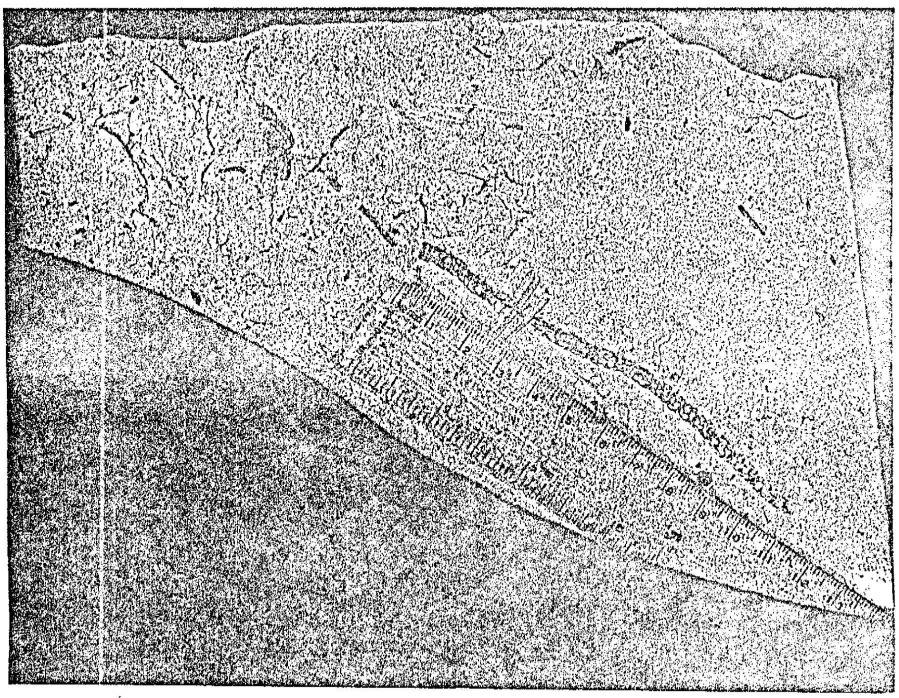

Figure 4. Shale displaying branch and needles of the genus Pinus.

tributary valleys, and with coarse sedimentary breccias and fanglomerates of local derivation along the margins.

The area studied displays a multitude of sedimentary features (mudcracks, ripple marks, etc.) which is in agreement with a lacustrine environment. Virtually all of the sediments display some type of paleoflora, primarily the Pinus and Acer genera (Fig. 4), and are devoid of any aquatic life remains.

Except for local areas of slumping, the beds are relatively undisturbed. All of the sections are essentially flat lying with dips averaging only 1 to 2 degrees. As one approaches the caldera rim, however, the beds begin to increase in dip since the beds were deposited in areas of increasing slope. Figure 5 shows a conjectural composite of all reference sections assuming all the beds can be approximated as horizontal due to the low dips measured.

The upper portions of the lacustrine facies are of very simple mineralogy (see Appendix 2). They are strikingly absent of authigenic minerals except for a few specimens which contain only trace amounts of montmorillonite.

While no marker beds nor syngenetic bedded mineral deposits were found in the areas studied, a massive zeolitized tuff of possible economic importance was found in Reference Section 1.

Table 1 lists the mean, standard deviation, and coefficient of variation of the major oxides of all the lithologic units of each section for comparative purposes.

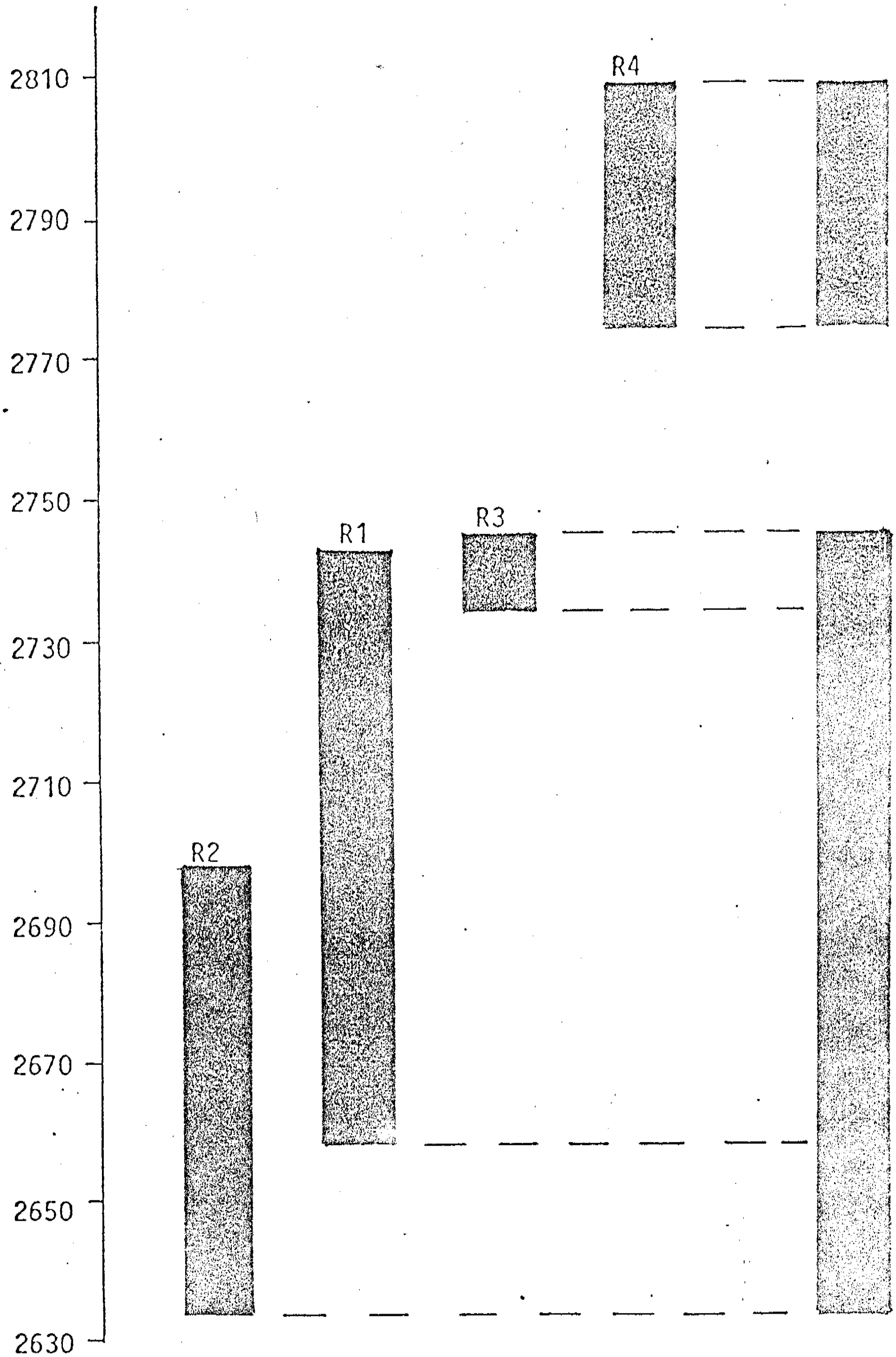

Fig. 5 Composite drawing of all reference sections. Elevation in meters.

Figure 1 shows locations of all reference sections, and Figures 6 and 7 show outcrops of Reference Sections 1 and 2, respectively. Plates 1, 2, and 3 are stratigraphic columns of the reference sections studied. Appendix 1 contains compilation charts of all the sections.

Arenites

The arenites are light gray (N7) to light brown (5Y 5/6) on a fresh surface and pale yellow-brown (10YR 6/2) on a weathered surface. They are relatively thin-bedded (.3 m thick or less) although some are as thick as 3.7 m. The arenites subtlely grade into the shales and siltstones and can be easily overlooked upon casual inspection. All arenites are moderate to well indurated with the detrital grains floating in either a cement of calcite or gypsum (Fig. 8) with several specimens being rich in a chalcedonic cement.

The average grain size of the detrital minerals is .312 mm for arenites of Reference Section 1 with poor sorting. The grains have an estimated roundness of .20-.30. The cements compose approximately 30% of the rock; quartz, 25%; hornblende, 4%; biotite, 3%; sanidine, 15%; magnetite, 3%; plagioclase, 15%; with the remainder cristobolite, pyrite and diopside-augite.

The arenites of Reference Section 2 and 3 are coarser, .608 mm, but are also poorly sorted and have a roundness of .20-.30. The plagioclase content is greater, being 20%, and

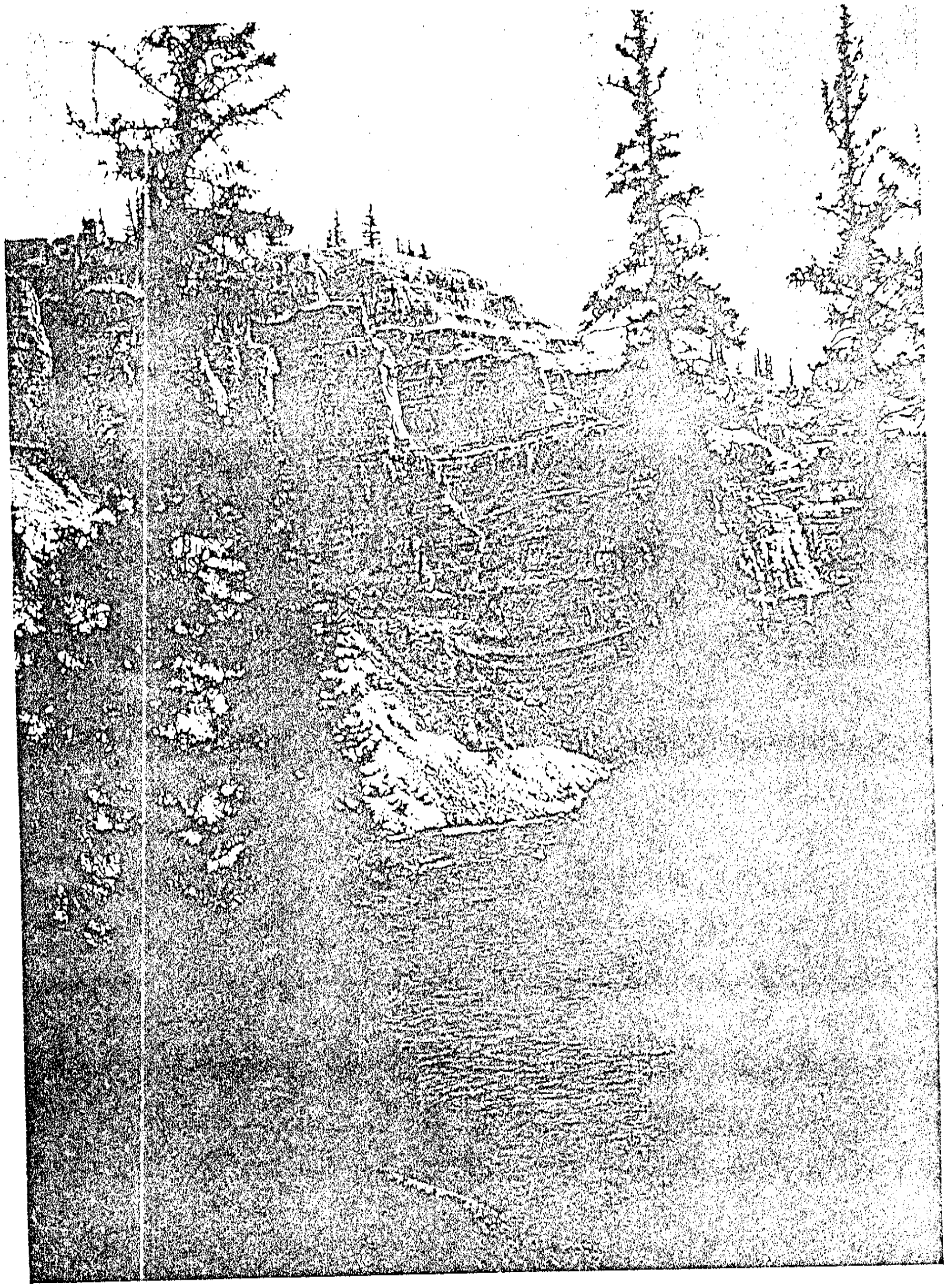

Figure 6. Vertical exposure of Reference Section 1 which displays slumping and chalk-colored beds of zeolitized tuff.

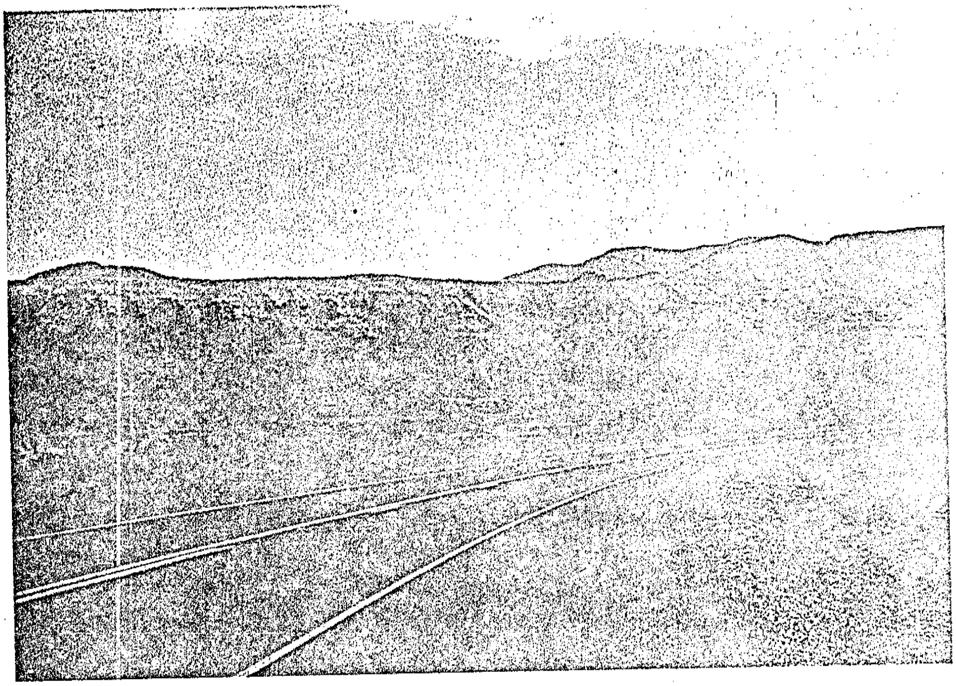

Figure 7. Vertical exposure of Reference Section 2 illustrating near horizontal attitude of beds.

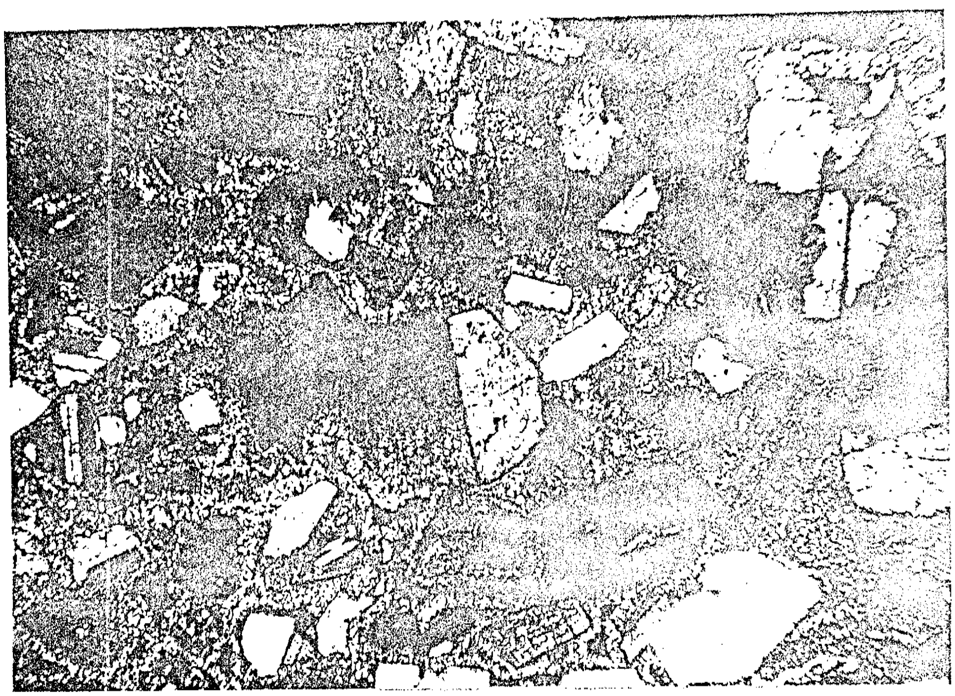

Figure 8. A calcite-cemented arenite. Plagioclase in the center shows moderate embayment. A poorly sorted arenite with grains suspended in a calcite cement.

are the largest grains in the arenites. Cements and quartz are lower by 5%; biotite, magnetite, and hornblende contents are unchanged; and sanidine approximately 10%. Analcime, identified by X-ray diffraction, was found only in the arenites and conglomerates of Reference Section 2.

The An content of the plagioclases of all the arenites averages 22%, ranges from 7 to 36%, and shows zoning and no alteration. Only minor embayments are observed on a few of the broken plagioclase crystals with arenites of Reference Section 2 being the most corroded and embayed. Trace amounts of clinoptilolite, smectites, authigenic quartz, and organics are also present with Reference Section 2 arenites showing a definitely greater abundance of authigenic quartz than any other section or lithology.

The arenites of Reference Section 2 showed a distinct increase in volcanic rock fragments. In several specimens, it was the dominant detrital grain. The fragments are subangular to subrounded, contain plagioclase crystals, biotite, magnetite, quartz, and microlaths of feldspar in a very finely crystalline matrix (Fig. 9). Sedimentary rock fragments are also found but never exceed 5% in abundance with the clasts being primarily of shales. The clasts are subrounded to rounded and never approach the size of the volcanic rock fragments (4.459 mm).

From Table 1 it can be seen that the coefficients of variation for Al_2O_3, CaO, MgO, and TiO_2 are nearly identical for Sections 1 and 2.The Na_2O content of Reference Section 2

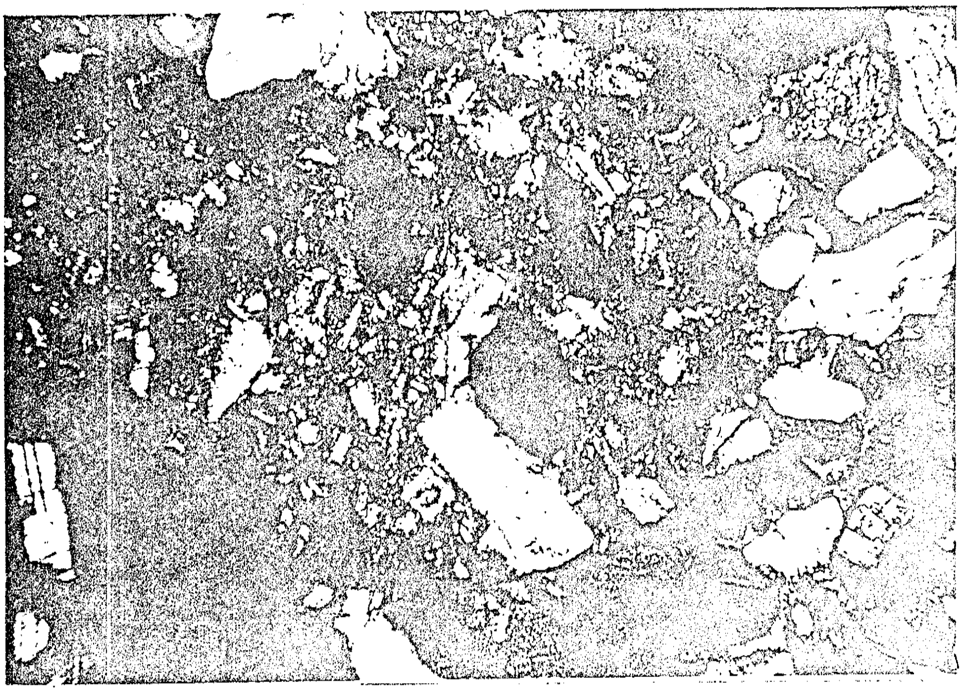

Figure 9. Volcanic rock fragment which occupies most of the photo shows laths of plagioclase set in a very finely crystalline matrix. Also present is sanidine and biotite. Crossed nicols.

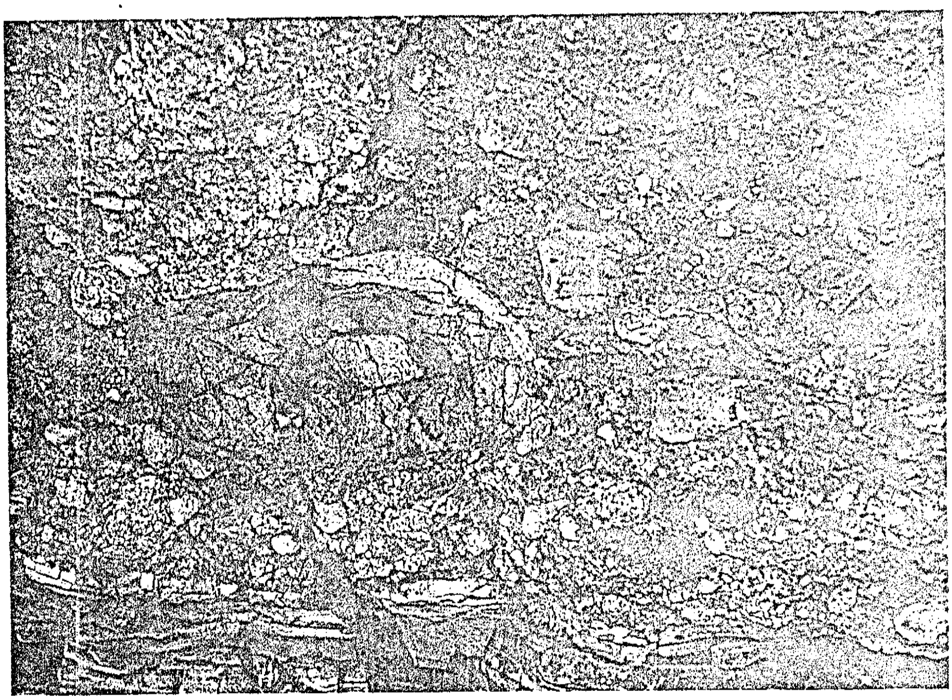

Figure 10. A very poorly sorted conglomerate of Reference Section 2 composed of rhyolitic and latitic pebbles and cobbles.

arenites is twice that of Reference Section 1 as well as the SiO_2 mean being higher. The Fe_2O_3 and K_2O content of Reference Section 1 arenites are considerably higher than those of Reference Section 2. Reference Section 3 arenites show the lowest coefficient of variation and standard deviation for the oxides.

Conglomerate

Conglomerates in the area studied are thin-bedded, averaging .6 m in thickness with the exception of one large thick-bedded deposit. The induration is poor even when cemented by calcite, gypsum, analcime, or clinoptilolite. The majority of the conglomerates contain clinoptilolite and montmorillonite in their matrix as determined by diffraction studies. The pebbles range in size from .32 mm to 7.62 cm with most less than 2.54 cm. Sorting is poor (Fig. 10), and the pebbles have a roundness of .30-.60. Volcanic pebbles which are chiefly rhyolites and latites, predominate, but some beds contain minor sedimentary rock fragments of the lower beds as well as pumice. The matrix comprises only 20% of the rock and also contains feldspar, quartz, biotite, magnetite, and hornblende. The conglomerates are moderate yellow-brown (10YR 5/4) to light olive-gray (5Y 6/1) for fresh surfaces and dark yellow-brown (10YR 4/2) on weathered surfaces.

The conglomerates of Reference Section 1 only contained clinoptilolite and montmorillonite in their matrix in resembling gaylussite or nacholite occur in the shales and contrast to those of Reference Section 2, which also contained analcime but never in association with clinoptilolite. Reference Section 3 conglomerates contain no authigenic minerals. Reference Section 2 also contained a mudflow conglomerate in the upper portion of the section. As can be seen from Figure 11, the sorting is very chaotic, and the pebbles more angular than the other conglomerates observed. Also present in the mudflow conglomerate are angular, undeformed clasts of lacustrine sediments up to 16.51 cm in length.

Shale

Shale is the predominate lithologic unit in the lacustrine facies. It is very pale orange (10YR 8/2) to yellow-gray (5Y 8/1) or a banding of both on fresh surfaces and light brown (5YR 5/6) on weathered. The shales are evenly bedded and average .6m in thickness, but can range up to 1.8m. Laminations vary from paper-thin to beds 2.5 to 5cm thick. A few shales display evenly bedded .13 cm-thick beds of calcite (Fig. 12). Detrital calcareous concretions, somewhat flattened parallel to the bedding planes present, are common in many of the shales. There is distortion of the shales around the concretions giving a flow-like texture around them (Fig. 13). This is probably due to differential compaction around the concretions while the shales were being deposited.

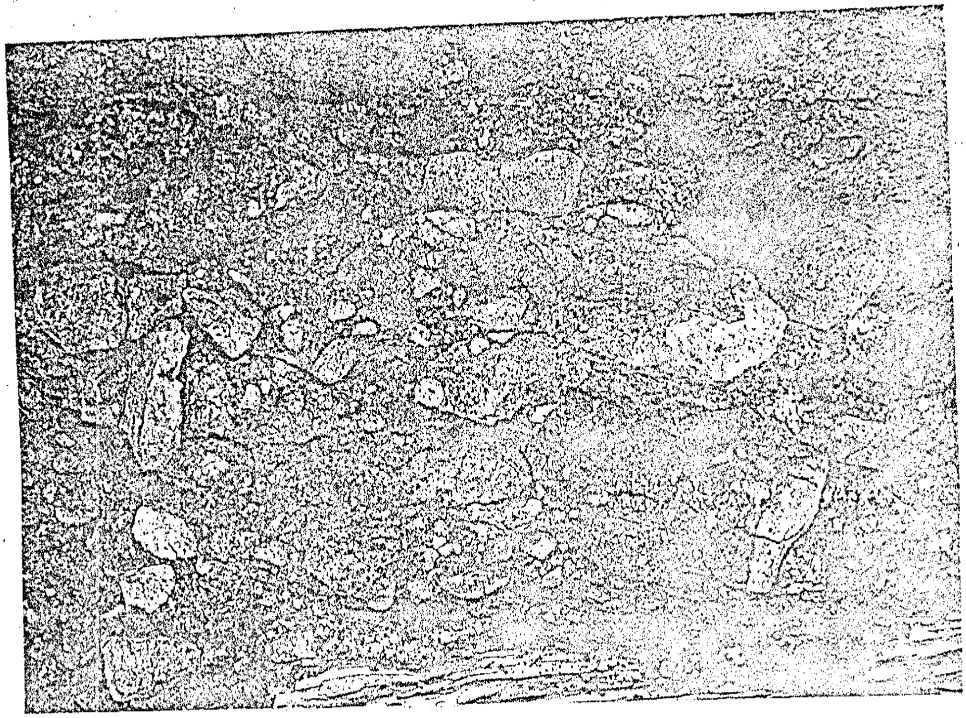

Figure 11. Mudflow conglomerate of Reference Section 2 displaying very chaotic sorting.

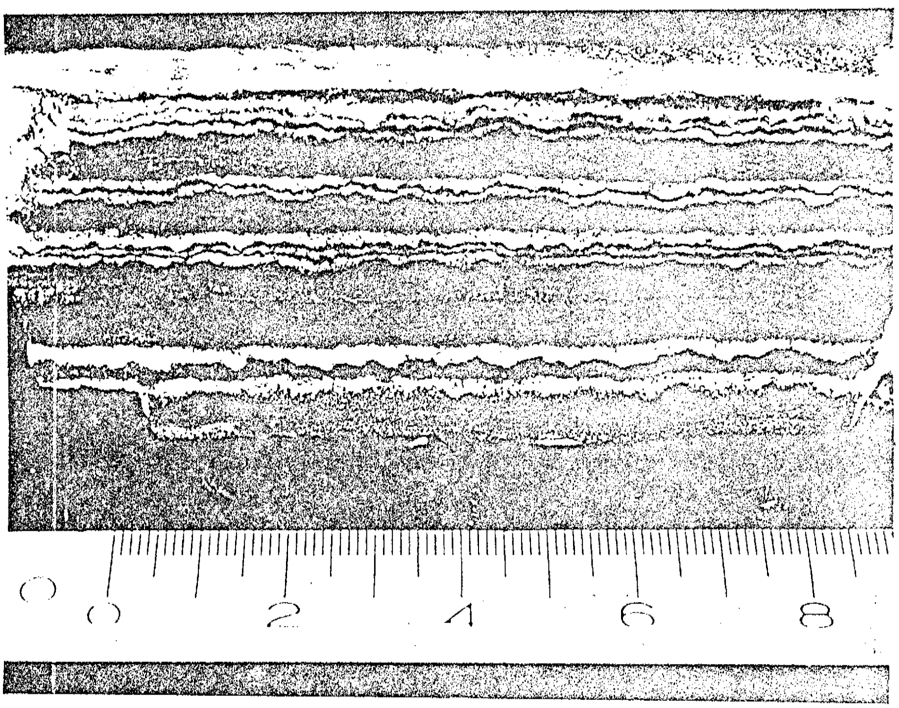

Figure 12. Primary authigenic calcite interbedded within a shale of Reference Section 2.

Figure 13. Distortion of matrix around a calcareous clast giving it a flow-like texture. Crossed nicols.

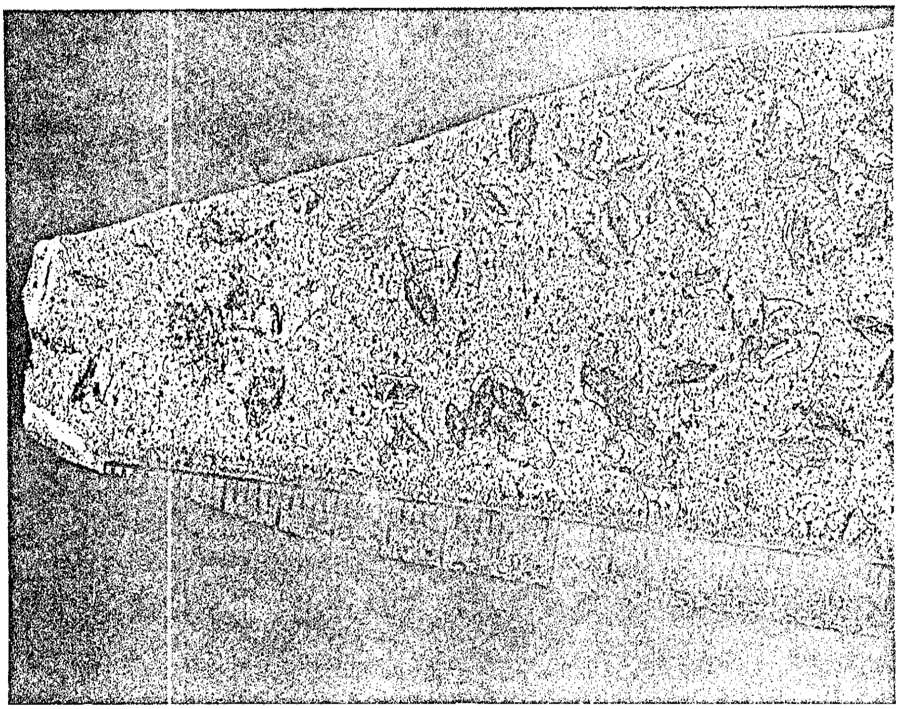

Figure 14. Calcite crystals filling molds of former crystals which were probably gaylussite or nacholite.

Also present are carbonized plant remains as well as mudcracks, ripple marks, and soft sediment deformation features. Every gradation exists between shale and the other lithologies present with arenaceous shales predominating. Most shales contain numerous crystal molds resembling gaylussite or nacholite, .13 to 5.0 cm long, with most averaging .64 cm in length. There is a tendency for the smaller crystal molds to occur in groups of two or three (Fig. 14). Calcite or gypsum occurs as clusters of subhedral to anhedral crystals, where it apparently precipitated in the molds that formed by solution of a readily soluble probably saline mineral.

Certain portions of Reference Section 2 display a green-yellow weathering rind 1-2 mm thick which smells of sulfur when crushed. This is probably due to the weathering of the pyrite in the shales. Also found in the shales are imbedded oblate spheroids of pumice (Fig. 15) ranging in size from 1.00 cm to 4.50 cm in length.

Authigenic clinoptilolite and montmorillonite are common in the shales. This is due to the alteration of the vitric material which averages 25% of the rock. Quartz averages .122 mm for Reference Section 1 and .081 mm for Reference Sections 2, 3, and 4, is subangular to subrounded, and is 10% in abundance. Other constituents are: biotite, 5%; plagioclase, 5%; organics, 8%; magnetite, 2%; and trace amounts of hornblende, sanidine, hematite, augite, diopside, apatite, pyrite, cristobalite, calcite, and gypsum. The matrix is primarily of silt size of which tuffaceous material dominates.

The coefficient of variation for the K_2O content of Sections 1 and 2 are very similar. All other oxides' coefficient of variation is much higher in Reference Section 2. The mean contents of the oxides are similar for both sections, but Reference Section 2 shows larger standard deviations for all oxides. K_2O content is identical for mean and standard deviation for Sections 1, 2, and 3.

Fissility is usually excellent (Fig. 16), and induration is moderate. The An content of the plagioclases ranged from 14 to 44% and averaged 25%. None of the plagioclases studied showed any alterations. Sorting of the sand fraction is poor. There are local areas of hematitic staining caused by the oxidation of the magnetite present. Sphericity of the derital minerals is .30-.40.

Siltstone

Siltstone is the second most abundant rock in the Creede Formation. It is grayish orange (10YR 7/4) to light olive-gray (5Y 6/1) for both fresh and weathered surfaces. The siltstones are moderately to well consolidated and moderately sorted. The beds, averaging 2 m in thickness, are massive and contain abundant organic material.

The siltstones have a sphericity of .20-.30. The average grain size is .065 mm, and the major detrital minerals present are: quartz, 10%; biotite, 2%; feldspar,

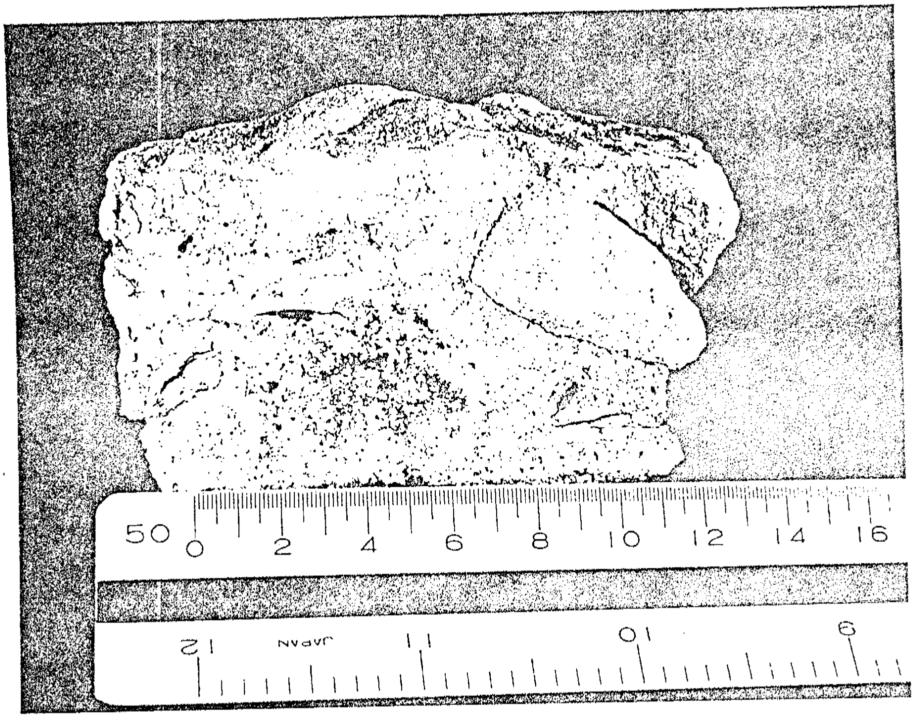

Figure 15. Pumice fragment in upper right of specimen which is common to the shales and siltstones.

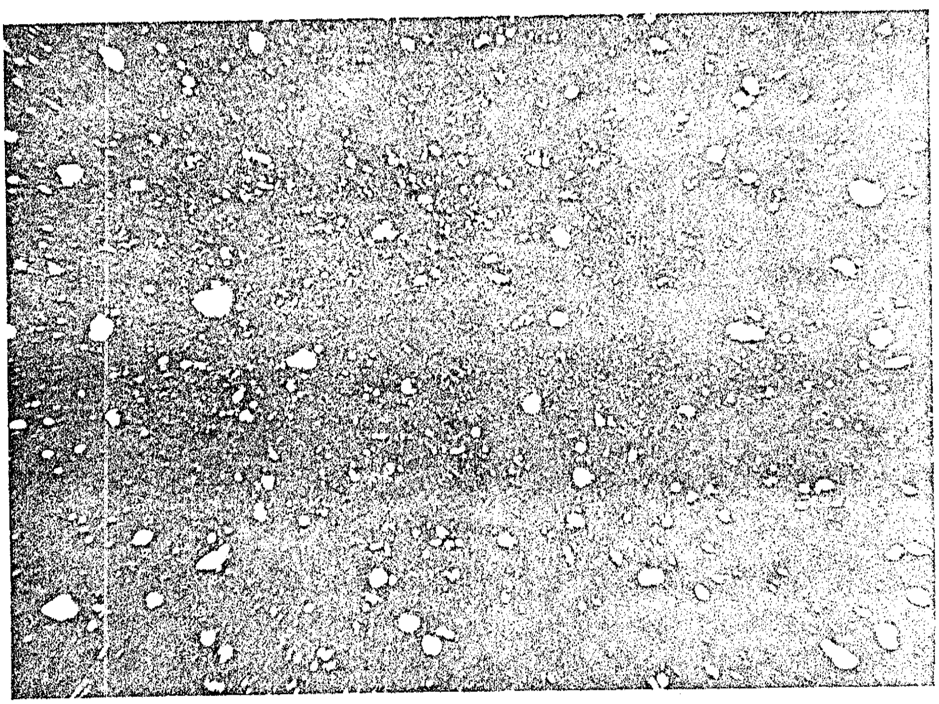

Figure 16. Thin-section photo displaying excellent fissility which is found in most shales. Crossed nicols.

5%; magnetite, 1%; and organics, 4%. Minor and accessory minerals observed were: hornblende, calcite, gypsum, pyrite, augite, apatite, montmorillonite, and clinoptilolite. The matrix is composed of altered shards and silt-size tuffaceous material.

Reference Section 2 showed a larger coefficient of variation for all oxides except CaO and TiO_2. It also displays greater standard deviations for all oxides except CaO.

Travertine

The Creede Formation has numerous bodies of travertine and tufa within it. They are more abundant near the borders of the formation than in the middle (Larsen and Cross, 1956). The travertine is light gray (N8) and ranges from dense, fine-grained calcite to a porous, highly cellular variety. Freshly broken travertine yields a fetid sulfurous odor. Within the travertine bodies are fragments of lacustrine sediments as well as deposits of opal, chalcedony, and quartz lining cavities or occurring as vein fillings.

The travertine, occurring in a variety of forms, were deposited by mineral springs as irregular masses surrounding cylindrical orifices. Some deposits appear to be leaflike extensions from a spring which crosscut and intertongue with lake strata. Also present are large masses of travertine surrounded by lacustrine sediments (Fig. 17). Steven and

Friedman, 1968, postulated that these structures are travertine terraces. Thin beds of virtually pure limestone are found interbedded within the Creede strata. These probably resulted from calcite precipitating out of shallow alkaline ponds fed by mineral springs as evaporation and/or supersaturation occurred. The carbonate in travertine in the Creede Formation was deposited from a sedimentary carbonate unit as based on geologic and isotopic evidence (Steven and Friedman, 1968).

Tuff

The tuffs of the northern portion of the Creede caldera were studied and described in 1971 by Steven and Van Loenen. Tuffs in the lacustrine deposits in the area studied make up approximately 10% of the sections and are the most conspicuous strata, as can be seen from Figure 5. From the distinct laminations present, the tuffs appear to be the result of ash falls into the lake. Eight tuffs were recognized. Ranging from .6 to 4.0 m in thickness, they are laterally continuous.

The fresh tuff is very pale orange (10YR 8/2) to very light gray (N8) and weathers to a light brown (5YR 5/6). Where zeolitized, the tuff is well indurated, extremely fine grained, and breaks with a conchoidal fracture. Only upon very careful examination can the laminations be detected. Non-zeolitized tuff is usually very friable and easily disaggregated.

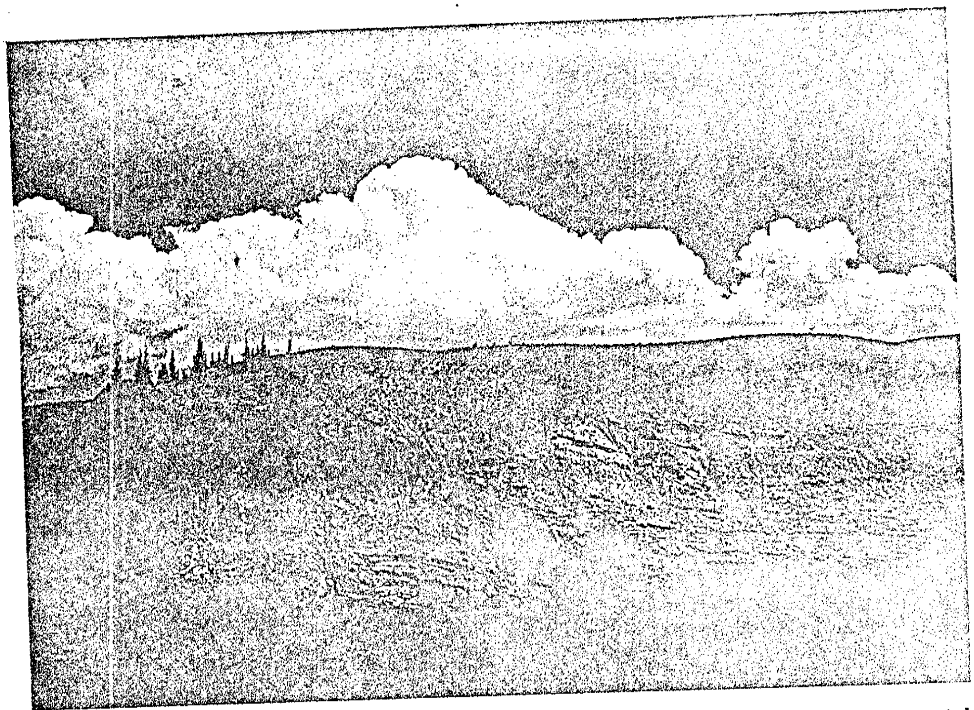

Figure 17. Massive body of travertine displaying distortion of lake sediments as they approached it.

Figure 18. Thin-section photo (plane polarized light) of a tuff displaying well-preserved glass fragments giving it a vitroclastic texture.

The tuffs contain minor carbonized plant remains and the same type of crystal molds as mentioned in the shales. The lower contact of the tuffs is very distinct, but the upper portions are usually gradational into the overlying lithologies.

As seen from Figure 18, the vitroclastic texture is well preserved with the relict shards and vesicles usually being replaced internally by clinoptilolite and the outer surfaces rimmed with sodium smectites. Both platy bubble-wall shards and pumice shards containing elongated bubbles are present with the former predominating. Pyrogenic phenocrysts of apatites, biotite, sanidine, hornblende, pyroxene, plagioclase, and quartz are distributed uniformly throughout the tuffs. The quartz and feldspar grains average .410 mm, are subangular to subrounded, and make up 5% of the tuffs. Organics and biotites each average 3% in abundance, while apatite, hornblende, gypsum, and pyroxene exist only in trace amounts. The only species of zeolite in the tuffs was clinoptilolite and was identified by the technique described under laboratory methods.

IV. MINERALOGY AND GEOCHEMISTRY

Laboratory Methods

X-ray diffractometer patterns were made of all samples collected and mineralogic compositions were estimated from these (see Appendix 2). The samples were ground to less than

200 mesh, made into either briquettes or fused disks and then exposed to copper radiation. The mineralogy determined from this data was then used to supplement both the petrographic and scanning electron microscopy (SEM) studies.

The petrographic studies were made by using thin sections and immersion oil mounts, and selective staining for calcite and potassium feldspar. The SEM studies were done on a Hitachi model HHS-2R unit and were made by carbon or gold-palladium coating freshly broken rock chips. These provided information on authigenic minerals and alterations present, and textural and age relationships of the authigenic minerals. The SEM was also equipped with an energy dispersive analyzer (EDAX) which yielded semi-quantitative chemical data (see Appendix 3) used in mineral identification and in detecting any elemental distributions.

A Rigaku X-ray fluorescence spectrometer interfaced with a PDP 11/23 computer was employed to determine the chemistry of all samples collected (see Appendix 4), except the conglomerates. Some duplicate samples were sent out to commercial labs for analysis. Fire assays and atomic absorption were done on two specimens to determine if any silver was present.

The types of clays present were identified by making several 2 and .25 micrometer oriented mounts of each sample. One mount of each sample was glycolated and the remainder

TABLE 1

Statistical Analyses of Lithologic Chemistry

	SiO_2	Al_2O_3	CaO	K_2O	MgO	TiO_2	Fe_2O_3	Na_2O
Reference Section 1 Arenites								
x	65.65	10.95	9.44	3.25	0.89	0.38	2.59	1.39
s	3.70	1.82	6.10	0.96	0.47	0.11	1.02	0.26
cv	5.64	16.62	64.61	29.67	52.48	28.31	39.40	18.41
Reference Section 2 Arenites								
x	60.46	13.80	7.57	2.57	1.30	0.50	3.07	2.76
s	5.38	2.16	4.75	0.50	0.71	0.14	0.80	0.97
cv	8.91	15.68	62.80	9.30	54.44	27.07	25.96	35.04
Reference Section 3 Arenites								
x	59.35	14.41	2.56	3.12	1.10	0.58	3.60	2.17
s	2.13	1.30	0.37	0.24	0.11	0.08	0.72	0.36
cv	3.58	8.99	14.58	7.69	9.98	13.75	20.08	16.40
Reference Section 1 Shales								
x	63.85	11.05	2.70	3.66	1.15	0.44	2.61	1.00
s	2.63	1.54	1.95	0.95	0.27	0.06	0.68	0.22
cv	4.11	13.91	72.07	26.05	23.34	14.71	26.18	22.58
Reference Section 2 Shales								
x	64.89	10.20	3.58	3.67	1.15	0.38	2.13	1.19
s	4.91	2.44	4.29	0.99	0.52	0.11	0.89	0.43
cv	7.56	23.93	119.70	27.07	45.76	30.02	41.79	35.92
Reference Section 3 Shales								
x	66.97	9.18	1.63	3.87	1.00	0.50	2.41	0.96
s	1.59	0.79	0.74	0.44	0.26	0.03	0.60	0.22
cv	2.38	8.60	45.34	11.45	26.05	6.90	25.12	23.15
Reference Section 4 Shales								
x	66.20	9.23	3.53	4.75	0.88	0.38	2.82	0.72
s	0.99	0.55	3.10	0.18	0.12	0.05	0.27	0.06
cv	1.50	5.99	87.58	3.71	14.21	13.41	9.64	8.26

Reference Section 1 Siltstones

	SiO_2	Al_2O_3	CaO	K_2O	MgO	TiO_2	Fe_2O_3	Na_2O
x	63.74	10.59	2.53	3.97	1.15	0.44	2.98	1.14
s	2.34	1.09	3.00	0.41	0.19	0.04	0.70	0.29
cv	3.68	10.25	118.66	10.29	16.47	9.16	23.48	25.04

Reference Section 2 Siltstones

x	61.99	11.44	1.80	3.63	1.51	0.45	2.98	1.52
s	5.27	2.31	0.71	0.81	0.88	0.03	1.20	0.65
cv	8.49	20.21	39.75	22.30	57.91	7.09	40.27	42.46

Reference Section 3 Siltstones

x	69.01	8.47	7.16	4.60	0.71	0.31	1.87	0.67
s	0.00	0.00	0.00	0.00	0.00	0.00	0.00	0.00
cv	0.00	0.00	0.00	0.00	0.00	0.00	0.00	0.00

Reference Section 4 Siltstones

x	64.89	9.87	1.97	4.72	1.00	0.42	2.72	0.71
s	1.98	0.99	1.63	0.33	0.09	0.06	0.43	0.08
cv	3.05	10.01	82.60	6.90	8.90	13.21	15.67	11.48

Reference Section 1 Tuffs

x	63.45	11.65	2.09	2.69	1.36	0.29	2.15	1.02
s	4.49	1.98	0.88	0.38	0.52	0.13	0.78	0.68
cv	7.08	17.01	41.89	14.16	38.03	43.59	36.08	66.46

Reference Section 2 Tuffs

x	71.67	11.15	1.18	4.30	0.82	0.36	1.39	1.43
s	1.00	1.55	0.16	0.68	0.21	0.21	0.07	0.12
cv	1.40	13.90	13.56	15.81	25.61	5.85	5.04	8.39

Reference Section 4 Tuffs

x	64.13	10.87	1.03	4.80	1.00	0.47	2.05	0.76
s	1.31	0.02	0.17	0.37	0.05	0.02	0.84	0.06
cv	2.04	0.21	16.83	7.62	4.74	4.69	41.06	7.28

TABLE 2
Statistical Analyses of Mineral Chemistry

	SiO_2	Al_2O_3	CaO	K_2O	MgO	TiO_2	Fe_2O_3	Na_2O
Reference Section 2 Analcime-Rich Rocks								
x	58.86	14.77	5.48	2.55	1.07	0.55	3.20	3.75
s	1.63	0.47	1.62	0.16	0.17	0.07	0.52	0.19
cv	2.77	3.19	29.55	6.09	16.08	13.44	16.31	5.07
Reference Section 1 Calcite-Rich Rocks								
x	50.80	5.01	16.00	3.32	0.96	0.35	2.52	1.49
s	17.34	5.48	8.71	1.23	0.40	0.47	0.73	0.54
cv	34.14	109.40	54.47	37.07	41.55	13.49	28.87	36.27
Reference Section 2 Calcite-Rich Rocks								
x	43.43	7.23	20.05	2.49	1.01	0.27	2.40	1.44
s	19.27	5.79	10.52	1.18	0.33	0.17	1.16	1.27
cv	44.36	80.08	52.45	47.60	32.88	60.43	48.32	88.20
Reference Section 1 Clinoptilolite-Rich Rocks								
x	62.96	12.06	2.94	2.88	1.30	0.41	2.91	1.02
s	2.46	1.28	1.32	0.41	0.22	0.12	0.99	0.42
cv	3.91	10.59	44.77	14.18	16.93	29.64	34.07	41.57
Reference Section 2 Clinoptilolite-Rich Rocks								
x	57.27	14.02	2.58	3.09	2.10	0.49	2.90	1.95
s	4.71	1.78	0.86	0.48	0.81	0.11	1.15	0.73
cv	8.22	12.72	33.38	15.37	38.46	21.85	39.62	37.34
Reference Section 1 Gypsum-Rich Rocks								
x	63.72	10.05	2.10	4.59	0.84	0.44	2.62	1.37
s	0.16	0.42	0.19	0.52	0.18	0.04	0.83	0.06
cv	0.24	4.22	9.11	11.26	21.89	8.77	31.85	4.13
Reference Section 2 Gypsum-Rich Rocks								
x	57.94	13.55	3.20	3.06	1.81	0.47	3.01	2.18
s	4.11	2.11	1.11	0.73	0.79	0.11	0.81	0.84
cv	7.10	15.57	34.74	23.80	43.50	22.68	26.93	38.45
Reference Section 1 Montmorillonite-Rich Rocks								
x	62.54	12.08	2.35	3.06	1.35	0.40	2.61	0.87
s	2.89	1.34	0.82	0.61	0.32	0.11	0.79	0.25
cv	4.62	11.11	34.80	19.95	23.63	28.53	30.36	28.79
Reference Section 2 Montmorillonite-Rich Rocks								
x	58.87	12.87	4.15	3.14	1.90	0.44	2.96	1.78
s	6.23	2.77	5.01	0.60	0.85	0.14	0.93	0.76
cv	10.58	21.53	120.65	19.20	44.89	32.99	31.42	42.86

heat treated at 350° and 550° C. The mounts were then subjected to nickel-filtered copper radiation. By observing the 001 peak shifts and/or destruction, the clays were identified (Carroll, 1970).

The species of zeolite of the heulandite structural group present was determined in a similar fashion. By following the procedures outlined by Boles (1972) and Alietti (1972), 2 micrometer oriented mounts were separately subjected to 200, 300, 400, 500, and 600° C heat treatments and then X-rayed. By observing at which point the 020 peak was destroyed, the species of zeolite was determined.

Table 2 lists the mean, standard deviation and coefficient of variation of lithologic units which are rich in a particular authigenic mineral. Appendix 5 shows various oxide plots of the authigenic minerals.

Table 3 is a comparison of Fisher Quartz Latite to the tuff found in the lacustrine facies. The analyses were first normalized, and assuming Al_2O_3 is immobile, the tuffs' oxides were recalculated for loss due to weathering. The gains and losses of the different oxides can now be compared.

Analcime

Analcime, also known as analcite, is one of the more commonly reported zeolites in sedimentary rocks. It has an ideal formula of $NaAlSi_2O_6 \cdot H_2O$, but is usually higher in silica ranging from a Si:Al of 2.0 to approximately 2.7

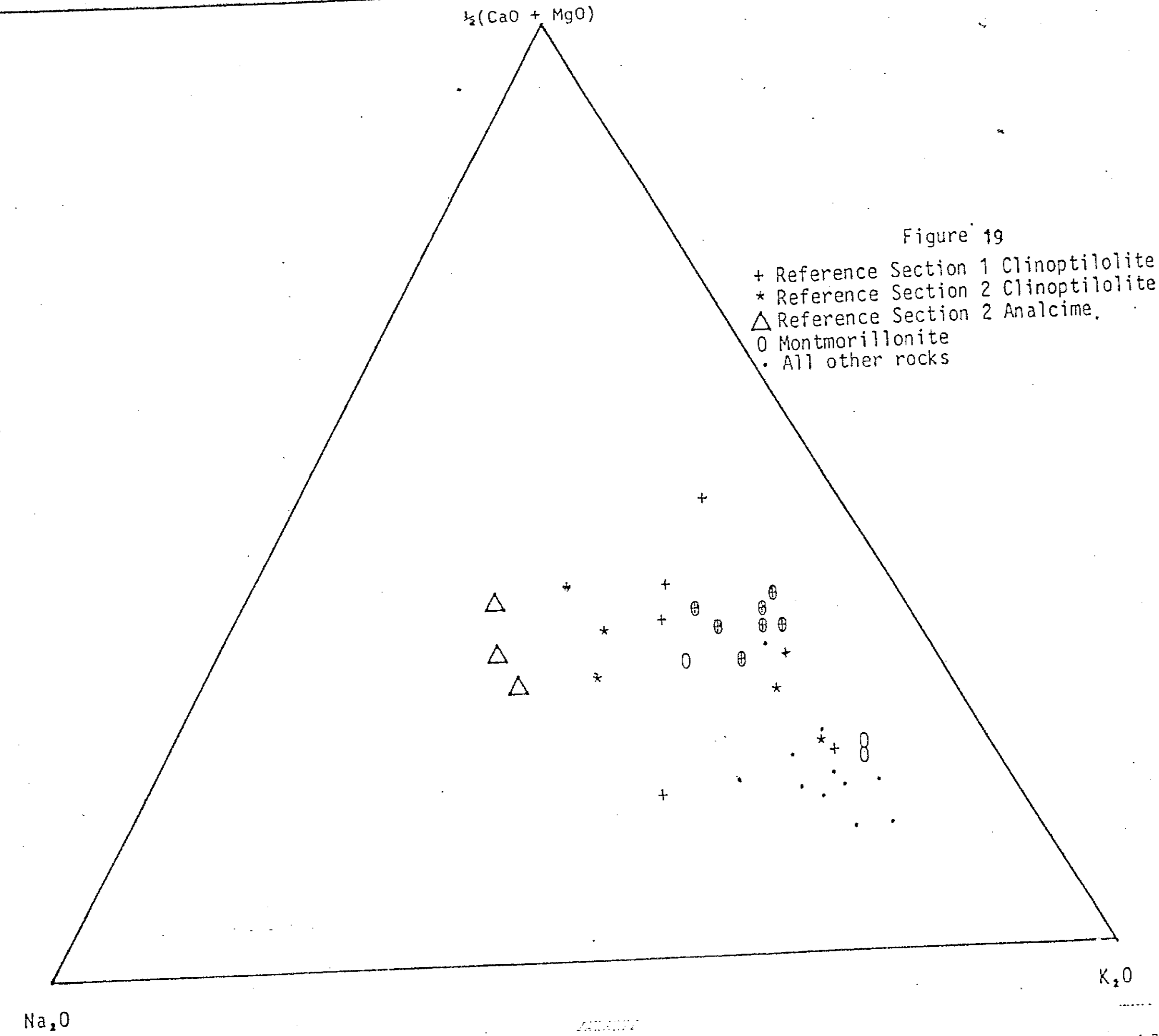
½(CaO + MgO)
Figure 19
+ Reference Section 1 Clinoptilolite
* Reference Section 2 Clinoptilolite
△ Reference Section 2 Analcime.
0 Montmorillonite
. All other rocks
Na_2O
K_2O

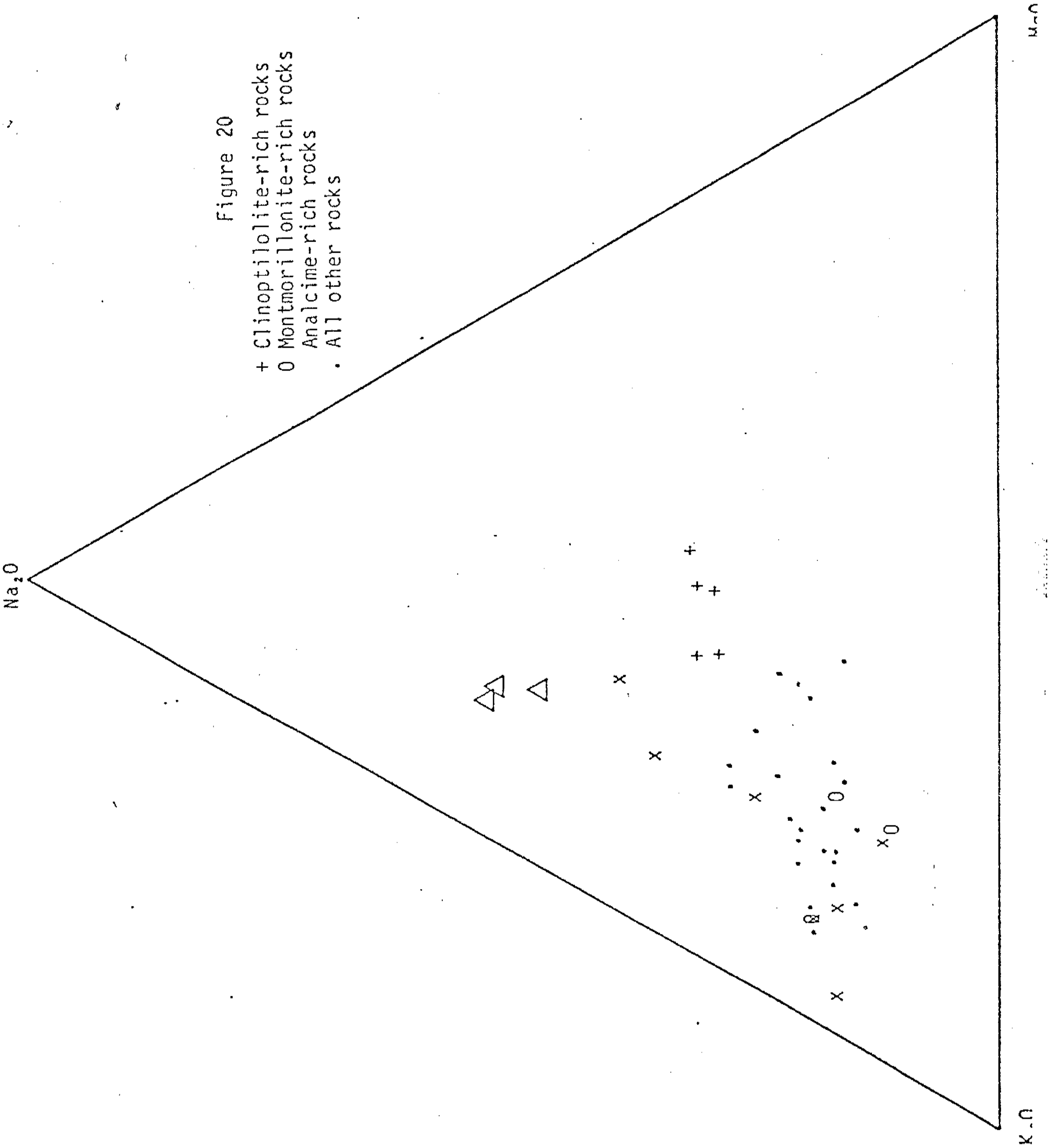
+ Clinoptilolite-rich rocks
O Montmorillonite-rich rocks
Analcime-rich rocks
. All other rocks
Na_2O
K_2O
H_2O

Figure 20

(Saha, 1959). Analcime occurs in rocks ranging from Late Paleozoic to Recent in age and is especially common in saline lacustrine deposits, regardless of age. Unlike the other zeolites, analcime occurs in rocks which lack evidence of vitric material.

Analcime was found only in Reference Section 2 and was restricted to the arenites and conglomerates (appendix 2). Relict vitric material was observable in only one thin section containing analcime, and the only authigenic silicate associated with the analcime based on X-ray diffraction and petrographic data was quartz. Gypsum was always found in association with analcime (appendix 2). Comparison of the analcime-rich arenites of Reference Section 2 to those found elsewhere in the formation shows the analcime-bearing rocks to be richer in sodium (Table 1).

As can be seen from the ternary diagrams (Fig. 19 and 20), the plotted analcime data occurs in a tight cluster for both systems. This is due to analcime being richer in sodium than any other authigenic mineral present.

Analcime was not recognized in thin section due to its very small crystal size. Studies of numerous size fractions show that the average size of the analcime is 4 micrometers, and at 2 micrometers it is virtually absent. Identification was based on X-ray diffraction studies and SEM analyses. The analcime occurs as subhedral to euhedral cubo-octahedral and trapezohedral crystals 2.7 to 4.0 um in size (Fig. 21).

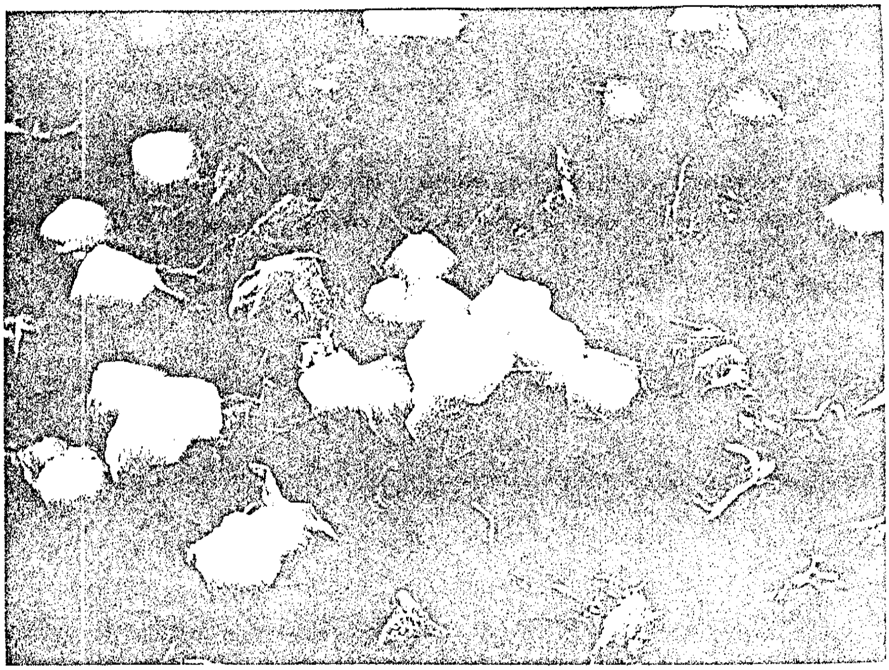

Figure 21. SEM photo of analcime crystals surrounded by authigenic clay. Average crystal size is 3 micrometers. Magnification 3,500x.

Figure 22. Thin-section photo (plane polarized light) of a calcitic peloid. All peloids displayed concentric bands and lacked any internal structures.

Calcite

Calcite occurs in a variety of forms in the sediments. It most commonly occurrs as a cement and may exceed 30% in some rocks. As mentioned in the stratigraphic section, it also occurs as crystals in molds. The more unusual form of calcite is that of peloids (Fig. 22) and thin bands of very pure crystalline calcite interbedded with shales (Fig. 23). The bands of calcite are primary deposits which either formed from calcite precipitating out of evaporating alkaline ponds or from hot springs enriching the waters in calcium carbonate beyond the saturation point of calcite (Love and Hawley, 1981).

Clay Minerals

Most of the sediments of the lacustrine facies of the Creede Formation contain authigenic clay. The clay minerals are associated with all the other authigenic minerals except analcime, and their content is generally less than 30% of the rock. By diffracting glycolated and heat-treated oriented mounts, the sodium-rich variety of montmorillonite was the only species of clay found. Scanning electron microscope photos of the clay (Fig. 21 and 24) show the irregular, wavy plates which are characteristic of the smectites. Figure 25 shows clay films coating the outer rims of shards indicating an authigenic origin. The occurrence of montmorillonite is more widespread than any of the other authigenic silicate minerals.

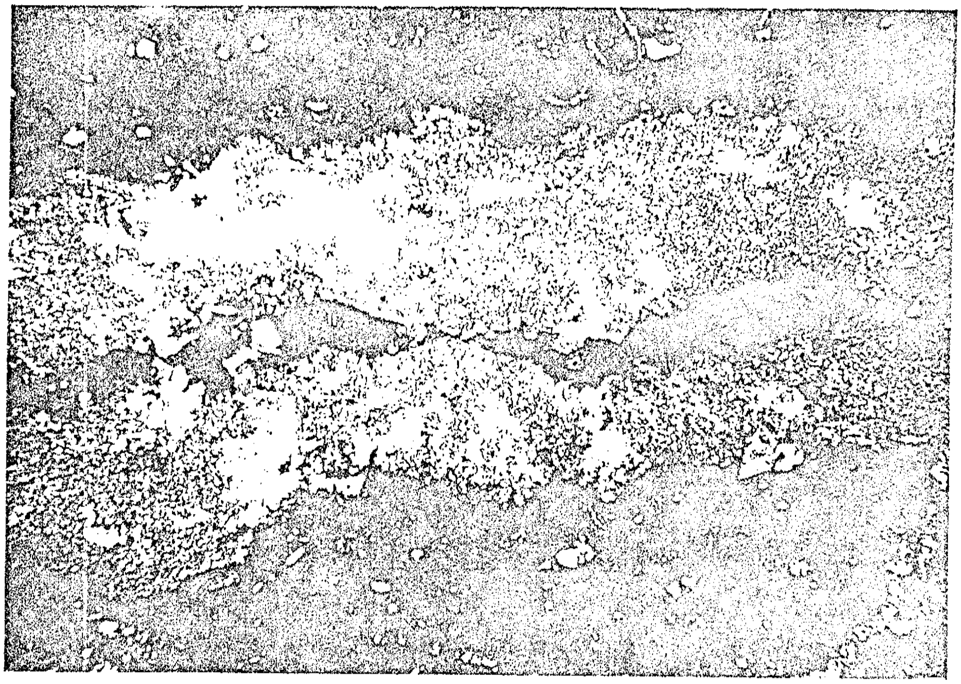

Figure 23. Thin-section photo (crossed nicols) of bands of primary calcite. This section was made from the specimen displayed in Figure 12.

Figure 24. SEM photo showing irregular wavy plates which are characteristic of the smectites. The clay shown is detrital. Magnification 1,000x.

Figure 25. Thin-section photo (crossed nicols) showing the occurrence of authigenic montmorillonite coating the outer surfaces of shards. The montmorillonite is identified by its high birefringence.

The rocks rich in montmorillonite occur in groups for Fe_2O_3 - K_2O+ Na_2O - MgO and Na_2O - K_2O - MgO ternary diagrams (Fig. 26 and 27).

Clinoptilolite

Clinoptilolite, described as early as 1890 by Pirsson, is the silica and alkali-rich member of the heulandite structural group. Extensive studies have found that it occurs chiefly in sedimentary rocks and ranks number one in abundance in comparison to the other zeolites.

Due to anomolous optical properties of the heulandite group and very small particle size, petrographic studies cannot be utilized in determining which species is present. Thermal treatments yielded clinoptilolite as the only species present.

Clinoptilolite is the most common zeolite found in the sediments of the Creede Formation. It is found in association with all of the other authigenic minerals. especially montmorillonite, but was never found in association with analcime. The clinoptilolite content ranges from trace amounts to approximately 75-80% of the rocks. It occurs as prismatic or platy crystals (Fig. 28) that average 10 um long, 9.5 um wide, and 1.5 um thick. The clinoptilolite in thin-section studies is found as crystals lining molds of former glass shards (Fig. 29) suggesting an authigenic origin. Examination by SEM also shows the clinoptilolite lining the inside of glass shards (Fig. 30) and as jumbled stacks of euhedral platy crystals

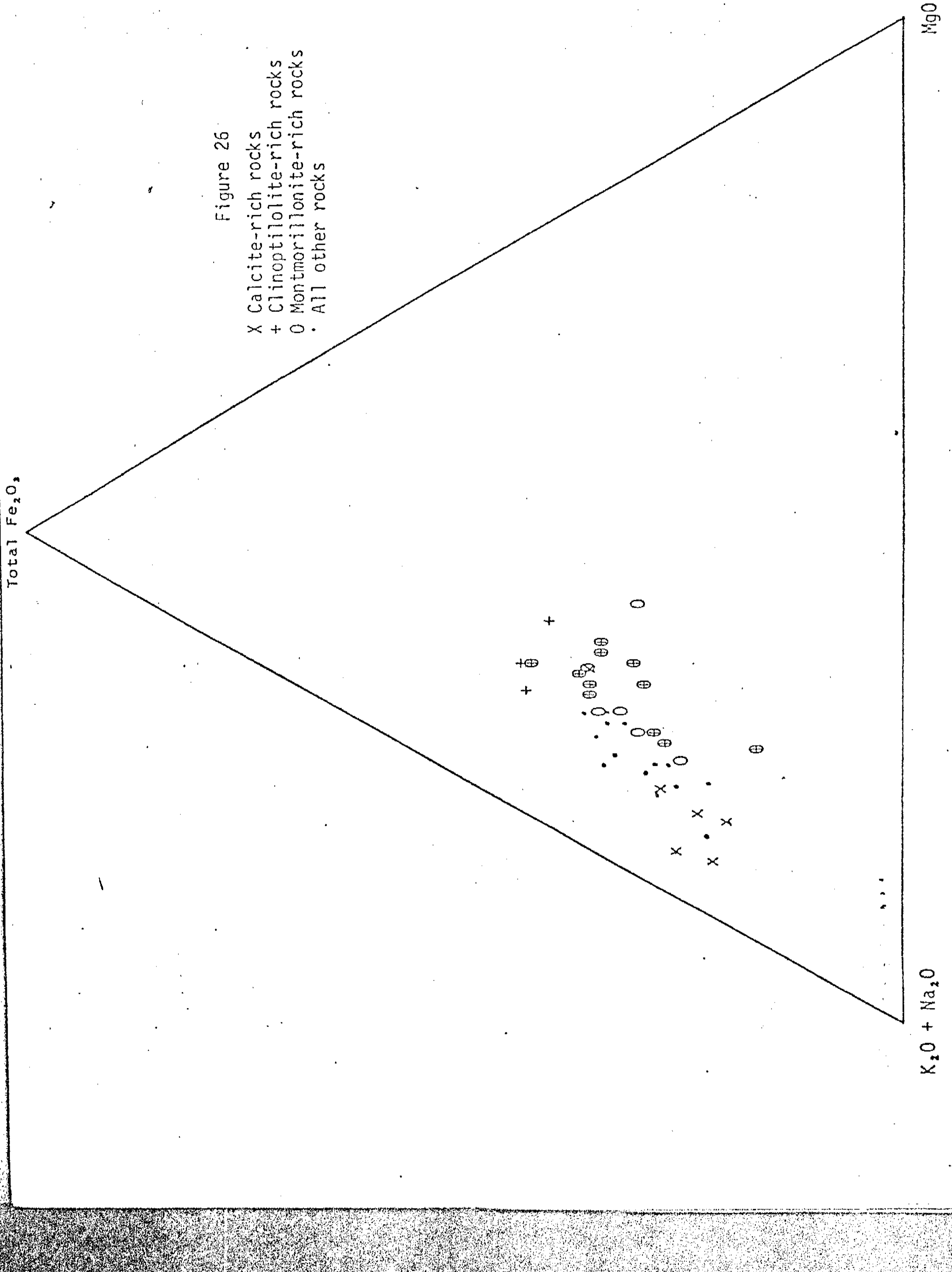
Total Fe_2O_3
MgO
$K_2O + Na_2O$
X Calcite-rich rocks
+ Clinoptilolite-rich rocks
O Montmorillonite-rich rocks
· All other rocks

Figure 26

Figure 27

X Calcite-rich rocks
+ Clinoptilolite-rich rocks
0 Montmorillonite-rich rocks
· All other rocks

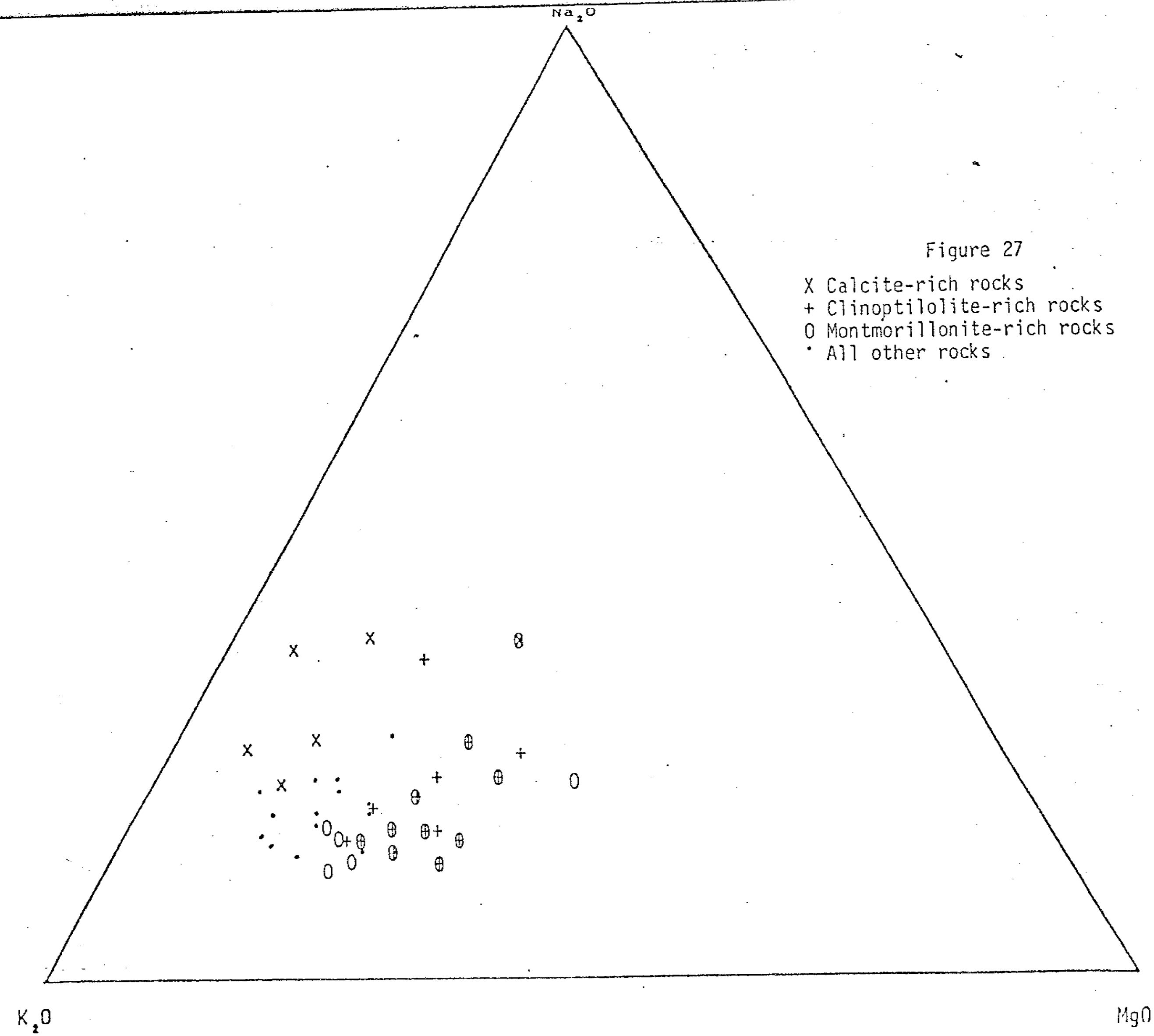

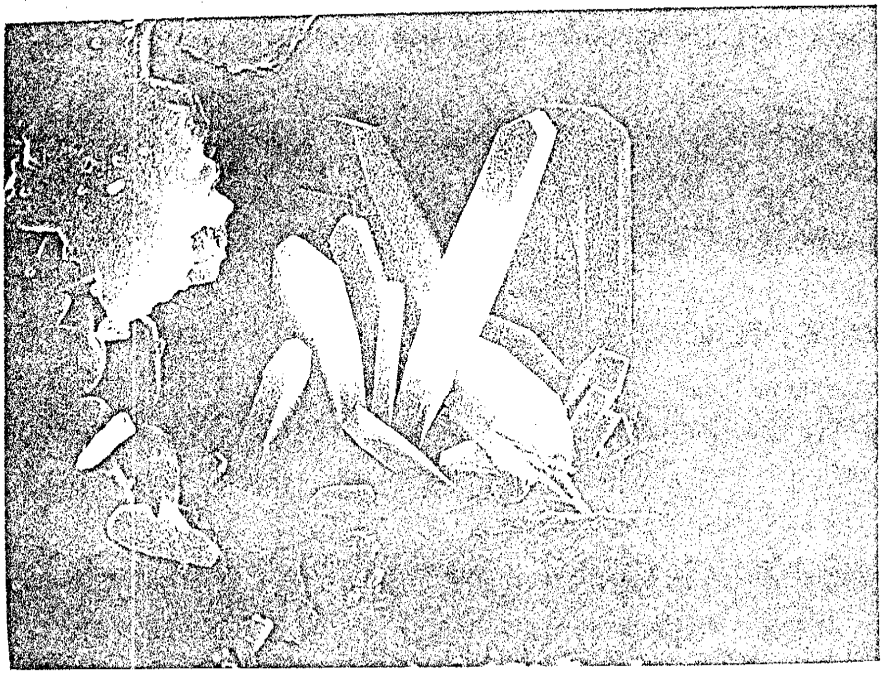

Figure 28. Clinoptilolite in SEM view. Although crystal morphology is very distinct, thermal treatment is the most certain method of identification. Magnification 3,000x.

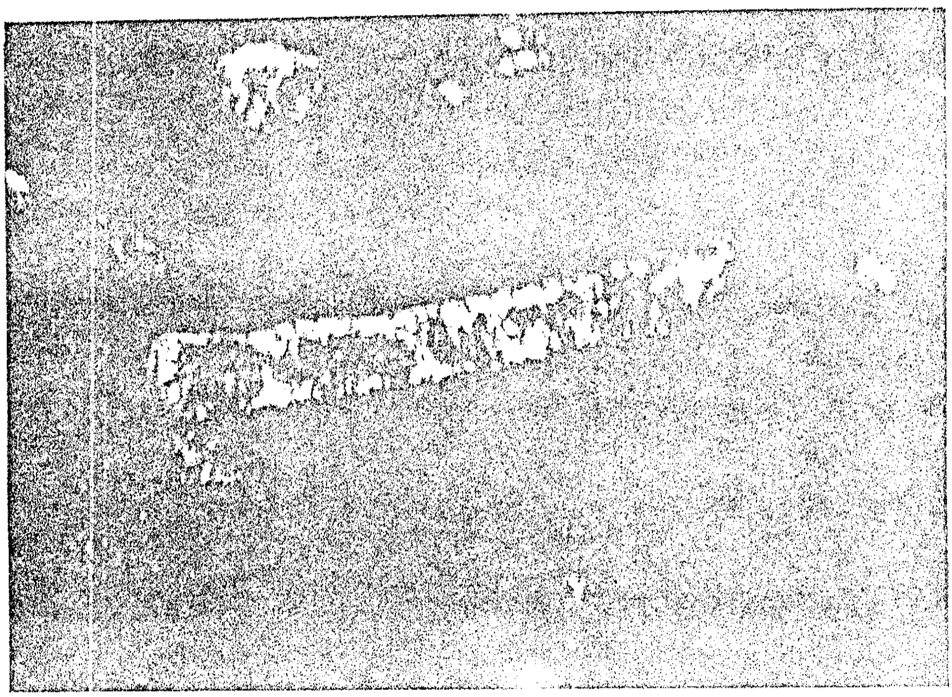

Figure 29. High magnification thin-section photo of platy crystals of clinoptilolite lining molds of former glass shards preserving the relict vitroclastic texture & indicating its authigenic origin. Crossed nicols.

(Fig. 31) filling veinlets and voids within the rocks. X-ray diffraction of size fractions indicates that the clinoptilolite still persists at a .25 um separation along with montmorillonite.

The clinoptilolite was found to occur in practically every rock type as long as there was once vitric material present for zeolitization to occur.

Clinoptilolite-rich rocks, when plotted on a Fe_2O_3 - $Na_2O + K_2O$ - MgO ternary diagram, show the closest grouping of points (Fig. 26). The Na_2O - K_2O - MgO ternary diagram showed nearly as good results, and the ternary diagram Na_2O - K_2 - CaO showed the greatest spread of points (Fig. 27 and 32).

Gypsum

Gypsum is found in a variety of forms and occurrences in the Creede Formation. Displacive veins of fibrous satin spar gypsum filling primarily vertical fractures and joints and minor discontinuous layers ranging from .6cm on the ends to 5 cm in the centers between bedding planes are found. In some of the open fractures, the walls are lined with masses of euhedral bladed crystals which average 1.3 cm in length, .25 cm thick, and .8 cm in height. Gypsum is also found as subhedral crystals within the rocks and as a cementing agent with Reference Section 2 having the greatest abundance of gypsum.

Both major reference sections display numerous .25 to .64 cm-thick displacive horizontal beds of gypsum which can

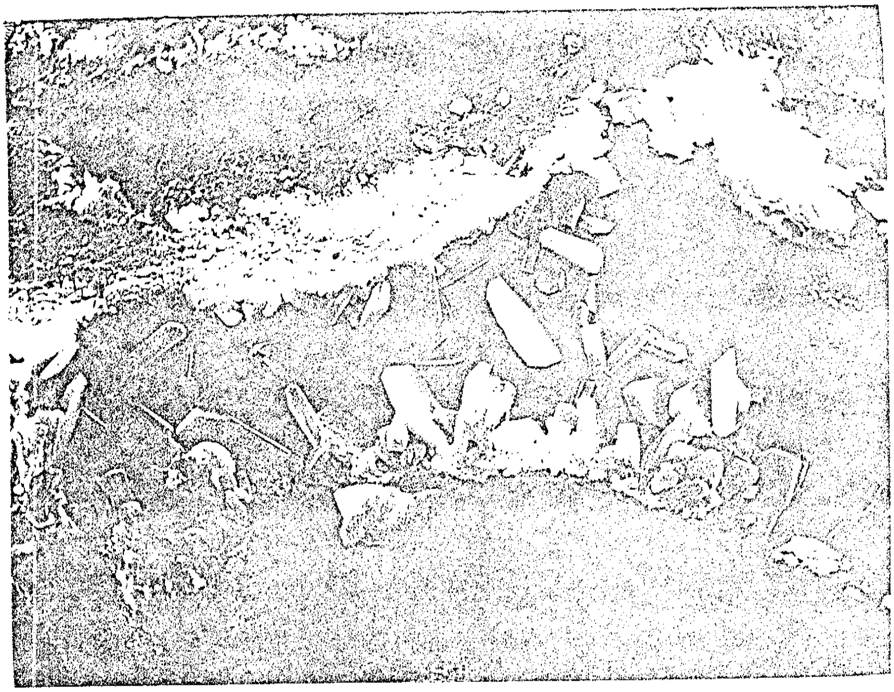

Figure 30. SEM view of clinoptilolite crystals occurring as a shard filling. Magnification 1,000x.

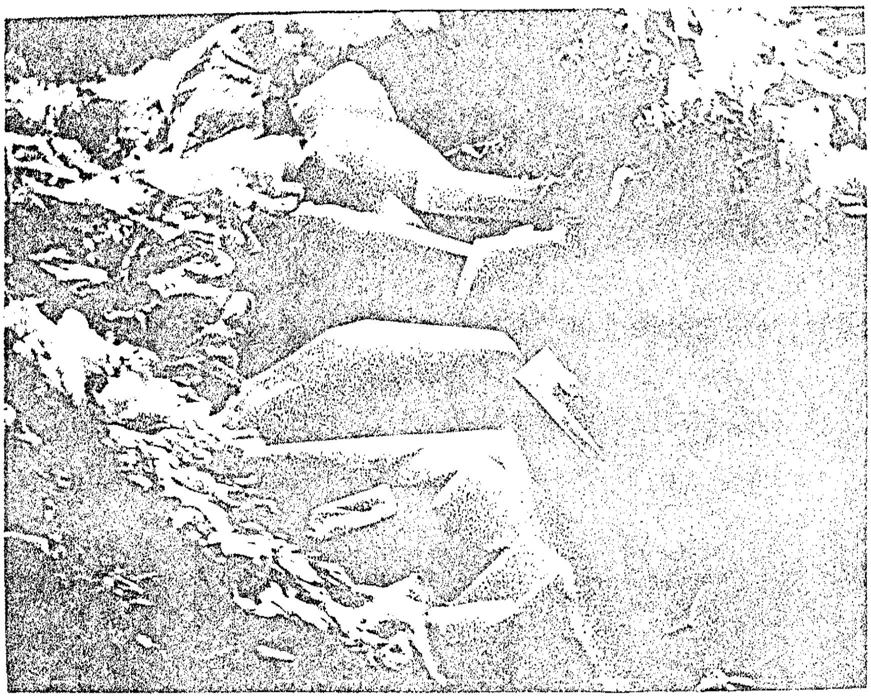

Figure 31. SEM photo of jumbled stacks of platy clinoptilolite crystals. Magnification 2,000x.

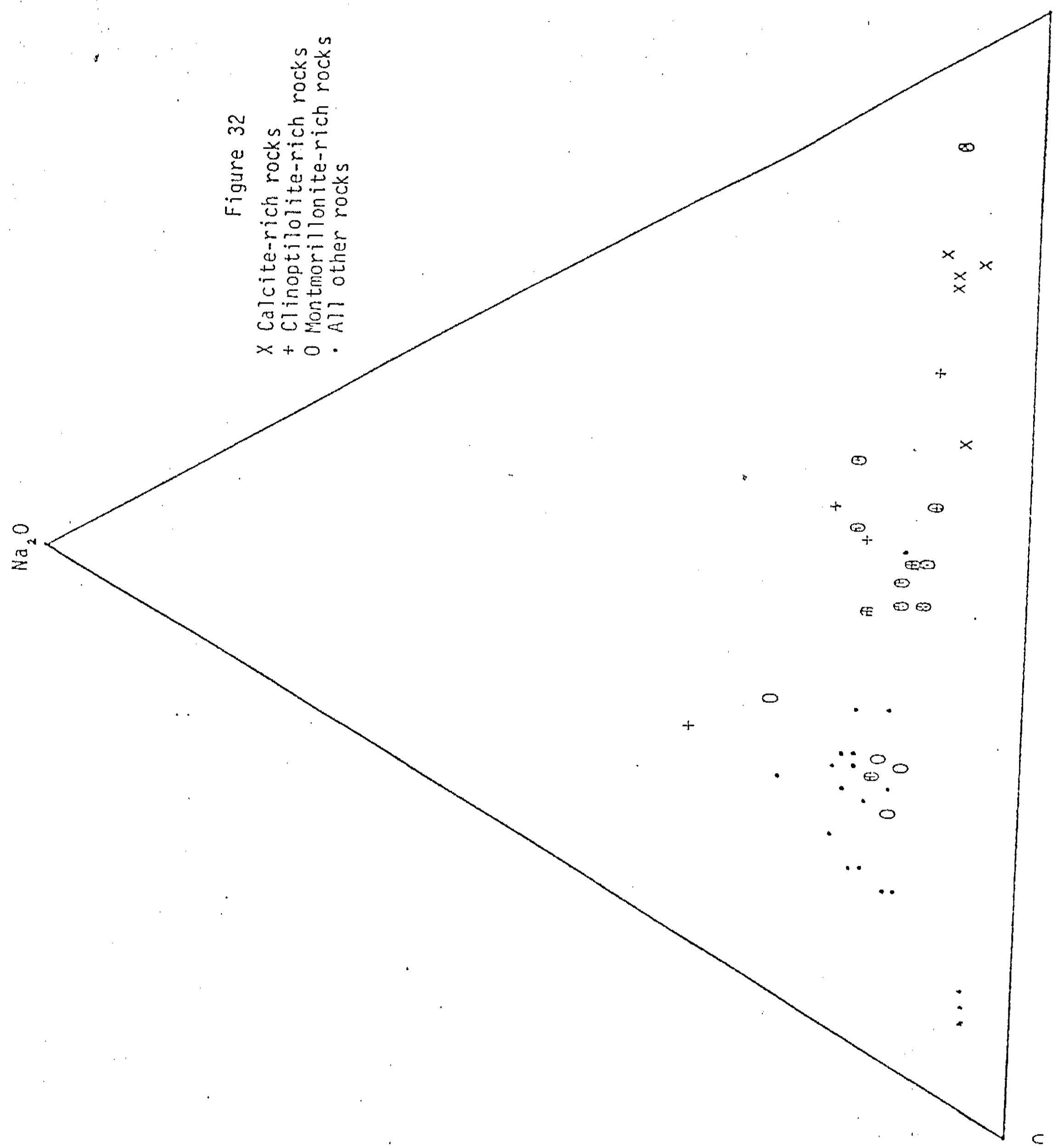
Na2O
X Calcite-rich rocks
+ Clinoptilolite-rich rocks
O Montmorillonite-rich rocks
· All other rocks

Figure 32

be traced as far laterally as the upper and lower sediments.

Gypsum-rich rocks of Reference Section 2 are 10 times the coefficient of variation for Na_2O for similar rocks of Reference Section 1. The coefficient of variation is also greater than Reference Section 1 for all oxides except Fe_2O_3. Reference Section 2 also showed higher standard deviations for all oxides and larger means for all oxides except K_2 and SiO_2.

Halite

Halite was never observed in X-ray diffraction or in petrographic studies. It was found during general SEM examinations of selected samples and occurs as both perfect cubes (Fig. 33) and nearly completely dissolved forms. Although clearly authigenic, the ease at which halite is mobilized and reprecipitated, and the fact that in none of the petrographic examinations were molds of former halite crystals observed, suggests that it is a post depositional secondary mineral.

Pyrite

Authigenic pyrite occurs as scattered groups of euhedral crystals ranging from 1 to 5um in length. As can be seen from Fig. 34, they are cubic and pyritohedral in form. Figures 35 and 36 show the iron and sulfur distributions, respectively for the pyrite.

Figure 33. SEM photo fo a perfect cube of halite. Magnification 1,000x.

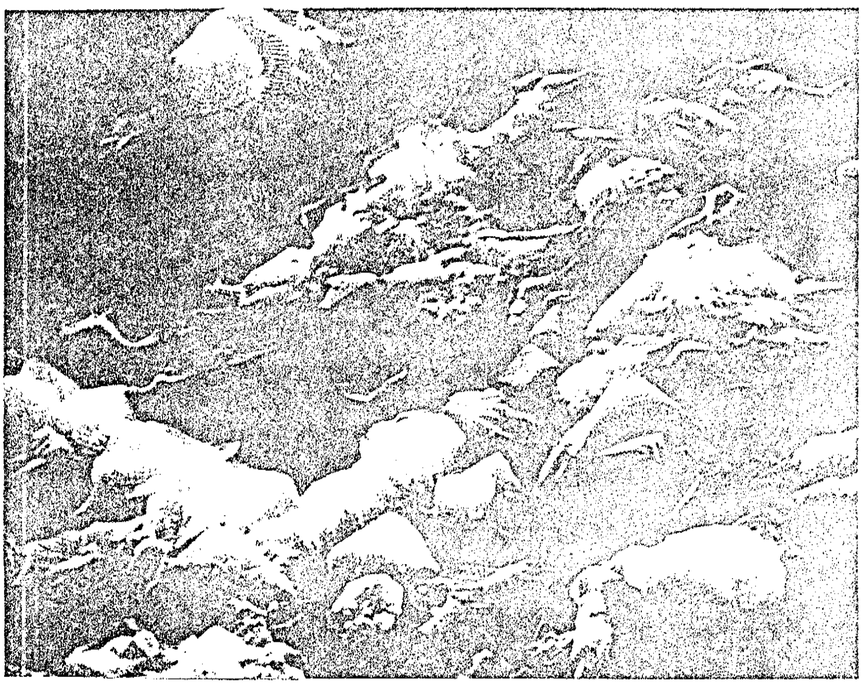

Figure 34. SEM photo of cubic and pyritohedral crystals of pyrite. The pyrite occurs primarily in the shales as disseminated crystals. Magnification 5,000x.

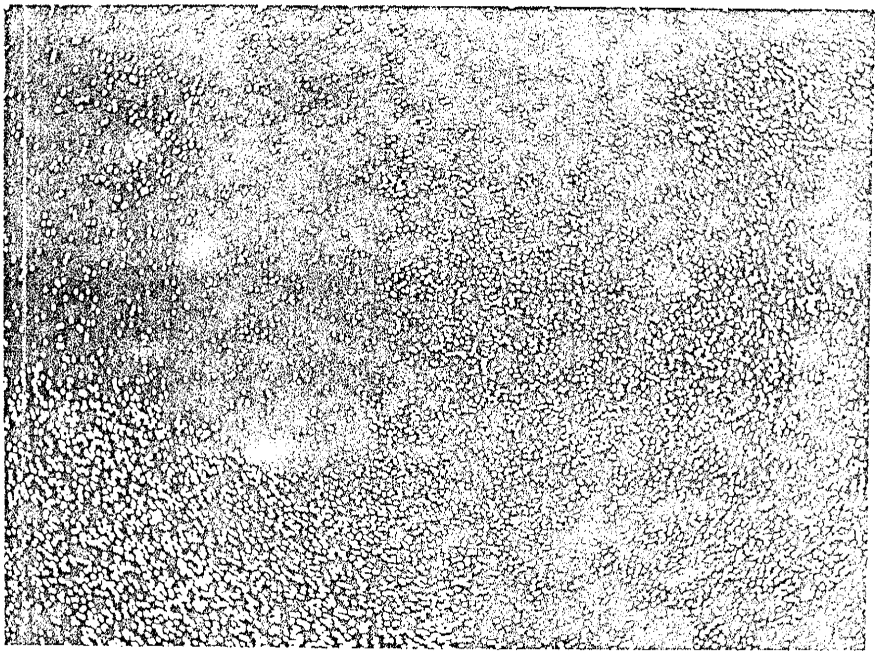

Figure 35. Elemental distribution of iron for Figure 34.

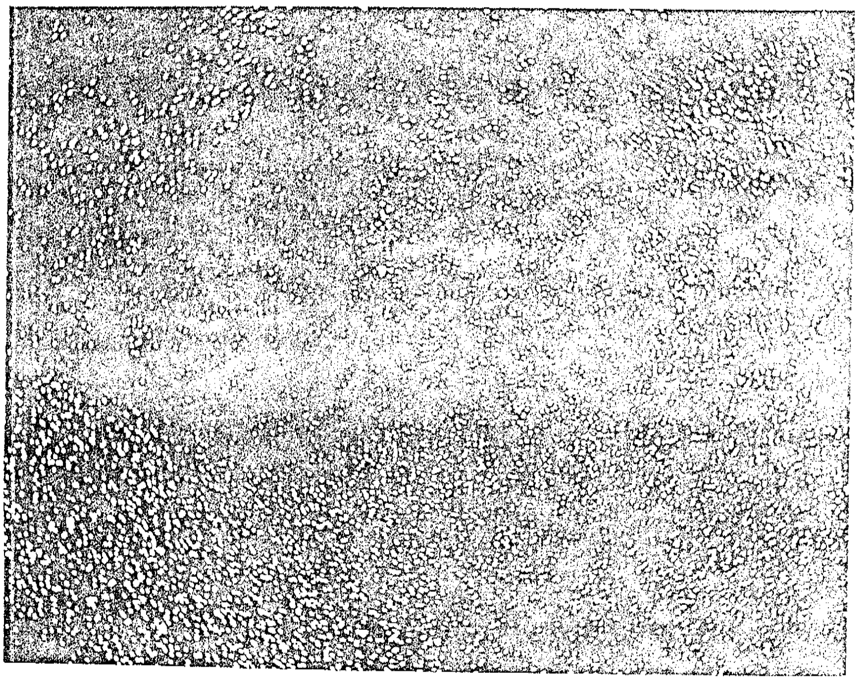

Figure 36. Elemental distribution of sulfur for Figure 34.

Quartz

Quartz is a common authigenic mineral in the Creede Formation. As determined by X-ray diffraction, it is associated wth all other authigenic minerals. Petrographic and SEM studies have confirmed the association of authigenic quartz with montmorillonite, clinoptilolite and analcime. Authigenic quartz was identified in every sample in which analcime occurred.

Quartz occurs in a variety of forms. Aggregates of anhedral, nearly equidimensional crystals (Fig. 37) were found with the individual crystals ranging from .40 to 20 um in diameter. The quartz also occurs as aggregates of fibers. SEM studies show authigenic quartz, identified by energy dispersive analysis and its euhedral, trigonal trapezohedral outline (Fig. 38), occurring as a void filling (Fig. 39) or covering of detrital grains (Fig. 40) rather than a replacement. Most of the quartz is chalcedonic based on its low index of refraction (less than 1.54).

Opal, because of its nondescript and isotropic character, was primarily identified by X-ray diffraction of bulk samples. It has characteristically broad peaks at 4.24A, 4.10A, 3.32A, 2.98A, and 2.50A d spacings. Opal was found only in one sample which was collected near a travertine orifice. It constitutes virtually 100% of the rock and is globular in form (Fig. 41).

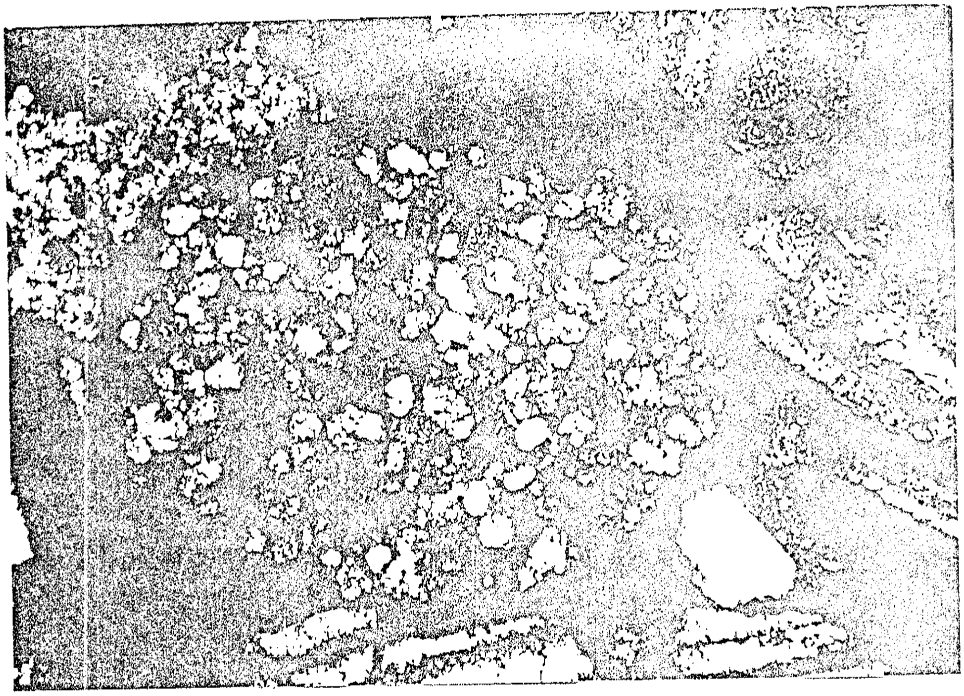

Figure 37. Thin-section photo (crossed nicols) of authigenic quartz.

Figure 38. SEM photo of trigonal trapezohedral crystals of quartz. This example appears to show authigenic quartz forming as a void filling rather than a replacement. Magnification 4,000x.

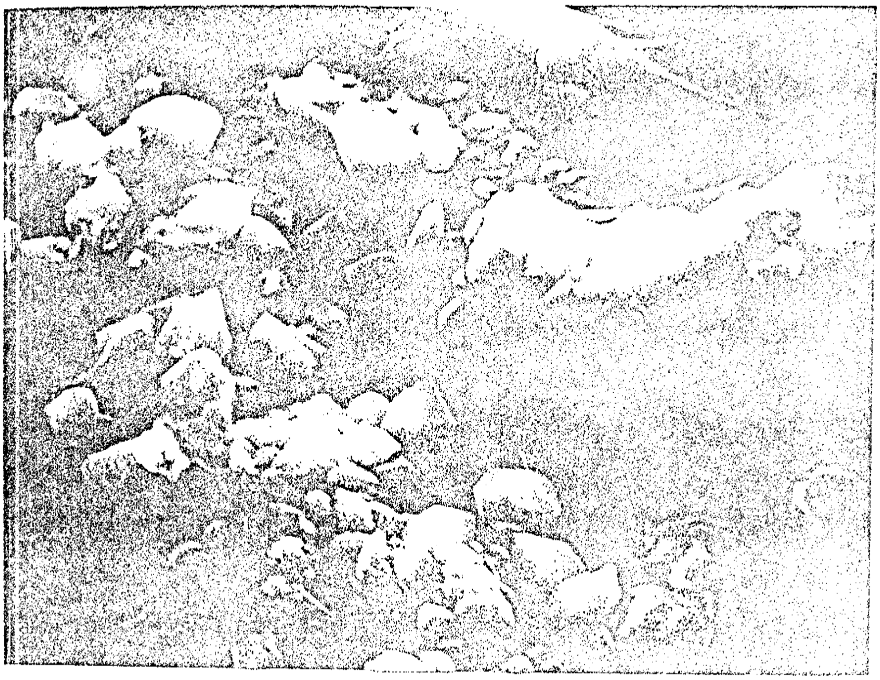

Figure 39. Authigenic quartz crystals lining a cavity. Magnification 3,400x.

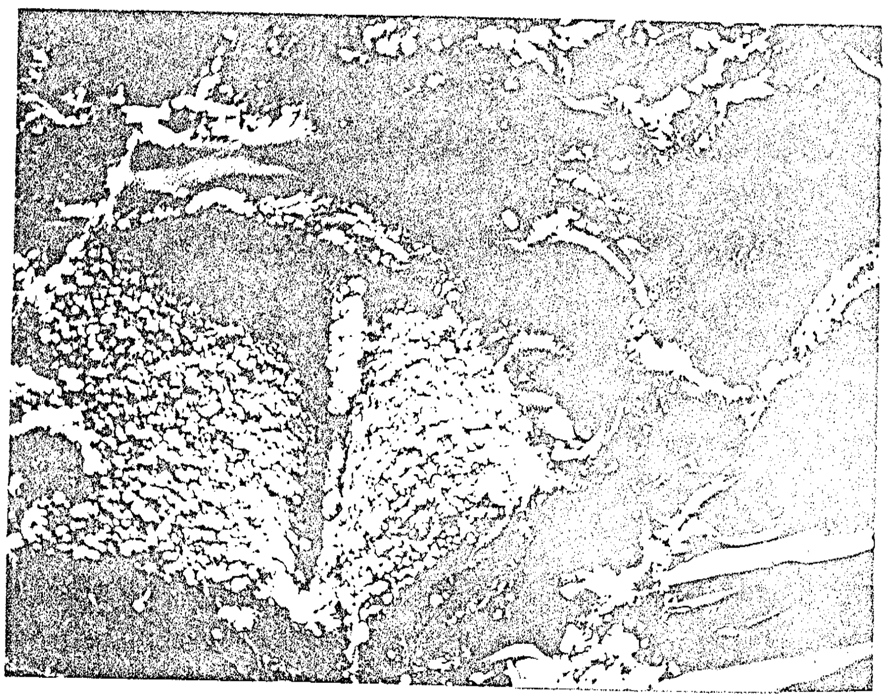

Figure 40. SEM photo showing authigenic quartz coating a detrital grain of feldspar. Magnification 500x.

Igneous Remnants

Igneous remnants are common in Creede sediments as both major and accessory minerals. The more common ones are: apatite, biotite, cristobalite, diopsidic-augite, hornblende, magnetite, plagioclase, and sanidine. The apatites are broken euhedral crystals common to all lithologies (Fig. 42). Biotite is found in virtually all sediments and undergoes little alteration. Only occassional oxidation around the rims of the grains is observed. Cristobolite was identified by diffraction techniques and thin-sections studies. It occurs as aggregates of small crystals, has a curved fracture, and low index of refraction. Hornblende and diopsidic-augite are most abundant in the arenites, and in some cases exceed 5% of the rock. Hornblende always exceeded diopsidic-augite in abundance, while both were usually partially to almost completely dissolved out of the rock. Plagioclase was found in all lithologies with the greatest percentage occurring in the arenites. The plagioclases were found as broken euhedra and were very fresh in appearance. All twinning was very sharp and distinct with no alteration observed except for minor corrosion and embayments. Approximately 10% of all plagioclases observed displayed very distinct zoning (Fig. 43). The An content ranged from 13 to 44% and averaged 24 percent. Sanidine, occurring as broken euhedral crystals, was found in all lithologies and was never the dominant detrital mineral. It never exceeded plagioclase in abundance. A few of the sanidine grains showed rims of sericite.

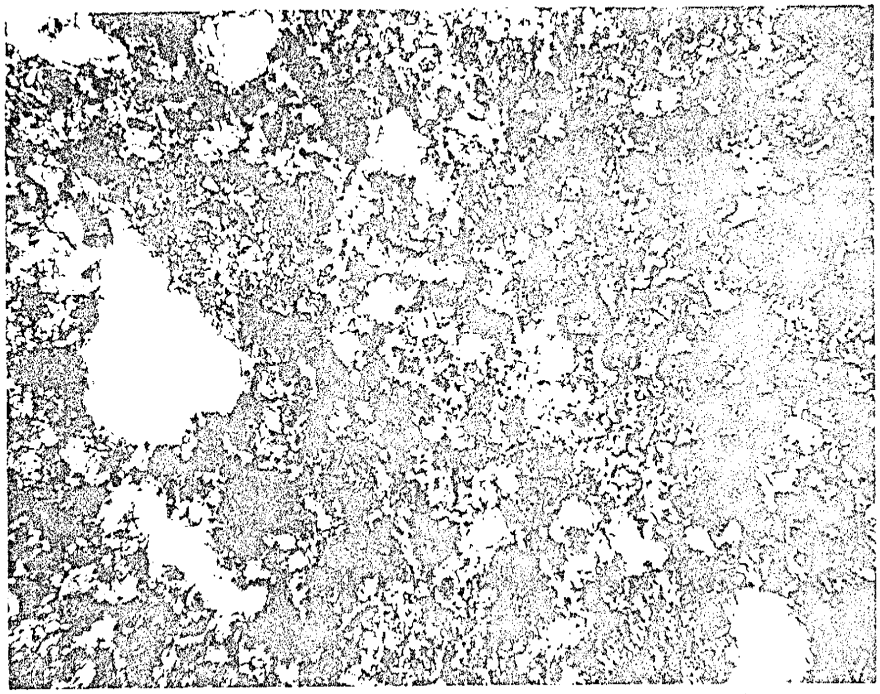

Figure 41. Thin-section photo (crossed nicols) of an opal-rich rock with the opal occurring as a globular form.

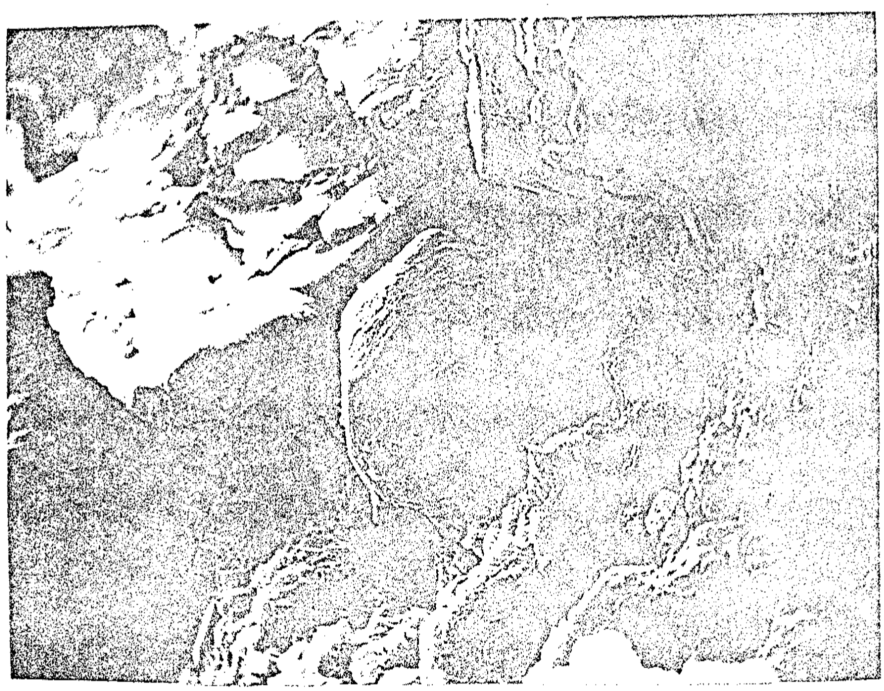

Figure 42. SEM photo of nearly euhedral crystal of apatite which is common to most lithologies. Magnification 950x.

V. DISCUSSION

Origin of the Zeolites

The formation and distribution of zeolites and associated authigenic minerals in sedimentary deposits is dependent upon the age and permeability of the sediments, temperature and pressure, pore-water chemistry, and composition of the host rock. Authigenic mineral assemblages in sedimentary rocks vary considerably as a function of age, regardless of burial depth or depositional environment (Hay, 1965). Figure 44 shows the variation in abundance of different zeolites as a function of age. As all sediments are coeval, this relationship does not apply.

Most zeolitic reactions require the addition of K, Na, and Ca ions and water. As zeolites were found in virtually all types of sediments, the permeability had no influence on zeolite distribution.

The total estimated thickness of the deposits is 732 m, which is equivalent to 190 bars and temperatures of 38 to 43 degrees C. assuming a normal geothermal gradient. For metamorphism to produce zeolites, it requires 240 to 1200 bars pressure and temperatures of 41 to 140 degrees C. (Hyndman, 1972). The less-hydrous calcic zeolites such as wairakite, scolecite, and laumontite are favored in such environments. The lack of these zeolites and the conditions necessary for metamorphic zeolites to occur removes temperature and pressure as an influencing factor.

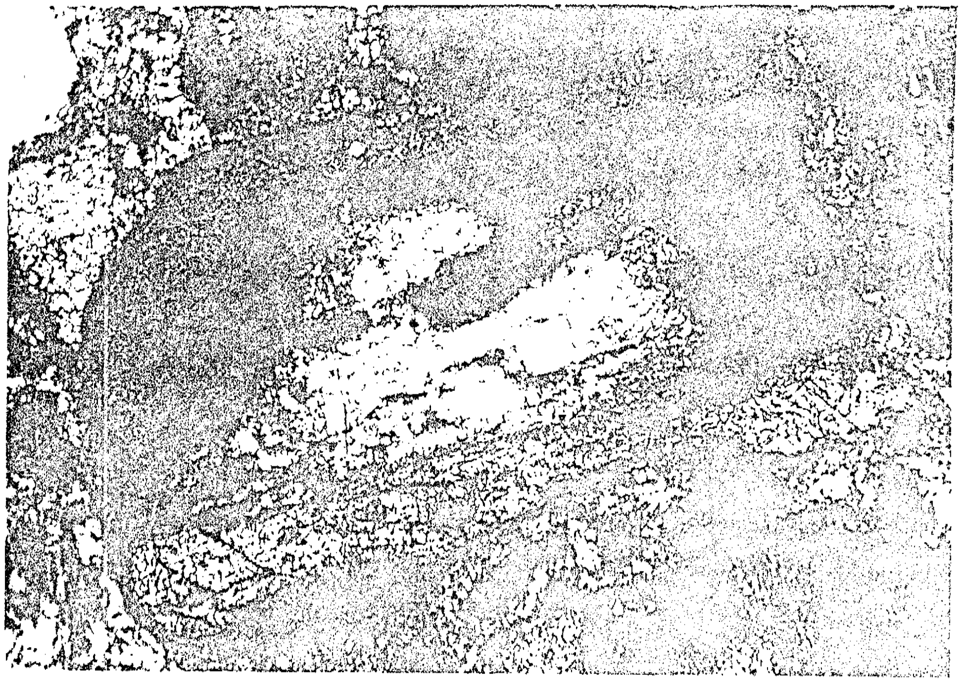

Figure 43. Thin-section photo (crossed nicols) showing a strongly zoned plagioclase grain.

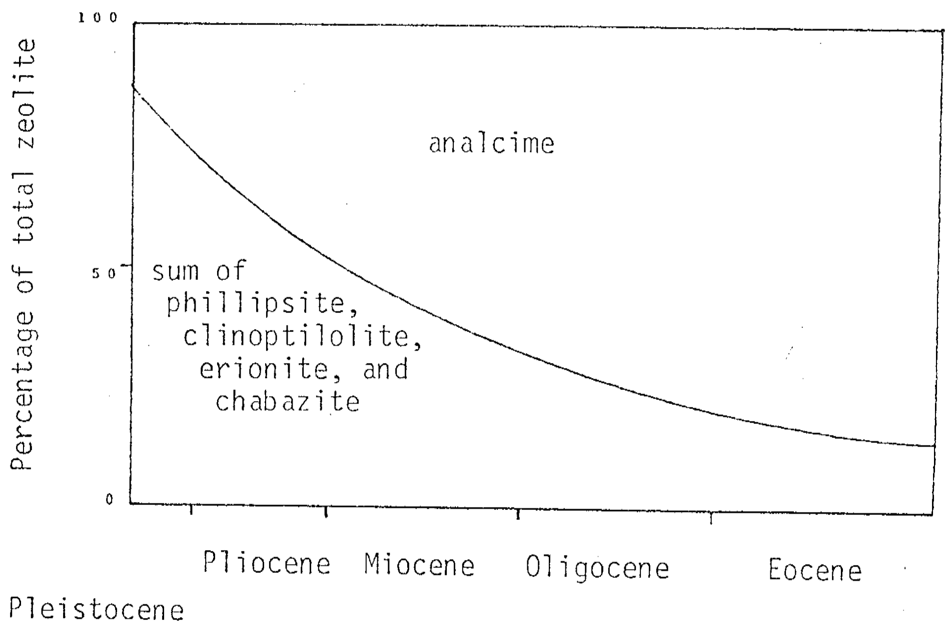

Figure 44. Schematic diagram showing the abundance of analcime relative to the sum of phillipsite, clinoptilolite, erionite, and chabazite as a function of age in Eocene to late Pleistocene silicic tuffs deposited in saline, alkaline lakes.

All sediments were derived from a common host rock, namely, Fisher Quartz Latite. As the composition of the solid phase present in the sediments is the same, the pore-water chemistry must be the determining parameter in zeolite genesis and distribution.

The documentation of zeolites and authigenic silicate minerals forming during diagenesis by reaction of volcanic glass with interstitial water is well established (Hay, 1966; Sheppard and Gude, 1968 and 1973; and Surdam and Parker, 1972) with the interstitial water originating as either meteoric water or connate water of a saline lake. Laboratory experiments indicate that the activity ratio of alkali ions to hydrogen ions and silica activity are the determining parameters of the pore water that governs which silicate mineral will form.

The initial action of the water is to exchange its hydrogen ions for sodium and potassium from the latitic glass surface, making the water alkaline and increasing the solubility of the glass. This process not only generates an alkaline fluid, but also acts as a self-accelerating process of dissolving the glass present (Mariner and Surdam, 1970). The silica-to-aluminum ratio decreases with the increasing alkalinity due to the fact that alumina activity increases faster than the silica activity. The zeolite mineralogy is postulated to be a function of the silica-to-aluminum relationship and pH. Initially, then, the $Na^+ + K^+/H^+$ ratio would be at its lowest value which would favor the formation of montmorillonite. Subsequent solution of the glass and/or the formation of montmorillonite by hydrolysis of the glass would cause an increase in pH and the alkali-to-hydrogen ratio. This change in the chemical environment would disfavor the formation of montmorillonite, and would instead be suitable for zeolite genesis. The species of zeolite(s) formed will be dependent upon the activity of H_2O and the Ca:Na + K and Si:Al ratios of the pore water. To form the clinoptilolite present in the sediments, the Si:Al and Ca:Na + K ratios must be high, while the H_2O activity must be low. The analcime, based on experimental studies, forms from alkalic, silicic zeolite precursors. Analcime formation is favored by a high Na:H ratio, and relatively low Si:Al ratio and H_2O activity in the pore fluids. The reaction of clinoptilolite to analcime is as follows:

$$\underset{\text{clinoptilolite}}{Na_2K_2CaAl_6Si_{30}O_{72}} \cdot 24H_2O + 4Na^+ + \longrightarrow \underset{\text{analcime}}{6NaAlSi_2O_6} \cdot H_2O$$

$$+ 18H_2O + 18SiO_2 + 2K^+ + Ca^{+2}$$

As can be seen from this reaction, there is a gain in sodium and a loss in H_2O, SiO_2, K, and Ca. Increased salinity should, therefore, be a determining parameter in analcime genesis. Increasing salinity may also lower H_2O activity favoring the transformation. Decreasing hydrogen ion concentration (increasing pH) would increase the Na+:H+ ratio and decrease the Si:Al ratio enhancing the probability of analcime formation. Both clinoptilolite and analcime may react to form potassium feldspar. The reactions for these transformations are as follows:

$$\underset{\text{clinoptilolite}}{Na_2K_2CaAl_6Si_{30}O_{72}} \cdot 24H_2O + 4K^+ \rightarrow \underset{\text{adularia}}{6KAlSi_3O_8} + 24H_2O + 12SiO_2 + Na^+ + Ca^{+2}$$

and $NaAlSi_2O_6 \cdot H_2O + SiO_2 + K^+ \rightarrow KAlSi_3O_8 + H_2O + Na^+$. Both reactions represent gains in potassium and losses in sodium and water. As no occurrence of adularia was reported, the potassium concentration must have been too low for the transition of zeolites to adularia. This also infers that the pH was too low since a high $K^+:H^+$ ratio also favors adularia crystallization. The absence of adularia could, therefore, by due to either the lack of potassium necessary for adularia formation and/or simply not finding outcrops in the basin which possess the necessary chemical parameters conducive to adularia genesis. The lack of potassium is probably due to its being retained in the unaltered detrital feldspars.

In summary, the trend of authigenic silicate mineral genesis is as follows (with increasing alkalinity):

glass --> montmorillonite or alkalic, silicic zeolites -->
analcime or adularia and analcime --> adularia

This same mineralogic transition is found to occur laterally within the lake sediments with the exception of adularia and was used to further subdivide the Creede Formation. The northwestern portion of the lacustrine facies is comprised of a fresh glass facies, a montmorillonite-clinoptilolite facies, and an analcime-clinoptilolite facies.

Synopsis of the Depositional Environment of Lake Creede

In order to interpret accurately the depositional environment of Lake Creede, hydrologic, sedimentary, biologic and structural features as well as authigenic minerals present must be examined. First and foremost is the correlation between water chemistry of the depositional environment and the authigenic minerals present. This transition of facies mentioned represents the change of fresh water to slightly saline to moderately saline water, respectively. This is the type of zonation one would expect in a closed basin lake. The outer perimeters of the lake would be fresh water due to streams and runoff from the caldera rim. As the center of the basin is approached, the alkalinity and salinity increases due to evaporation and concentration of alkalies from hot spring activity and alkalies from dissolved volcanic glass. The mudcracks indicate that at times only portions of the lake existed and were probably concentrated brines. By looking at the mineralogies of the columns (plates 1, 2, and 3), the stratigraphic relationship of each (Fig. 5), and block diagram 45, the diagenetic facies reflect this compositional variation in the lake. Reference Sections 3 and 4 should contain very small amounts of authigenic minerals; Section 1, authigenic minerals related to slightly alkaline, saline solutions; and Section 2 should contain authigenic minerals stable in a moderate saline, alkaline lake. As can be seen, this is indeed the exact sequence of authigenic minerals

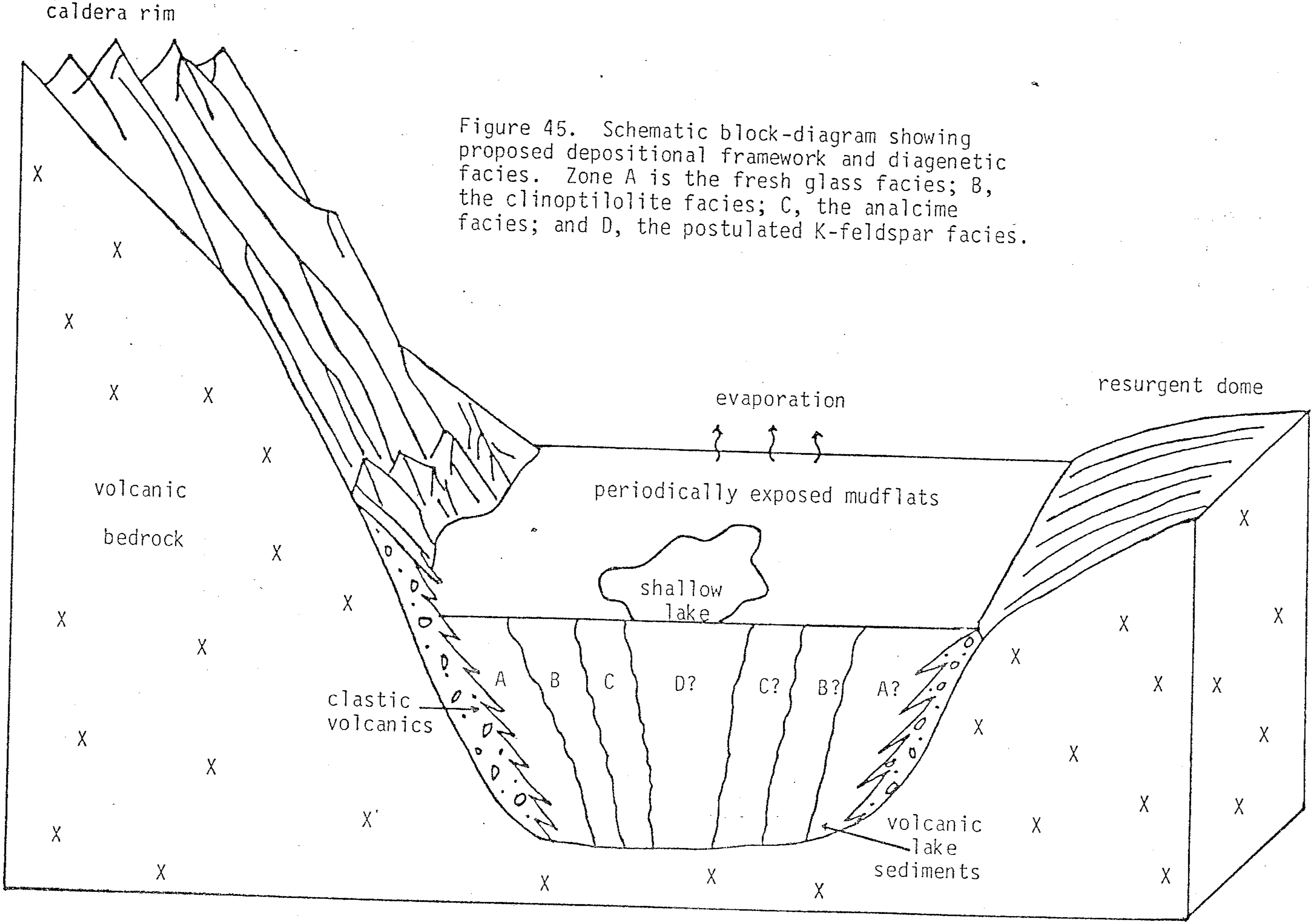

Figure 45. Schematic block-diagram showing proposed depositional framework and diagenetic facies. Zone A is the fresh glass facies; B, the clinoptilolite facies; C, the analcime facies; and D, the postulated K-feldspar facies.

found in the area studied. Reference Section 2 displays primary deposition of calcite which requires the solution to have a pH of 7.8 or higher, and analcime which also forms in high pH, moderately saline and alkaline environments. Reference Section 1 contains very abundant clinoptilolite and montmorillonite indicative of lower pH's and only slightly saline and alkaline conditions. The remaining two sections contained virtually no authigenic silicate minerals. This type of distribution is identical to other saline, alkaline lakes as reported by Sheppard and Gude (1968, 1969 and 1973), Surdam (1977), and Hay (1966). The well-preserved, original vitroclastic textures and sedimentary features in the tuffaceous sediments indicate that alteration probably occurred after burial. The pore waters retained the chemical signature of the lake water and reacted with the glass to form the present diagenetic facies.

Table 3 lists the normalized host rock, Fisher Quartz Latite, and various tuffs and authigenic silicate-rich rocks also normalized. Weight gain or loss as well as present gain or loss was determined by assuming Al_2O_3 constant (Krauskopf, 1967). By examining the percent gain or loss of oxides, the following was found. The montmorillonite-rich rocks lose iron, titanium, and sodium but gain silica, water and potassium. Therefore, as montmorillonite forms, the salinity should increase. This change in pore-water chemistry would then favor zeolite formation.

Table 3

Comparison of Fisher Quartz Latite to tuffs and authigenic silicate-rich rocks in the Creede Formation.

Oxide	Fisher Quartz Latite	R1 Clin Norm	R1 Clin Al corr	Weight change	Percent change
SiO2	61.76	62.96	83.53	21.77	35.25
Al2O3	16.00	12.06	16.00	0.00	0.00
CaO	4.93	2.94	3.90	-1.03	-20.89
K2O	3.23	2.88	3.82	0.59	18.27
MgO	1.95	1.30	1.72	-0.23	-11.79
TiO2	0.88	0.41	0.54	-0.34	-38.64
Fe2O3	6.15	2.91	3.86	-2.29	-37.24
Na2O	3.54	1.02	1.35	-2.19	-61.86
LOI	1.56	13.52	17.94	16.38	1050.00
Sum	100.00	100.00	132.67		

Oxide	Fisher Quartz Latite	R2 Clin Norm	R2 Clin Al corr	Weight change	Percent change
SiO2	61.76	57.27	65.36	3.60	5.83
Al2O3	16.00	14.02	16.00	0.00	0.00
CaO	4.93	2.58	2.94	-1.99	-40.37
K2O	3.23	3.09	3.53	0.30	9.29
MgO	1.95	2.10	2.40	0.45	23.08
TiO2	0.88	0.49	0.56	-0.32	-36.36
Fe2O3	6.15	2.90	3.31	-2.84	46.18
Na2O	3.54	1.95	2.23	-1.31	-37.01
LOI	1.56	15.60	17.80	16.24	1041.03
SUM	100.00	100.00	114.12		

Oxide	Fisher Quartz Latite	R1 Mont Norm	R1 Mont Al corr	Weight change	Percent change
SiO2	61.76	64.54	85.48	23.72	38.41
Al2O3	16.00	12.08	16.00	0.00	0.00
CaO	4.93	2.35	3.11	-1.82	-36.92
K2O	3.23	3.06	4.05	0.82	25.39
MgO	1.95	1.35	1.79	-0.16	-8.21
TiO2	0.88	0.40	0.53	-0.35	-39.77
Fe2O3	6.15	2.61	3.46	-2.69	-43.74
Na2O	3.54	0.87	1.15	-2.39	-67.51
LOI	1.56	12.74	16.87	15.31	981.41
SUM	100.00	100.00	132.45		

Oxide	Fisher Quartz Latite	R2 Mont Norm	R2 Mont Al corr	Weight change	Percent change
SiO2	61.76	58.87	73.19	11.43	18.51
Al2O3	16.00	12.87	16.00	0.00	0.00
CaO	4.93	4.15	5.16	0.23	4.67
K2O	3.23	3.14	3.90	0.67	20.74
MgO	1.95	1.90	2.36	0.41	21.03
TiO2	0.88	0.44	0.55	-0.33	-37.50
Fe2O3	6.15	2.96	3.68	-2.47	-40.16
Na2O	3.54	1.78	2.21	-1.33	-37.57
LOI	1.56	13.89	17.27	15.71	1007.05
SUM	100.00	100.00	124.32		

Oxide	Fisher Quartz Latite	R2 Anal Norm	R2 Anlm Al corr	Weight change	Percent change
SiO2	61.76	58.86	63.76	2.00	3.24
Al2O3	16.00	14.77	16.00	0.00	0.00
CaO	4.93	5.48	5.94	1.01	20.49
K2O	3.23	2.55	2.76	-0.47	-14.55
MgO	1.95	1.06	1.15	-0.08	-4.10
TiO2	0.88	0.55	0.60	-0.28	-31.82
Fe2O3	6.15	3.20	3.47	-2.68	-43.58
Na2O	3.54	3.75	4.06	0.52	14.69
LOI	1.56	9.78	10.59	9.03	578.85
SUM	100.00	100.00	108.33		

Oxide	Fisher Quartz Latite	R1 Tuff Norm	R1 Tuff Al corr	Weight change	Percent change
SiO2	61.76	64.00	87.14	25.38	27.66
Al2O3	16.00	11.75	16.00	0.00	0.00
CaO	4.93	2.11	2.87	-2.06	-41.78
K2O	3.23	2.71	3.69	0.46	14.24
MgO	1.95	1.03	1.87	-0.08	-4.10
TiO2	0.88	2.17	0.40	-0.48	-183.33
Fe2O3	6.15	0.29	2.95	-3.20	-52.03
Na2O	3.54	1.37	1.87	-1.67	-47.18
LOI	1.56	14.57	19.83	18.27	1171.15
SUM	100.00	100.00	136.16		

Clinoptilolite-rich rocks also lose sodium and titanium as well as calcium. Gains are in silica, potassium, and water. Clinoptilolite formation would further increase the salinity and alkalinity of the solution. The solution existing in the pore water would now be moderately alkaline and saline and should favor analcime crystallization. The analcime comparison in Table 3 displays only a minor gain in silica and water when compared to montmorillonite and clinoptilolite-rich rocks. The comparison also exhibits the only gain in sodium and loss in potassium. This agrees exactly with the above equation of clinoptilolite and sodium reacting to form analcime and losing water, silica, and potassium. Thus, the comparison of the authigenic silica-rich rocks also reflects the chemical zonation of ancient Lake Creede which was preserved in the pore water.

Structural conditions also favor the formation of a saline, alkaline lake. The resurgent doming produced a closed basin surrounded by the caldera rim that trapped precipitation. The Creede paleoflora suggests a montane environment, with a cool temperate climate and a moderate seasonal rainfall on the higher slopes and a warmer, drier climate on the lower slopes (Steven and Eaton, 1975). Given these data, the basin floor should have consisted of a shallow body of water that periodically expanded and then shrank to a saline, alkaline lake. Both sedimentary features and authigenic mineral distributions seem to confirm this.

The sediments show many features indicative of deposition in shallow water or under playa conditions. The most obvious of these features are the ripple marks and mudcracks which are extensive throughout the facies. The presence of uniform textured arenites and the dominance of shale over all other lithologies are also suggestive of lake deposits.

Having established that the deposits were lacustrine and the structural and climatic conditions were favorable for a saline, alkaline lake, biologic information must be examined next in order to determine the chemical characteristics of the lake. Although the Creede Formation contains abundant paleoflora, it is devoid of any evidence of aquatic life. This suggests either a penesaline or hypersaline environment. Since the most obvious evidence of a saline, alkaline depositional environment is lacking, bedded saline minerals, it is inferred that only penesaline and alkaline conditions prevailed. Disseminated crystal molds resembling gaylussite or nacholite occur in the shales and siltstones and suggest saline conditions during deposition.

Although all evidence points towards a closed system for zeolite genesis (saline, alkaline lake), this does not preclude the validity of some other type of system. As sampling was taken only from available outcrops in the area, there is the possibility that key authigenic mineral assemblages which would favor some other system were present but unobtainable in surface exposures.

Analcime-clinoptilolite-bearing units between sections 1 and 2 and clinoptilolite-montmorillonite units between sections 1 and 3 at approximately the same elevations would favor an open system for zeolite genesis.

Hot spring activity, as mentioned by Steven and Van Loenen, 1971, and the possiblility of circulating hydrothermal fluids (Bethke and Rye, 1979 and Steven and Eaton, 1975) could have also played an important role in zeolite distribution as well as reaction kinetics. Only by a more detailed analysis of these sediments, possibly by coring selected areas of the formation, can the authigenic mineral distribution to a specific hydrologic model be assigned.

Summary and Conclusions

The Creede Formation consists of an upper fluviate and a lower lacustrine facies. The latter can be subdivided into a fresh glass facies, a clinoptilolite-montmorillonite facies, and an analcime-clinoptilolite facies. From the biologic and sedimentary features present, and diagenetic distribution, it is inferred that the paleodepositional chemical environment of the lake was saline and alkaline. The chemical characteristics and zonation of its waters were retained after deposition in the pore waters. It was this variation in pore-water chemistry which was responsible for the diagenetic facies present.

APPENDIX I

COMPILATION CHART OF REFERENCE SECTION 1

Measured at a vertical exposure along the Rio Grande River NW1/4, SW1/4, NE1/4, section 16, T41N, R1W, Creede quadrangle.

Elevation in Meters	Lithologic Unit	Sample #	Thickness in Meters
Base of section is not exposed.			
2657.9	siltstone	1	0.61
2658.5	siltstone	2	2.10
2660.6	siltstone	3	0.91
2661.5	siltstone	4	1.20
2662.0	conglomerate	5	13.10
2675.1	arenite	6	3.80
2678.9	conglomerate	7	0.15
2679.0	shale	8	0.91
2680.0	arenite	9	0.08
2680.1	shale	10	0.66
2680.7	arenite	11	0.15
2680.8	siltstone	12A	4.27
2685.1	tuff	12B	3.35
2688.5	tuff	12C	3.81
2692.3	conglomerate	13	0.13
2692.4	shale	14	0.46
2692.9	shale	15	0.76
2693.6	siltstone	16A	3.48
2697.1	siltstone	16B	2.13
2699.3	shale	17	1.68
2700.9	shale	18A	3.35
2704.3	shale	18B	0.61
2704.9	siltstone	19	1.52
2706.4	conglomerate	20	0.10
2706.5	tuff	21	1.68
2708.2	conglomerate	22	0.46
2708.6	shale	23	1.52
2710.2	arenite	24	0.30
2710.5	shale	25	0.91
2711.4	conglomerate	26	0.46
2711.8	arenite	24	0.15
2712.0	conglomerate	26	0.61
2712.6	siltstone	27A	2.13
2714.7	siltstone	27B	2.13
2716.9	shale	27C	2.13
2719.0	shale	27D	1.98
2721.0	shale	27E	0.61
2721.6	tuff	28A	1.52
2723.1	tuff	28B	3.35
2726.5	shale	28C	1.83
2728.3	shale	28D	0.61

2728.9	arenite	28E	0.61
2729.5	conglomerate	29	0.30
2729.8	shale	30A	1.83
2731.7	siltstone	30B	1.83
2733.5	arenite	30C	1.83
2735.3	siltstone	30D	1.83
2737.1	siltstone	31	1.83
2739.0	siltstone	32	2.13
2741.1	siltstone	33	2.13
2743.2	top of column eroded.		

COMPILATION CHART OF REFERENCE SECTION 2

Measured at a vertical exposure along the Rio Grande River NW1/4, SE1/4, NW1/4, section 10, T41N, R1W, Creede quadrangle.

Elevation in Meters	Lithologic Unit	Sample #	Thickness in Meters
Base of section is not exposed.			
2633.5	alluvium	-	1.68
2635.2	conglomerate	1	0.61
2635.8	arenite	2	0.20
2636.0	conglomerate	1	0.20
2636.2	shale	3	0.15
2636.3	conglomerate	1	0.12
2636.5	siltstone	4	0.19
2636.7	conglomerate	1	0.20
2636.9	siltstone	5	0.15
2637.0	conglomerate	6	0.37
2637.4	shale	7	0.05
2637.4	conglomerate	6	0.20
2637.6	shale	8	0.08
2637.7	conglomerate	6	0.11
2637.8	shale	9	0.17
2638.0	arenite	10	0.21
2638.2	shale	11	0.62
2638.8	arenite	12	0.15
2639.0	shale	13	0.15
2639.1	limestone	14	0.06
2639.2	shale	15	0.24
2639.4	limestone	14	0.10
2639.5	shale	16	2.80
2642.3	arenite	12	0.05
2642.4	tuff	17	1.04
2643.4	arenite	12	0.05
2643.5	shale	18	2.90
2646.4	arenite	12	0.05
2646.4	shale	19	1.98

2648.4	arenite	20	0.76
2649.2	shale	21	1.07
2650.3	arenite	20	3.00
2653.3	shale	22	1.37
2654.6	arenite	20	0.30
2654.9	shale	23	1.89
2656.8	conglomerate	24	1.22
2658.0	arenite	25	1.10
2659.1	conglomerate	24	1.52
2660.7	siltstone	26	1.01
2661.7	conglomerate	24	0.61
2662.3	siltstone	27	3.30
2665.6	conglomerate	28	0.66
2666.2	siltstone	29	0.22
2666.5	conglomerate	28	0.82
2667.3	shale	30	1.30
2668.6	conglomerate	28	0.05
2668.6	shale	31	0.98
2669.6	conglomerate	28	0.18
2669.8	shale	32	0.95
2670.7	shale	33	0.70
2671.4	limestone	34	0.10
2671.5	siltstone	35	2.56
2674.1	arenite	36	1.66
2675.8	shale	37A	0.61
2676.4	shale	37B	1.52
2677.9	tuff	37BT	0.61
2678.5	shale	37C	0.91
2679.4	shale	37D	2.47
2681.9	conglomerate	38	0.61
2682.5	shale	39	3.05
2685.5	conglomerate	38	2.29
2687.8	shale	40	1.22
2689.0	conglomerate	38	0.46
2689.5	shale	41A	2.44
2691.9	shale	41B	2.90
2694.8	arenite	42	0.15
2695.0	siltstone	43	5.49
2700.5	top of column eroded.		

COMPILATION CHART OF REFERENCE SECTION 3

Measured at an outcrop located at SE1/4, NW1/4 SE1/4, section 9, T41N, R1W, Creede quadrangle.

Elevation in Meters	Lithologic Unit	Sample #	Thickness in Meters
Base of section is not exposed.			
2735.6	shale	1	1.68
2737.3	arenite	2	0.10
2737.4	shale	3	1.68
2739.0	arenite	4	1.68
2740.7	shale	5	1.68
2742.4	arenite	6	1.22
2743.6	shale	7	1.22
2744.8	siltstone	8	0.15
2745.0	conglomerate	9	0.15
2745.1	top of column not exposed.		

COMPILATION CHART OF REFERENCE SECTION 4

Measured at an outcrop located at NE1/4, NW1/4, SE1/4, section 9, T41N, R1W, Creede quadrangle.

Elevation in Meters	Lithologic Unit	Sample #	Thickness in Meters
Base of section is not exposed.			
2773.7	shale	1	1.68
2775.4	shale	2	1.68
2777.0	tuff	3	0.91
2778.0	shale	4	1.68
2779.6	siltstone	5	1.68
2781.3	siltstone	6	0.91
2782.2	tuff	7	0.61
2782.8	siltstone	8	1.83
2784.7	siltstone	9	1.83
2786.5	tuff	10	1.52
2788.0	shale	11	1.52
2789.5	shale	12	1.83
2791.4	shale	13	2.44
2793.8	shale	14	1.83
2795.6	siltstone	15	1.83
2797.5	siltstone	16	1.83
2799.3	shale	17	1.83
2801.1	shale	18	2.44
2803.6	shale	19	3.05
2806.6	shale	20	2.13
2808.7	top of column eroded.		

APPENDIX II

SEMI-QUANTITATIVE MINERALOGICAL COMPOSITION OF LACUSTRINE SEDIMENTS FROM THE CREEDE FORMATION, MINERAL COUNTY, COLORADO

Estimated from X-ray diffractometer patterns of bulk samples: O, abundant, more than 50%; O, 10 to 50%; X, trace to 10%; –, looked for, but not found.

Also looked for, but not found were: adularia, celadonite, chabazite, erionite, mordenite, and phillipsite.

Reference Section 1

Sample No.	Glass	Crstb	Clay	Clin	Anlcm	Gyp	Qtz	Cal	Feld	Biot	Horn
1	–	–	X	–	–	X	●	–	X	X	–
2	–	–	X	–	–	X	O	–	O	X	X
3	X	–	–	–	–	X	O	O	O	X	–
4	X	–	–	–	–	X	●	–	O	X	–
5	–	–	X	–	–	X	O	–	O	X	–
6A	X	–	–	–	–	O	O	–	O	X	–
6B	X	–	–	–	–	X	O	O	X	X	–
7	–	–	O	O	–	X	O	–	O	X	X
8	X	X	–	–	–	X	O	–	O	X	–
9	X	–	–	–	–	X	O	O	O	X	–
10	X	–	–	–	–	X	●	–	O	X	–
11	X	X	–	–	–	X	O	O	O	X	–
12A	–	–	X	X	–	X	O	–	X	X	X
12B	–	–	O	O	–	–	O	–	X	X	–
12C	–	–	X	O	–	X	●	–	X	X	–
13	–	–	X	O	–	–	O	–	O	X	–
14	–	–	O	O	–	–	O	–	O	X	–
15	–	–	O	O	–	–	O	–	O	X	X
16A	–	–	–	X	–	–	●	–	X	X	X
16B	–	–	X	–	–	X	●	–	O	X	–
17	–	–	–	X	–	–	●	–	O	X	–
18	–	–	X	O	–	–	O	X	O	X	–
19	–	–	X	O	–	–	●	–	X	X	–
20	–	–	X	X	–	X	X	●	X	X	X
21	–	–	O	O	–	–	O	–	X	X	–
22	–	–	O	O	–	–	O	–	O	X	X
23	–	–	X	O	–	–	O	–	O	X	X
24	–	–	X	–	–	X	X	O	O	X	X
25	–	–	X	O	–	–	O	–	O	X	X
26	–	–	X	X	–	X	X	O	O	X	–
27A	–	–	O	X	–	–	●	–	X	X	X
27B	–	–	X	O	–	–	●	–	O	X	–
27C	–	–	–	–	–	–	O	O	O	X	–

Sample No.	Glass	Crstb	Clay	Clin	Anlcm	Gyp	Qtz	Cal	Feld	Biot	Horn
27D	-	-	X	-	-	-	●	-	X	X	-
27E	-	-	X	-	-	-	●	-	X	X	-
28A	-	-	O	●	-	-	O	-	X	X	-
28B	-	-	O	●	-	-	O	-	X	X	-
28C	-	-	O	O	-	-	●	-	X	X	-
28D	-	-	O	O	-	-	O	-	O	X	-
28E	-	X	X	O	-	-	O	X	X	X	X
29	-	-	-	X	-	-	X	O	O	X	-
30A	-	-	X	X	-	-	●	-	X	X	-
30B	-	-	O	O	-	-	O	-	O	X	X
30C	-	-	X	X	-	-	O	-	O	X	X
30D	-	-	X	O	-	-	O	-	X	X	X
31	-	-	-	X	-	-	●	X	X	X	-
32	-	-	-	X	-	-	●	-	X	X	-
33	-	X	X	X	-	-	O	-	X	X	-

Reference Section 2

Sample No.	Glass	Crst	Clay	Clin	Anlcm	Gyp	Qtz	Cal	Feld	Biot	Horn
1	-	-	X	-	-	X	O	-	O	X	X
2	-	-	X	X	-	O	X	-	O	O	X
3	-	-	X	X	-	-	●	-	X	X	-
4	-	-	O	O	-	O	O	-	O	O	X
5	-	-	O	O	-	-	O	-	O	O	X
6	-	-	X	X	-	X	O	-	O	X	-
7	-	-	X	X	-	X	●	-	X	X	X
8	-	-	X	X	-	X	O	-	O	X	X
9	-	-	X	X	-	-	●	-	X	X	-
10	-	X	-	-	O	X	O	O	O	O	X
11	-	-	X	O	-	-	O	-	X	O	X
12	-	-	-	-	O	O	O	-	O	X	X
13	-	-	X	X	-	X	●	-	X	X	-
14	-	-	-	-	X	X	O	O	X	X	-
15	-	-	O	O	-	X	O	-	X	X	X
16	-	-	-	X	-	-	O	-	O	X	-
17	-	-	-	X	-	O	●	-	X	X	-
18	-	-	-	-	-	X	●	-	X	X	-
19	-	-	-	-	-	X	X	●	-	-	X
20	-	-	-	X	-	X	O	O	O	X	X
21	-	-	-	X	-	-	●	-	X	X	-
22	-	-	-	X	-	-	●	-	X	X	-
23	-	-	-	X	-	-	●	-	X	X	X
24	-	-	-	-	O	O	O	X	O	X	X
25	-	-	-	-	-	X	●	-	O	X	-
26	-	-	-	X	-	-	●	-	X	X	-

Sample No.	Glass	Crst	Clay	Clin	Anlcm	Gyp	Qtz	Cal	Feld	Biot	Horn
27	-	-	X	X	-	-	●	-	O	X	-
28	-	-	-	X	-	X	O	-	O	X	X
29	-	-	-	O	-	X	O	-	O	X	X
30	-	-	X	X	-	-	O	-	O	X	X
31	-	-	X	X	-	X	O	-	O	X	X
32	-	-	-	X	-	X	●	-	O	X	X
33	-	-	-	-	-	-	●	-	X	X	-
34	-	-	X	X	-	X	O	O	O	X	-
35	-	-	X	X	-	X	●	-	O	X	-
36	-	-	-	-	O	O	O	-	O	X	X
37A	-	-	-	-	-	-	●	-	O	X	-
37B	-	-	-	-	-	X	O	O	X	X	-
37BT	-	-	-	X	-	-	●	-	X	X	-
37C	-	-	-	X	-	-	O	O	X	X	-
37D	-	-	X	X	-	-	O	O	X	X	-
38	-	-	X	-	-	X	O	O	O	X	X
39	-	-	-	X	-	-	●	-	O	X	-
40	-	-	-	X	-	-	O	-	O	X	-
41A	-	-	-	X	-	-	●	-	O	X	X
41B	-	-	O	O	-	-	O	-	O	X	X
42	-	-	-	X	-	-	O	O	O	X	X
43	-	-	-	X	-	-	●	-	O	X	-

Reference Section 3

Sample No.	Glass	Crstb	Clay	Clin	Anlcm	Gyp	Qtz	Cal	Feld	Biot	Horn
1	O	-	X	-	-	-	●	-	O	X	-
2	O	-	-	-	-	-	O	-	O	X	-
3	O	-	-	-	-	-	●	-	O	X	-
4	O	-	-	-	-	-	O	-	O	X	-
5	O	-	-	-	-	-	O	-	O	X	-
6	O	-	-	-	-	-	O	-	O	X	-
7	O	-	X	-	-	-	O	-	O	X	-
8	O	-	X	-	-	-	O	O	O	X	-
9	O	-	-	-	-	-	O	-	O	X	-

Reference Section 4

Sample No.	Glass	Crstb	Clay	Clin	Anlcm	Gyp	Qtz	Cal	Feld	Biot	Horn
1	O	-	-	-	-	-	O	O	O	X	-
2	O	-	-	-	-	-	O	O	X	X	-
3	●	-	-	-	-	-	O	-	X	X	-
4	O	-	X	-	-	-	O	-	O	X	-
5	O	-	-	-	-	-	O	-	O	X	-
6	O	-	-	-	-	-	O	-	O	X	-
7	O	-	-	-	-	-	O	-	X	X	-
8	O	-	-	-	-	-	●	-	X	X	-
9	O	-	-	-	-	-	●	-	X	X	-
10	●	-	-	-	-	-	O	-	X	X	-
11	O	-	-	-	-	-	O	O	X	X	-
12	O	-	-	-	-	-	O	O	X	X	-
13	O	-	-	-	-	-	●	-	X	X	-
14	O	-	-	-	-	-	●	-	X	X	-
15	O	-	-	-	-	-	O	-	O	X	-
16	O	-	-	-	-	-	●	O	X	X	-
17	O	-	-	-	-	-	●	-	X	X	-
18	O	-	-	-	-	-	●	-	X	X	-
19	O	-	-	-	-	-	●	-	X	X	-
20	O	-	-	-	-	-	●	-	X	X	-

APPENDIX III

APPENDIX III

Accuracy of Energy Dispersive Analysis

The following charts represent only semi-quantitative abundances of the elements shown above the peaks. This is primarily because of instrumentation, but is also affected by the irregular specimen surfaces and low absorption coefficients of the lighter elements (sodium, magnesium, etc.). The gold and palladium peaks present are due to the coating used on the specimens. The vertical axis represents counts per second and the horizontal axis KeV. The energy dispersive unit used in this study was manufactured by Ortec.

EDAX of Figure 19

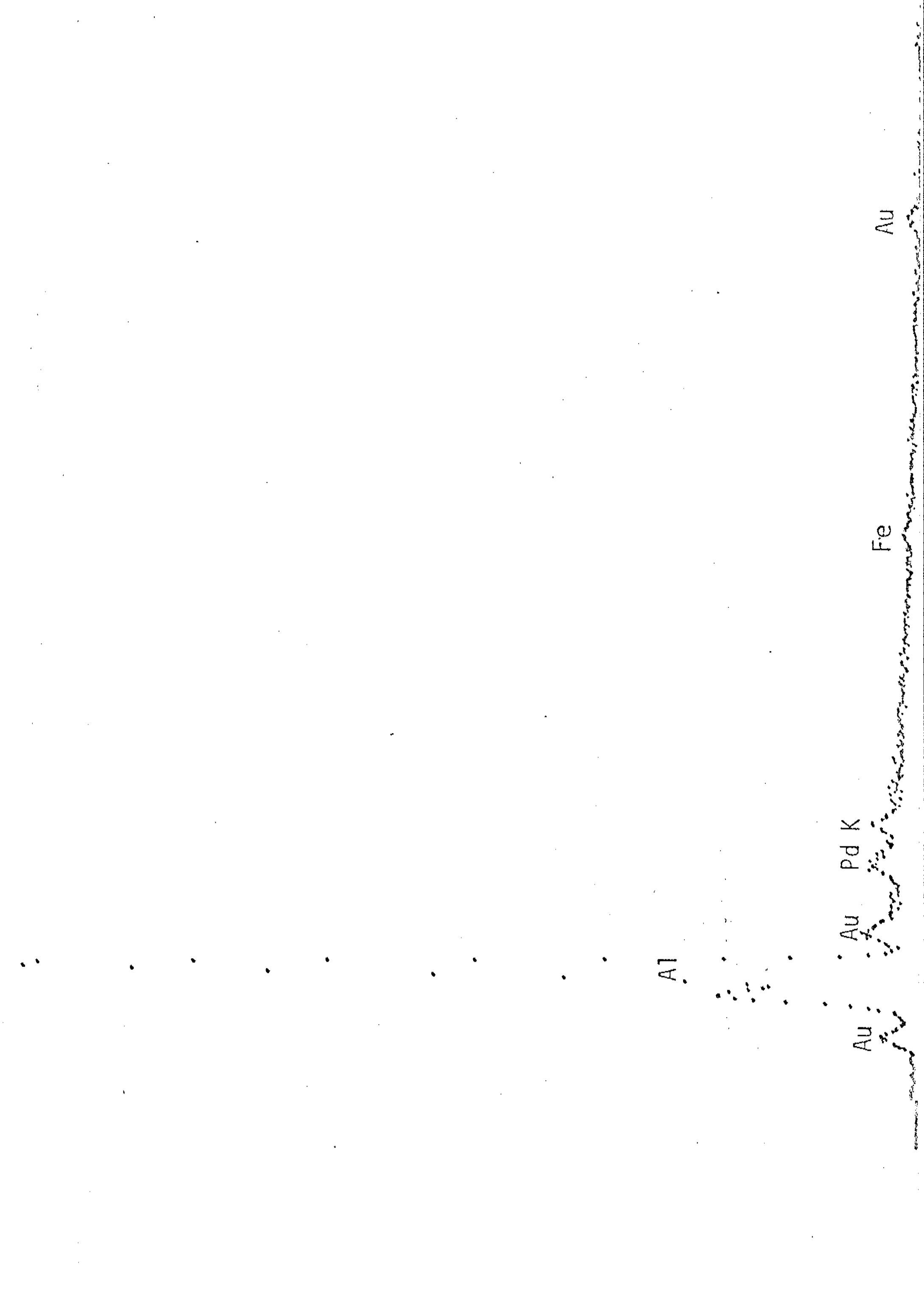

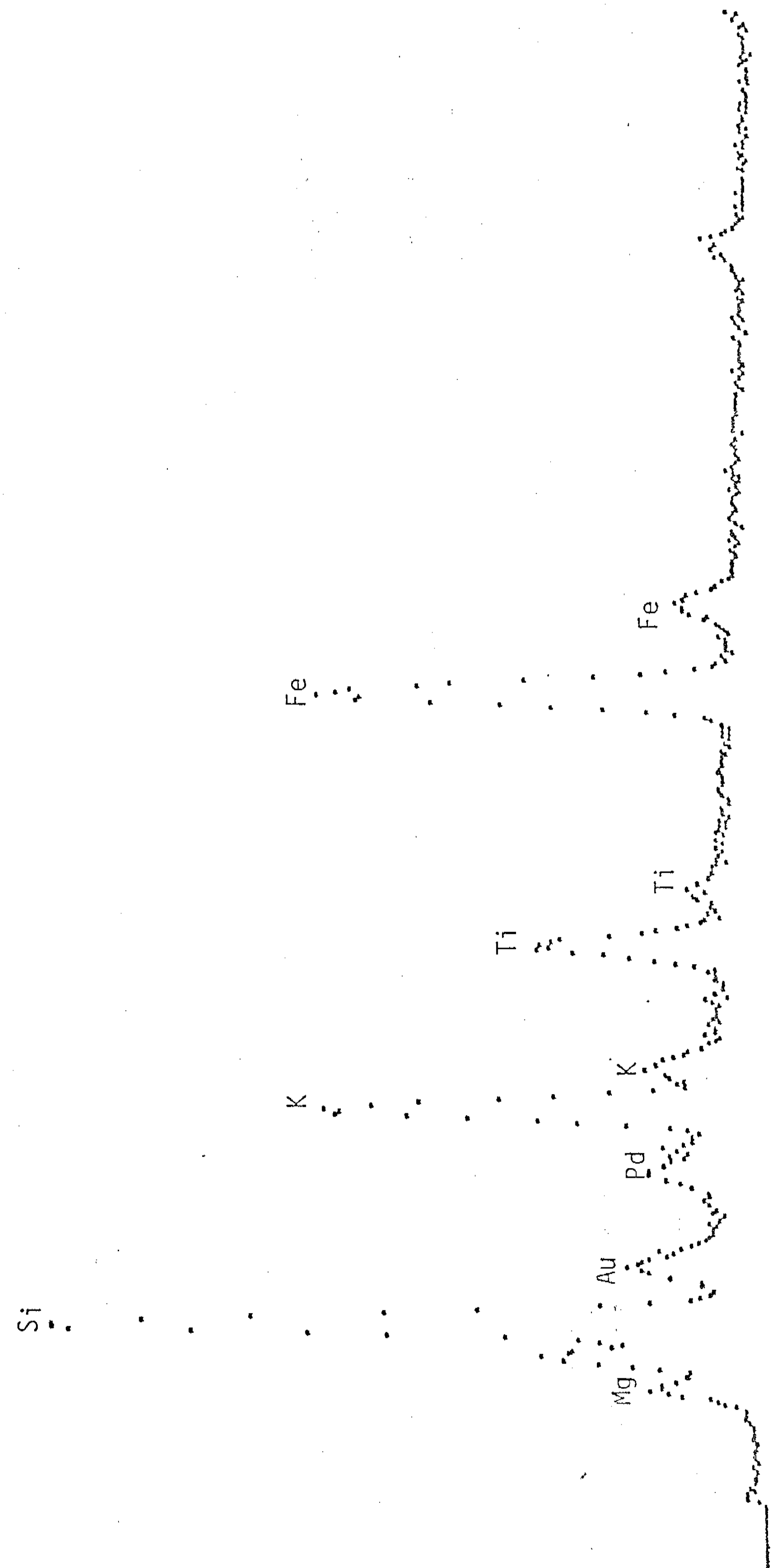

EDAX of Figure 24

EDAX of Figure 28

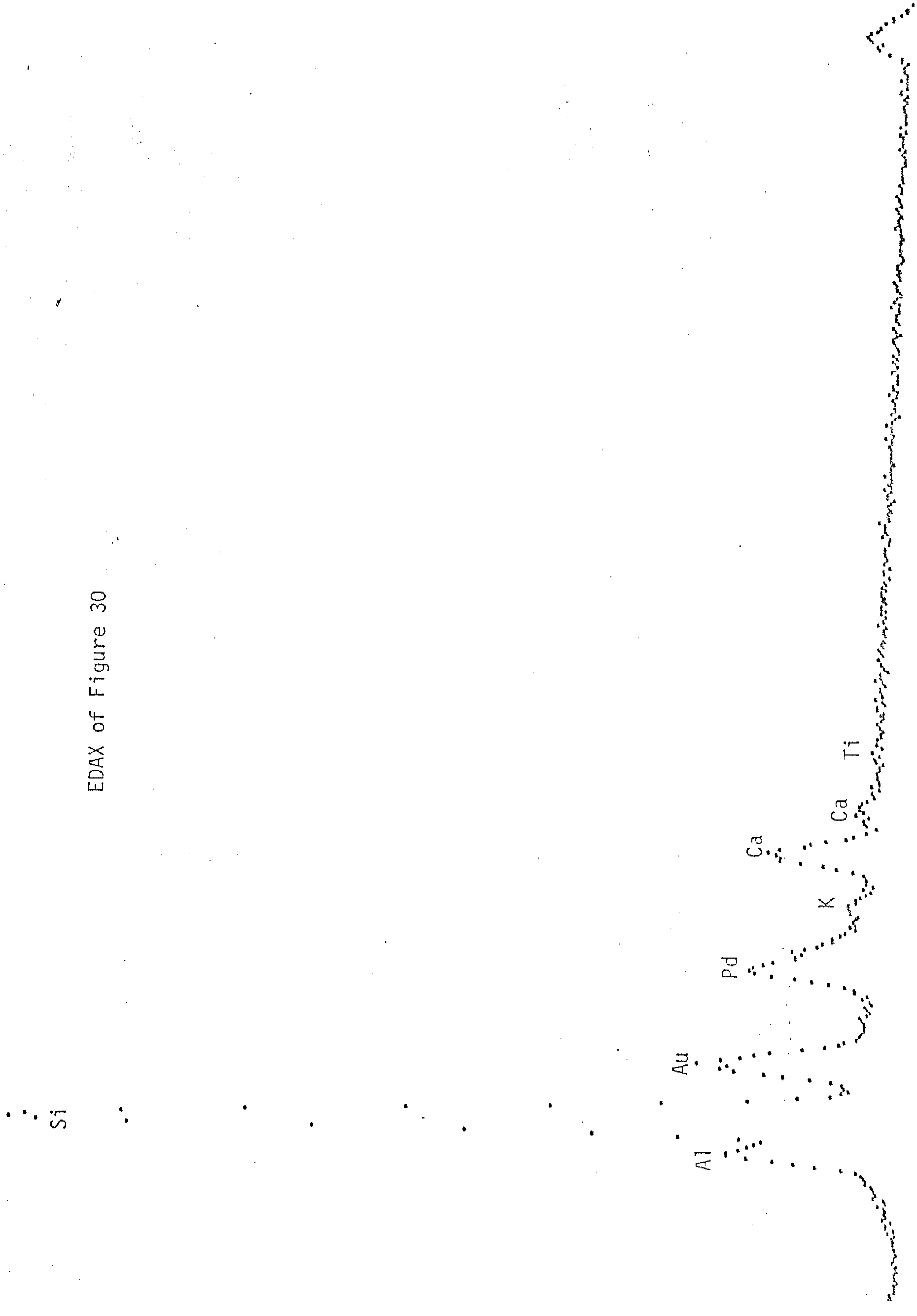

EDAX of Figure 30

EDAX of Figure 31

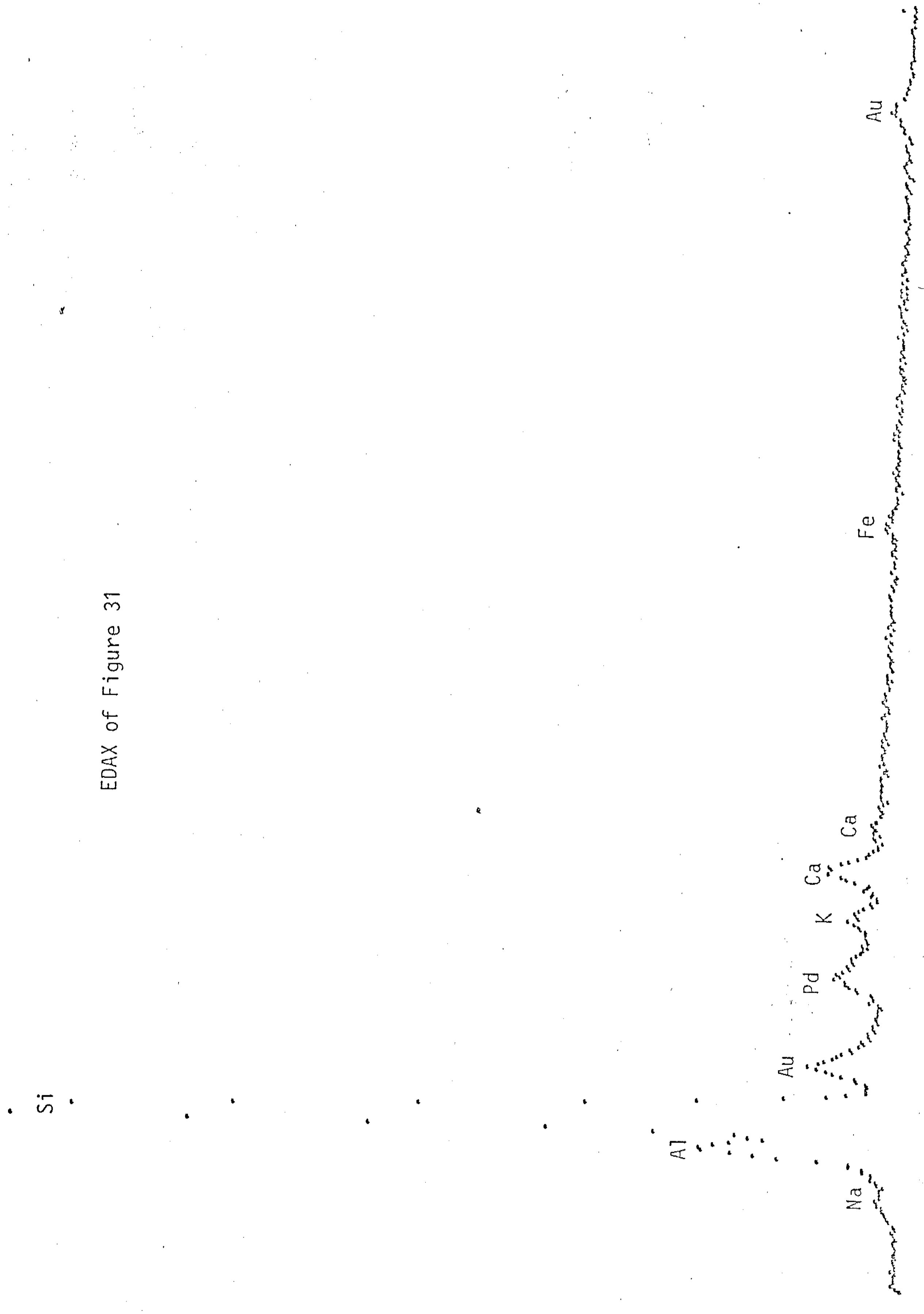

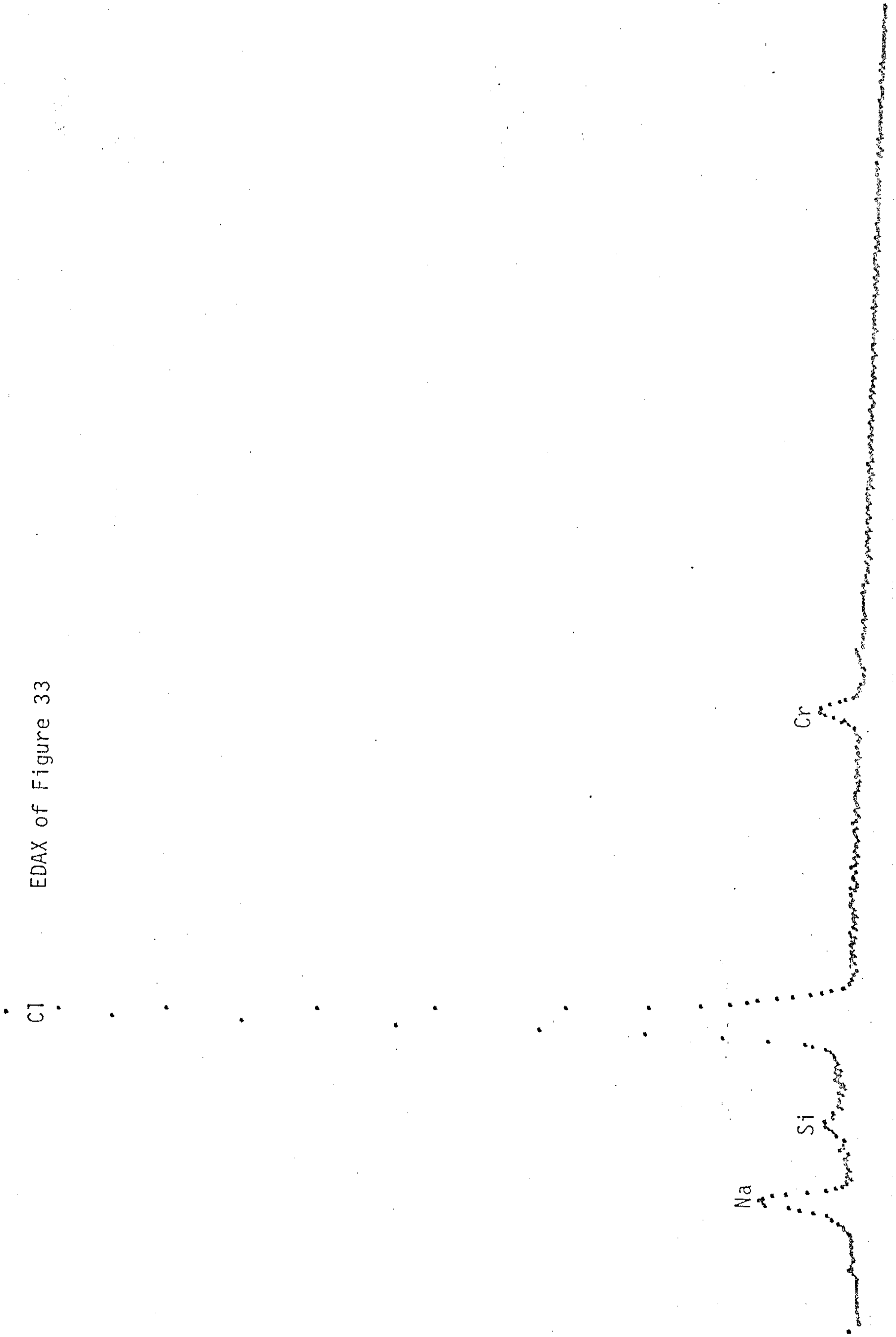

EDAX of Figure 33

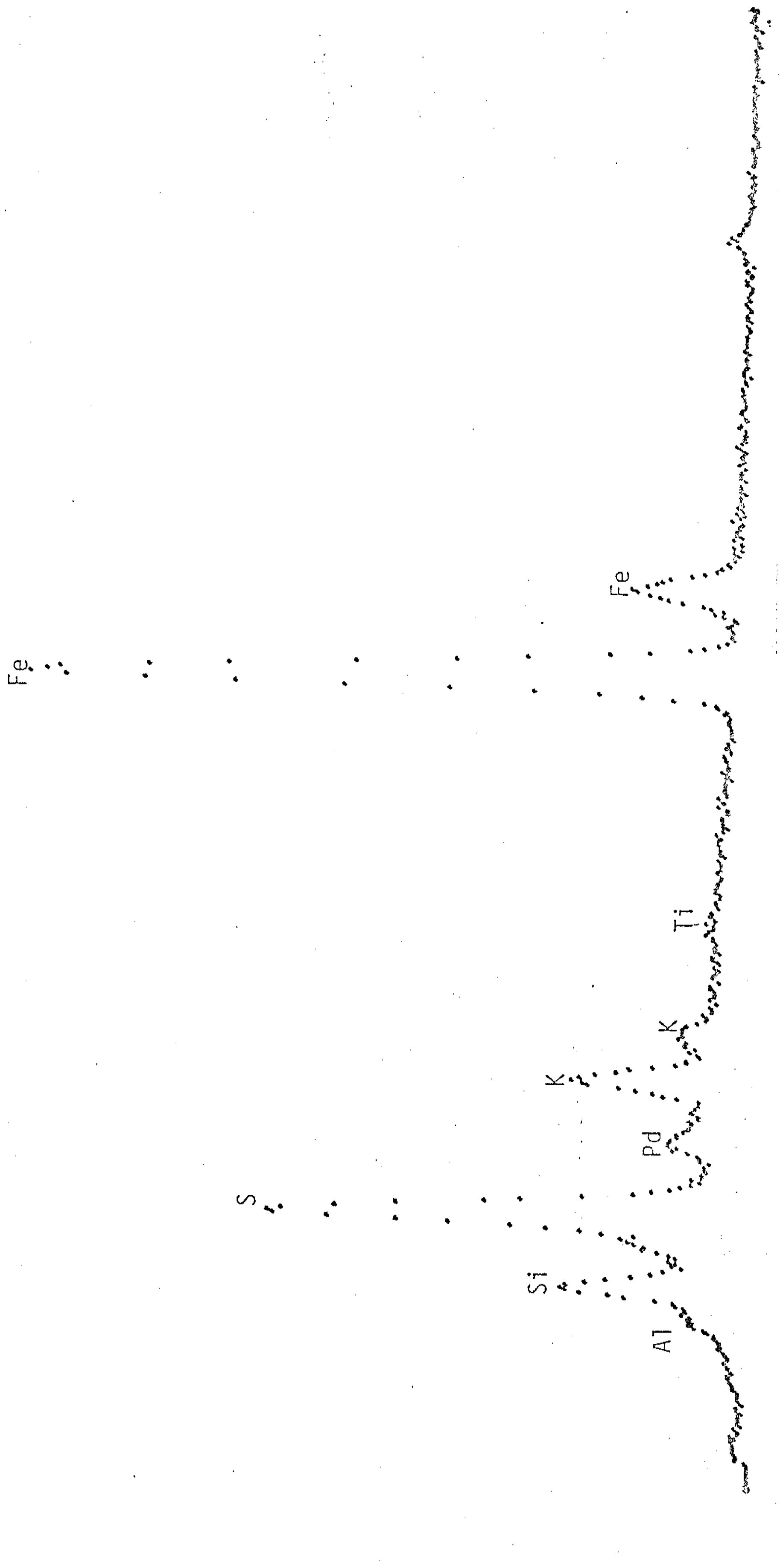

EDAX of Figure 34

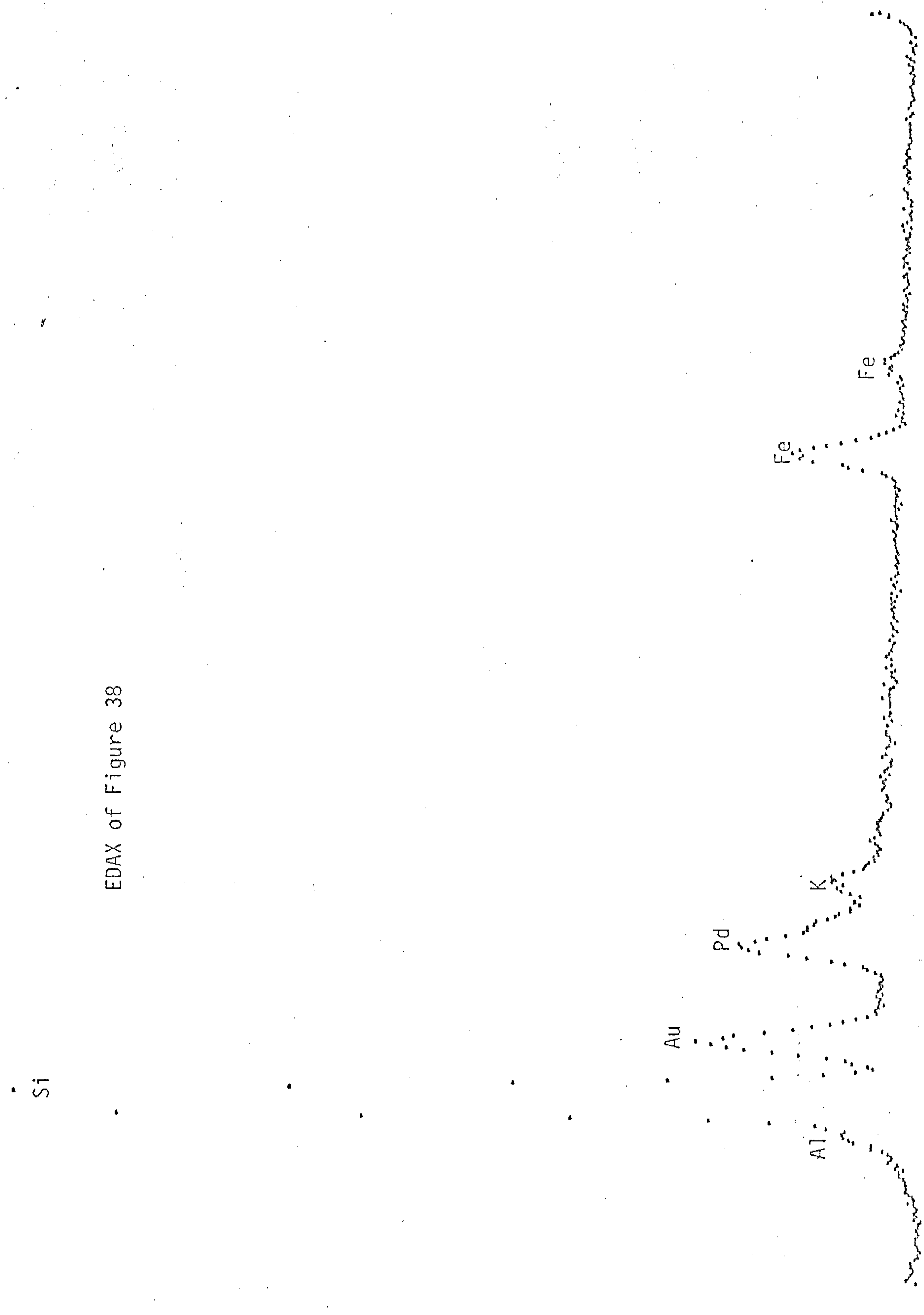

EDAX of Figure 38

EDAX of Figure 39

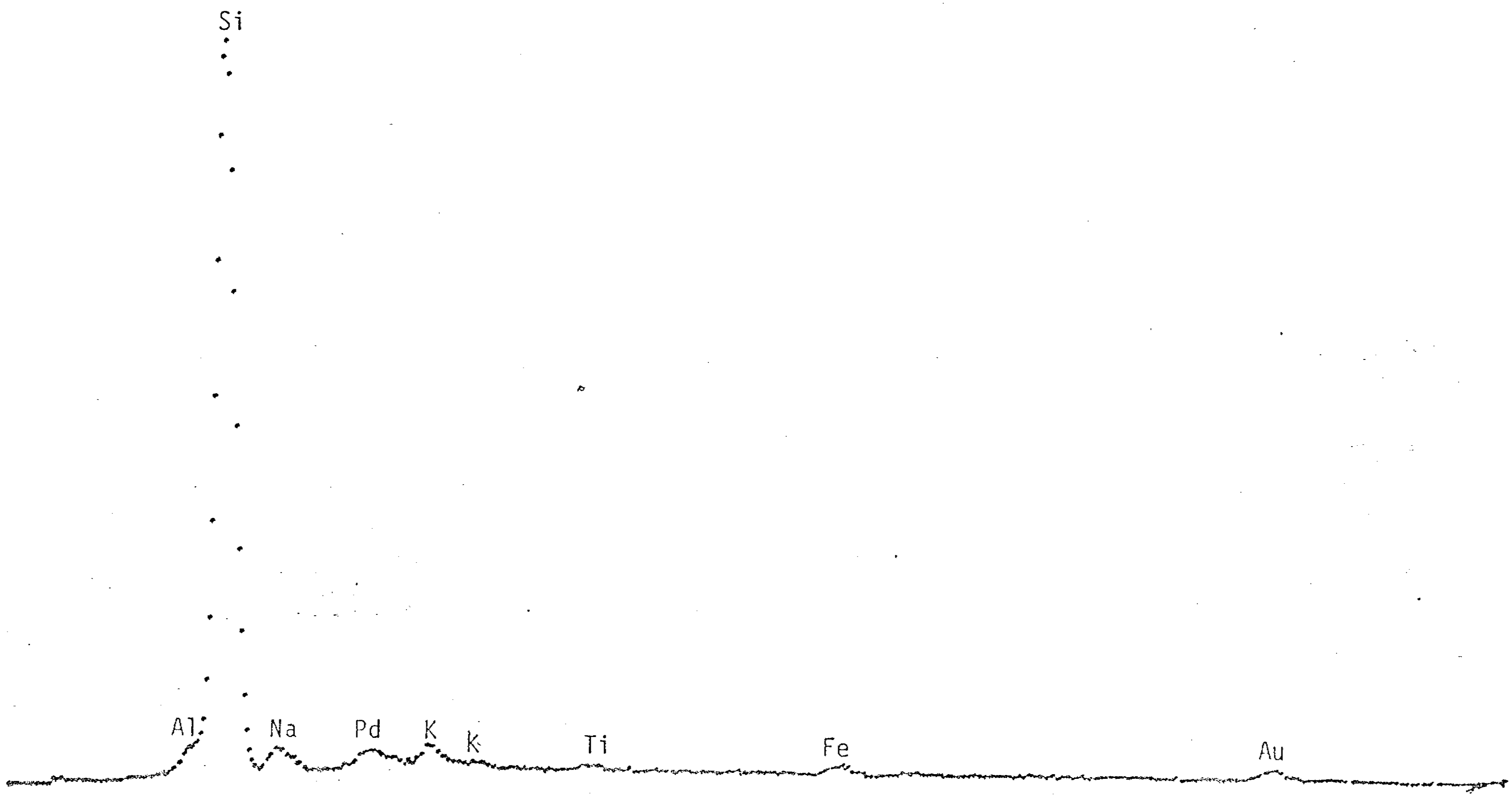

EDAX of Figure 40

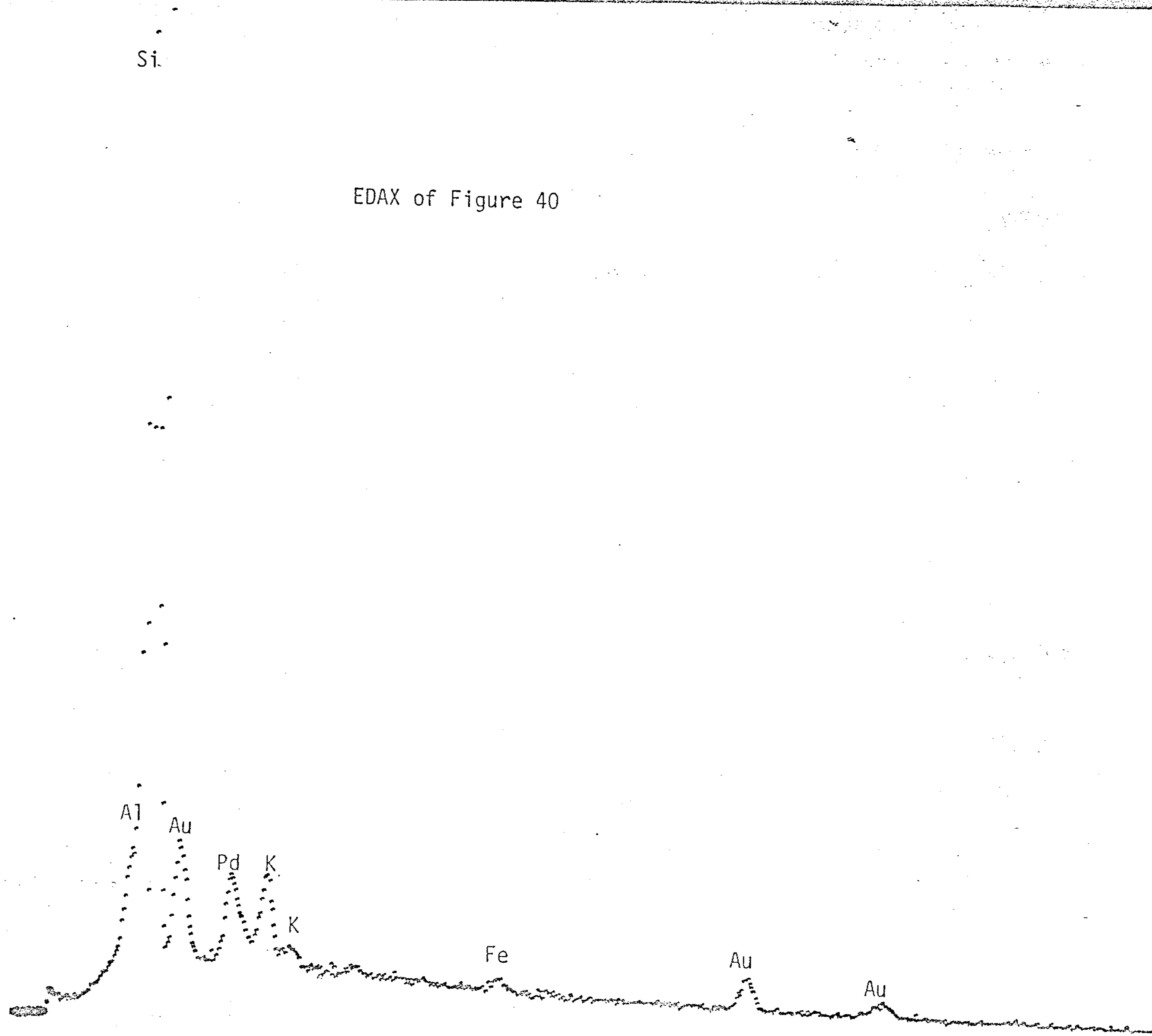

EDAX of Figure 42

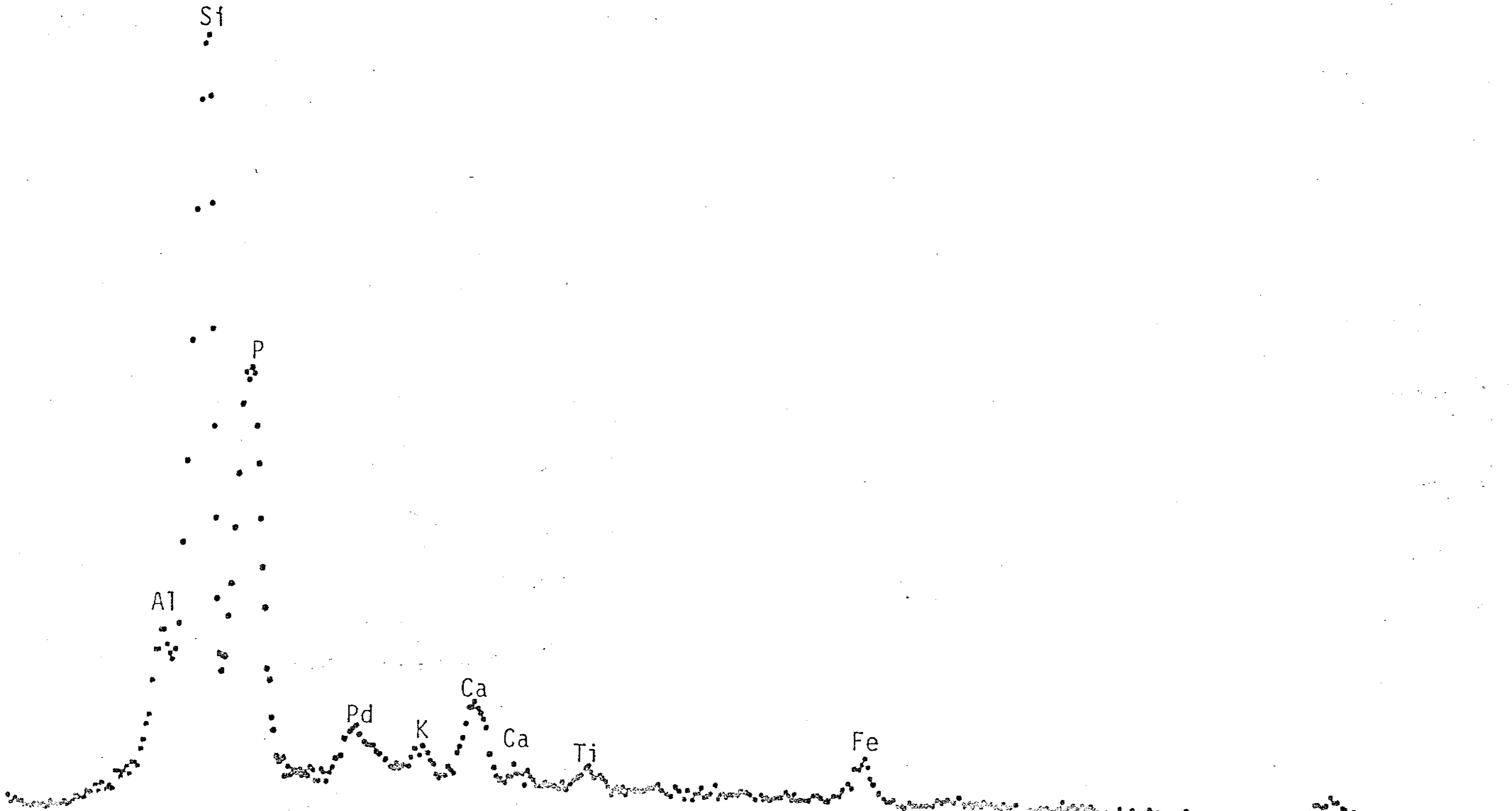

APPENDIX IV

Reference Section 1 Chemistry

#	SiO_2	Al_2O_3	CaO	K_2O	MgO	TiO_2	Fe_2O_3	Na_2O	DIFF
1	62.94	10.49	1.45	4.17	1.10	.430	3.12	1.29	15.01
2	60.28	11.10	1.09	4.29	1.44	.468	4.01	1.34	15.98
3	66.95	10.37	13.06	3.68	0.72	.339	2.33	1.52	1.03
4	63.53	9.85	1.24	3.72	1.32	.456	3.34	1.68	14.86
6A	63.61	10.35	2.23	4.22	0.97	.471	3.21	1.33	13.61
6B	70.96	7.83	13.37	3.69	0.65	.336	1.60	1.10	0.46
8	63.83	9.75	1.96	4.95	0.71	.416	2.03	1.41	14.94
9	67.47	11.26	14.15	3.22	0.28	.270	1.81	1.85	-0.31
10	64.21	9.54	1.09	4.94	0.88	.474	2.72	1.22	14.93
11	67.77	10.00	14.11	4.28	0.40	.267	1.77	1.50	-0.10
12A	65.67	9.66	3.88	3.77	1.03	.418	3.13	1.15	11.29
12B	56.17	14.39	1.13	2.25	2.16	.328	2.33	1.16	20.08
12C	66.40	8.83	1.18	3.18	1.21	.356	2.79	2.16	13.89
14	61.44	11.78	2.59	2.54	1.42	.449	2.46	0.68	16.64
15	60.24	13.65	3.00	2.60	1.68	.485	2.94	1.17	14.24
16A	64.55	9.63	1.57	4.06	1.07	.440	3.05	1.33	14.30
16B	62.59	10.75	1.95	4.62	1.09	.475	2.95	1.47	14.11
17	65.08	10.05	1.53	3.71	1.27	.511	2.69	1.07	14.09
18	67.27	10.51	6.84	3.09	1.04	.306	2.11	0.95	7.88
19	60.76	11.66	1.46	3.92	1.24	.498	4.50	0.93	15.03
21	62.33	12.07	2.51	2.95	1.52	.441	2.38	0.65	15.15
23	62.40	12.90	2.88	2.66	1.27	.490	3.96	1.08	12.36
24	67.29	11.25	15.51	1.52	1.06	.308	2.19	1.44	-0.57
25	61.60	12.71	3.10	2.41	1.38	.517	3.73	1.33	13.22
27A	61.49	11.58	1.71	4.10	1.23	.439	3.26	0.73	15.46
27B	62.19	11.24	1.57	4.58	1.14	.483	3.28	1.16	14.36
27C	69.63	8.43	7.07	4.37	0.77	.368	1.51	0.87	6.98
27D	62.19	11.58	1.00	5.09	1.02	.479	2.48	0.97	15.19
27E	62.51	11.00	1.30	3.90	1.31	.510	2.90	0.74	15.83
28A	67.36	11.41	3.02	2.41	0.82	.125	0.80	0.56	13.50
28B	65.01	11.55	2.62	2.66	1.07	.200	2.45	0.59	13.85
28C	64.68	10.76	1.28	4.29	1.00	.388	1.75	0.80	15.05
28D	62.03	12.56	2.63	3.15	1.26	.422	2.95	0.83	14.17
28E	61.12	13.41	4.09	2.64	1.48	.528	3.25	1.39	12.09
30A	66.75	9.48	1.54	3.59	1.10	.369	2.31	0.82	14.04
30B	62.16	13.27	2.64	2.89	1.38	.422	2.15	0.79	14.30
30C	61.30	12.58	2.63	3.16	1.40	.459	4.33	1.11	13.03
30D	65.61	10.36	1.49	3.96	1.10	.393	2.05	0.94	14.10
31	67.48	9.22	2.06	3.86	0.96	.423	2.14	0.96	12.90
32	67.06	9.12	1.24	3.93	1.02	.421	2.31	0.96	13.94
33	62.81	10.56	1.47	3.96	1.38	.474	3.11	0.89	15.35

Reference Section 2 Chemistry

#	SiO_2	Al_2O_3	CaO	K_2O	MgO	TiO_2	Fe_2O_3	Na_2O	DIFF
2	51.86	16.87	4.03	2.51	2.87	.692	4.37	2.53	14.27
3	65.70	9.41	2.11	2.79	1.90	.543	2.24	0.92	14.39
4	54.95	14.67	3.14	2.84	2.70	.471	3.22	2.33	15.68
5	55.01	14.65	2.18	2.90	2.72	.488	3.51	2.55	15.99
7	64.64	10.21	2.60	3.01	1.91	.454	1.96	1.47	13.75
8	62.68	12.50	3.08	3.41	1.57	.422	1.71	1.74	12.89
9	64.22	10.70	1.28	3.49	1.30	.438	2.75	1.43	14.39
10	60.21	14.86	7.24	2.56	1.04	.511	2.85	3.96	6.77
11	58.04	13.28	3.12	2.67	1.82	.431	3.33	1.90	15.41
12	59.33	14.26	5.13	2.39	0.88	.508	2.95	3.70	10.85
13	62.52	11.05	0.85	4.03	1.40	.378	2.51	1.11	16.15
14	71.24	7.40	13.87	3.10	0.91	.175	1.59	1.39	0.33
15	55.94	13.58	1.69	2.95	1.99	.406	3.13	2.24	18.07
16	61.28	12.68	1.65	3.80	1.18	.467	2.64	1.92	14.38
17	64.13	10.15	2.81	4.43	0.92	.369	2.07	1.45	13.67
18	66.93	8.00	1.03	4.02	0.97	.372	3.00	1.10	14.58
19	77.44	3.17	14.41	-0.02	-1.00	-.020	-0.02	0.40	4.58
20	68.80	10.27	15.48	1.70	0.91	.290	2.07	1.69	-1.21
22	62.88	9.77	0.74	4.15	1.31	.329	2.56	1.21	17.05
23	62.70	11.35	1.34	4.24	1.14	.438	2.45	1.42	14.92
25	61.41	12.47	4.03	3.36	1.24	.401	2.35	1.81	12.93
26	68.05	8.98	1.24	4.60	0.70	.445	1.56	1.42	13.01
27	61.02	10.43	1.20	3.05	1.71	.445	5.10	1.19	15.86
29	64.93	11.06	2.08	3.38	0.94	.388	2.38	1.19	13.65
30	61.31	12.44	2.14	3.88	1.43	.430	2.56	1.04	14.77
31	61.32	12.04	2.46	3.65	1.48	.424	1.99	1.11	15.53
32	63.98	10.29	1.61	5.03	0.96	.394	2.14	1.23	14.37
33	69.10	8.62	1.18	4.40	0.53	.412	0.69	1.19	13.88
34	71.74	8.05	16.30	3.08	0.41	.169	1.21	0.85	-1.81
35	66.38	9.50	1.35	3.84	0.96	.431	1.82	1.02	14.70
36	57.05	15.19	4.06	2.70	1.25	.638	3.80	3.59	11.72
37A	70.12	7.74	1.45	4.24	0.63	.394	1.23	1.21	10.99
37B	74.59	5.52	14.55	3.45	0.15	.175	2.32	0.76	-1.52
37C	67.22	9.87	10.50	3.92	1.12	.220	2.57	0.74	3.84
37D	71.18	8.46	11.48	3.90	0.64	.260	1.52	0.92	1.64
39	65.37	10.68	1.08	5.20	0.76	.428	0.65	0.99	14.84
40	62.78	10.18	1.78	4.00	1.18	.409	3.65	0.90	15.12
41A	64.54	12.33	2.00	3.69	0.86	.429	1.15	0.94	14.06
41B	60.86	10.83	1.90	4.11	1.30	.466	2.43	0.74	17.36
42	64.53	12.71	13.00	2.78	0.92	.473	3.08	2.05	0.46
43	63.57	10.82	1.39	4.81	0.87	.449	3.27	0.96	13.86

Reference Section 3 Chemistry

#	SiO_2	Al_2O_3	CaO	K_2O	MgO	TiO_2	Fe_2O_3	Na_2O	DIFF
1	68.56	8.38	1.06	3.94	1.07	.503	1.70	0.70	14.09
2	61.48	13.55	2.82	2.88	0.99	.662	3.15	1.99	12.48
3	68.10	8.74	0.99	4.11	0.87	.544	2.15	0.85	13.65
4	59.35	13.78	2.13	3.12	1.11	.498	4.43	1.94	13.64
5	65.73	9.41	1.92	4.19	0.73	.458	3.07	1.15	13.34
6	57.23	15.90	2.72	3.36	1.21	.591	3.21	2.58	13.20
7	65.47	10.17	2.53	3.22	1.33	.477	2.71	1.14	12.95
8	69.01	8.47	7.16	4.60	0.71	.313	1.87	0.67	7.20

Reference Section 4 Chemistry

#	SiO_2	Al_2O_3	CaO	K_2O	MgO	TiO_2	Fe_2O_3	Na_2O	DIFF
1	66.45	9.40	5.89	4.88	0.80	.364	2.44	0.76	9.02
2	66.32	9.84	5.98	4.98	0.78	.358	2.31	0.71	8.72
3	62.79	10.88	1.23	5.22	1.05	.473	2.56	0.70	15.10
4	64.59	10.09	1.28	4.63	1.11	.473	2.72	0.74	14.37
5	63.44	10.30	1.97	5.26	1.05	.402	2.90	0.64	14.04
6	64.26	9.85	1.18	4.27	1.09	.465	3.19	0.78	14.92
7	64.19	10.84	0.97	4.55	0.96	.492	2.52	0.81	14.67
8	65.54	9.87	0.97	4.72	0.96	.451	2.06	0.77	14.66
9	63.64	10.74	0.92	4.63	1.04	.459	2.79	0.76	15.02
10	65.41	10.88	0.90	4.63	0.98	.448	1.08	0.76	14.91
11	68.28	8.63	8.59	4.88	0.69	.288	2.61	0.59	5.44
12	66.96	9.30	8.57	4.79	0.85	.315	2.83	0.66	5.73
13	66.27	8.71	2.06	4.74	0.87	.388	3.08	0.80	13.08
14	65.23	9.80	1.20	4.41	1.03	.449	3.07	0.78	14.03
15	63.83	10.47	1.59	4.84	1.01	.416	3.01	0.70	14.13
16	68.62	7.98	5.19	4.60	0.84	.317	2.36	0.58	9.51
17	65.25	9.53	2.27	5.00	0.81	.399	2.89	0.77	13.08
18	66.69	8.49	0.92	4.68	0.91	.381	3.02	0.71	14.20
19	65.78	8.99	1.09	4.68	0.80	.379	3.12	0.70	14.46
20	66.35	8.72	1.03	4.61	1.00	.387	2.95	0.73	14.22

Reference Section 2 Analcime-Rich Rocks Chemistry

#	SiO_2	Al_2O_3	CaO	K_2O	MgO	TiO_2	Fe_2O_3	Na_2O	DIFF
10	60.21	14.86	7.24	2.56	1.04	.511	2.85	3.96	6.77
12	59.33	14.26	5.13	2.39	0.88	.508	2.95	3.70	10.85
14	71.24	7.40	13.87	3.10	0.91	.175	1.59	1.39	0.33
36	57.05	15.19	4.06	2.70	1.25	.638	3.80	3.59	11.72

Reference Section 1 Calcite-Rich Rocks Chemistry

#	SiO_2	Al_2O_3	CaO	K_2O	MgO	TiO_2	Fe_2O_3	Na_2O	DIFF
3	60.76	12.15	5.17	4.42	1.04	.443	3.14	1.67	11.21
6B	70.96	7.83	13.37	3.69	0.65	.336	1.60	1.10	0.46
9	39.98	0.20	22.33	2.77	0.79	.319	2.68	2.25	28.68
11	40.46	0.15	20.90	3.57	0.80	.314	2.58	1.67	29.56
24	27.13	0.15	26.83	1.12	1.72	.340	3.38	1.55	37.78
27C	65.29	9.56	7.39	4.32	0.73	.359	1.72	0.68	9.95

Reference Section 2 Calcite-Rich Rocks Chemistry

#	SiO_2	Al_2O_3	CaO	K_2O	MgO	TiO_2	Fe_2O_3	Na_2O	DIFF
10	60.21	14.86	7.24	2.56	1.04	.511	2.85	3.96	6.77
14	47.73	7.73	18.20	2.70	1.06	.196	2.10	1.41	18.27
19	1.99	0.12	43.04	-0.03	0.83	-.055	0.09	-0.03	53.93
20	32.84	9.91	24.81	1.42	1.58	.337	2.93	2.07	24.10
34	34.26	0.09	25.46	2.51	0.98	.207	1.80	0.68	34.01
37B	49.26	0.07	17.66	3.13	0.41	.199	3.16	0.54	25.57
37C	67.22	9.87	10.50	3.92	1.12	.220	2.57	0.74	3.84
37D	55.77	8.84	13.76	3.66	0.76	.269	1.84	0.79	14.31
42	41.59	13.55	19.76	2.49	1.30	.530	4.30	2.79	13.69

Reference Section 1 Clinoptilolite-Rich Rocks Chemistry

#	SiO_2	$Al_2O_3$3	CaO	K_2O	MgO	TiO_2	Fe_2O_3	Na_2O	DIFF
12C	66.40	8.83	1.18	3.18	1.21	.356	2.79	2.16	13.89
14	61.44	11.78	2.59	2.54	1.42	.449	2.46	0.68	16.64
15	60.24	13.65	3.00	2.60	1.68	.485	2.94	1.17	14.24
18	67.27	10.51	6.84	3.09	1.04	.306	2.11	0.95	7.88
19	60.76	11.66	1.46	3.92	1.24	.498	4.50	0.93	15.03
21	62.33	12.07	2.51	2.95	1.52	.441	2.38	0.65	15.15
23	62.40	12.90	2.88	2.66	1.27	.490	3.96	1.08	12.36
25	61.60	12.71	3.10	2.41	1.38	.517	3.73	1.33	13.22
28A	67.36	11.41	3.02	2.41	0.82	.125	0.80	0.56	13.50
28B	65.01	11.55	2.62	2.66	1.07	.200	2.45	0.59	13.85
28D	62.03	12.56	2.63	3.15	1.26	.422	2.95	0.83	14.17
28E	61.12	13.41	4.09	2.64	1.48	.528	3.25	1.39	12.09
30B	62.16	13.27	2.64	2.89	1.38	.422	2.15	0.79	14.30
30C	61.30	12.58	2.63	3.16	1.40	.459	4.33	1.11	13.03

Reference Section 2 Clinoptilolite-Rich Rocks Chemistry

#	SiO_2	Al_2O_3	CaO	K_2O	MgO	TiO_2	Fe_2O_3	Na_2O	DIFF
2	51.86	16.87	4.03	2.51	2.87	.692	4.37	2.53	14.27
4	54.95	14.67	3.14	2.84	2.70	.471	3.22	2.33	15.68
5	55.01	14.65	2.18	2.90	2.72	.488	3.51	2.55	15.99
15	55.94	13.58	1.69	2.95	1.99	.406	3.13	2.24	18.07
31	61.32	12.04	2.46	3.65	1.48	.424	1.99	1.11	15.53
41A	64.54	12.33	2.00	3.69	0.86	.429	1.15	0.94	14.06

Reference Section 1 Gypsum-Rich Rocks Chemistry

#	SiO_2	Al_2O_3	CaO	K_2O	MgO	TiO_2	Fe_2O_3	Na_2O	DIFF
1	62.94	10.49	1.45	4.17	1.10	.430	3.12	1.29	15.01
2	60.28	11.10	1.09	4.29	1.44	.468	4.01	1.34	15.98
3	60.76	12.15	5.17	4.42	1.04	.443	3.14	1.67	11.21
4	63.53	9.85	1.24	3.72	1.32	.456	3.34	1.68	14.86
6A	63.61	10.35	2.23	4.22	0.97	.471	3.21	1.33	13.61
6B	70.96	7.83	13.37	3.69	0.65	.336	1.60	1.10	0.46
8	63.83	9.75	1.96	4.95	0.71	.416	2.03	1.41	14.94
9	39.98	0.20	22.33	2.77	0.79	.319	2.68	2.25	28.68
10	64.21	9.54	1.09	4.94	0.88	.474	2.72	1.22	14.93
11	40.46	0.15	20.90	3.57	0.80	.314	2.58	1.67	11.21
12A	65.67	9.66	3.88	3.77	1.03	.418	3.13	1.15	11.29
12C	66.40	8.83	1.18	3.18	1.21	.356	2.79	2.16	13.89
16B	62.59	10.75	1.95	4.62	1.09	.475	2.95	1.47	14.11
24	67.29	11.25	15.51	1.52	1.06	.308	2.19	1.44	-0.57

Reference Section 2 Gypsum-Rich Rocks Chemistry

#	SiO_2	Al_2O_3	CaO	K_2O	MgO	TiO_2	Fe_2O_3	Na_2O	DIFF
2	51.86	16.87	4.03	2.51	2.87	.692	4.37	2.53	14.27
4	54.95	14.67	3.14	2.84	2.70	.471	3.22	2.33	15.68
11	58.04	13.28	3.12	2.67	1.82	.431	3.33	1.90	15.41
12	59.33	14.26	5.13	2.39	0.88	.508	2.95	3.70	10.85
15	55.94	13.58	1.69	2.95	1.99	.406	3.13	2.24	18.07
17	64.13	10.15	2.81	4.43	0.92	.369	2.07	1.45	13.67
31	61.32	12.04	2.46	3.65	1.48	.424	1.99	1.11	15.53

Reference Section 1 Montmorillonite-Rich Rocks Chemistry

#	SiO_2	Al_2O_3	CaO	K_2O	MgO	TiO_2	Fe_2O3	Na_2O	DIFF
12B	63.14	14.70	1.50	2.46	1.96	.294	2.34	1.57	12.04
14	61.44	11.78	2.59	2.54	1.42	.449	2.46	0.68	16.64
15	60.24	13.65	3.00	2.60	1.68	.485	2.94	1.17	14.24
21	62.33	12.07	2.51	2.95	1.52	.441	2.38	0.65	15.15
24	27.13	0.15	26.83	1.12	1.72	.340	3.38	1.55	37.78
27A	61.49	11.58	1.71	4.10	1.23	.439	3.26	0.73	15.46
27E	62.51	11.00	1.30	3.90	1.31	.510	2.90	0.74	15.83
28A	67.36	11.41	3.02	2.41	0.82	.125	0.80	0.56	13.50
28B	65.01	11.55	2.62	2.66	1.07	.200	2.45	0.59	13.85
28D	62.03	12.56	2.63	3.15	1.26	.422	2.95	0.83	14.17
28E	61.12	13.41	4.09	2.64	1.48	.528	3.25	1.39	12.09
30A	66.75	9.48	1.54	3.59	1.10	.369	2.31	0.82	14.04
30B	62.16	13.27	2.64	2.89	1.38	.422	2.15	0.79	14.30
30C	61.30	12.58	2.63	3.16	1.40	.459	4.33	1.11	13.03
30D	65.61	10.36	1.49	3.96	1.10	.393	2.05	0.94	14.10

Reference Section 2 Montmorillonite-Rich Rocks Chemistry

#	SiO_2	Al_2O_3	CaO	K_2O	MgO	TiO_2	Fe_2O_3	Na_2O	DIFF
2	51.86	16.87	4.03	2.51	2.87	.692	4.37	2.53	14.27
4	54.95	14.67	3.14	2.84	2.70	.471	3.22	2.33	15.68
5	61.42	14.56	2.76	2.90	2.36	.434	3.74	2.89	8.94
11	58.04	13.28	3.12	2.67	1.82	.431	3.33	1.90	15.41
13	62.52	11.05	0.85	4.03	1.40	.378	2.51	1.11	16.15
15	55.94	13.58	1.69	2.95	1.99	.406	3.13	2.24	18.07
34	71.74	8.05	16.30	3.08	0.41	.169	1.21	0.85	-1.81
41B	60.86	10.83	1.90	4.11	1.30	.466	2.43	0.74	17.36

Reference Section 1 Arenite Chemistry

#	SiO_2	Al_2O_3	CaO	K_2O	MgO	TiO_2	Fe_2O_3	Na_2O	DIFF
6A	63.61	10.35	2.23	4.22	0.97	.471	3.21	1.33	13.61
6B	70.96	7.83	13.37	3.69	0.65	.336	1.60	1.10	0.46
9	67.47	11.26	14.15	3.22	0.28	.270	1.81	1.85	-0.31
11	67.77	10.00	14.11	4.28	0.40	.267	1.77	1.50	-0.10
24	67.29	11.25	15.51	1.52	1.06	.308	2.19	1.44	0.57
28E	61.12	13.41	4.09	2.64	1.48	.528	3.25	1.39	12.09
30C	61.30	12.58	2.63	3.16	1.40	.459	4.33	1.11	13.03

Reference Section 2 Arenite Chemistry

#	SiO_2	Al_2O_3	CaO	K_2	MgO	TiO_2	Fe_2O_3	Na_2O	DIFF
2	51.86	16.87	4.03	2.51	2.87	.692	4.37	2.53	14.27
10	60.21	14.86	7.24	2.56	1.04	.511	2.85	3.96	6.77
12	59.33	14.26	5.13	2.39	0.88	.508	2.95	3.70	10.85
20	68.80	10.27	15.48	1.70	0.91	.290	2.07	1.69	-1.21
25	61.41	12.47	4.03	3.36	1.24	.401	2.35	1.81	12.98
36	57.05	15.19	4.06	2.70	1.25	.638	3.80	3.59	11.72
42	64.53	12.71	13.00	2.78	0.92	.473	3.08	2.05	0.46

Reference Section 3 Arenite Chemistry

#	SiO_2	Al_2O_3	CaO	K_2O	MgO	TiO_2	Fe_2O_3	Na_2O	DIFF
2	61.48	13.55	2.82	2.88	0.99	.662	3.15	1.99	12.48
4	59.35	13.78	2.13	3.12	1.11	.498	4.43	1.94	13.64
6	57.23	15.90	2.72	3.36	1.21	.591	3.21	2.58	13.20

Reference Section 1 Shale Chemistry

#	SiO_2	Al_2O_3	CaO	K_2O	MgO	TiO_2	Fe_2O_3	Na_2O	DIFF
8	63.83	9.75	1.96	4.95	0.71	.416	2.03	1.41	14.94
10	64.21	9.54	1.09	4.94	0.88	.474	2.72	1.22	14.93
14	61.44	11.78	2.59	2.54	1.42	.449	2.46	0.68	16.64
15	60.24	13.65	3.00	2.60	1.68	.485	2.94	1.17	14.24
17	65.08	10.05	1.53	3.71	1.27	.511	2.69	1.07	14.09
18	67.27	10.51	6.84	3.09	1.04	.306	2.11	0.95	8.02
23	62.40	12.90	2.88	2.66	1.27	.490	3.96	1.08	12.36
25	61.60	12.71	3.10	2.41	1.38	.517	3.73	1.33	13.22
27C	69.63	8.43	7.07	4.37	0.77	.368	1.51	0.87	6.98
27D	62.19	11.58	1.00	5.09	1.02	.479	2.48	0.97	15.19
27E	62.51	11.00	1.30	3.90	1.31	.510	2.90	0.74	15.83
28C	64.68	10.76	1.28	4.29	1.00	.388	1.75	0.80	15.05
28D	62.03	12.56	2.63	3.15	1.26	.422	2.95	0.83	14.73
30A	66.75	9.48	1.54	3.59	1.10	.369	2.31	0.82	14.04

Reference Section 2 Shale Chemistry

#	SiO_2	Al_2O_3	CaO	K_2O	MgO	TiO_2	Fe_2O_3	Na_2O	DIFF
3	65.70	9.41	2.11	2.79	1.90	.543	2.24	0.92	14.39
7	64.64	10.21	2.60	3.01	1.91	.454	1.96	1.47	13.75
8	62.68	12.50	3.08	3.41	1.57	.422	1.71	1.74	12.89
9	64.22	10.70	1.28	3.49	1.30	.438	2.75	1.43	14.39
11	58.04	13.28	3.12	2.67	1.82	.431	3.33	1.90	15.41
13	62.52	11.05	0.85	4.03	1.40	.378	2.51	1.11	16.15
15	55.94	13.58	1.69	2.95	1.99	.406	3.13	2.24	18.07
16	61.28	12.68	1.65	3.80	1.18	.467	2.64	1.92	14.38
18	66.93	8.00	1.03	4.02	0.97	.372	3.00	1.10	14.58
19	77.44	3.17	14.41	-0.02	-1.00	-.020	-0.02	0.40	4.58
22	62.88	9.77	0.74	4.15	1.31	.329	2.56	1.21	17.05
23	62.70	11.35	1.34	4.24	1.14	.438	2.45	1.42	14.92
30	61.31	12.44	2.14	3.88	1.43	.430	2.56	1.04	14.77
31	61.32	12.04	2.46	3.65	1.48	.424	1.99	1.11	15.53
32	63.98	10.29	1.61	5.03	0.96	.394	2.14	1.23	14.37
33	69.10	8.62	1.18	4.40	0.53	.412	0.69	1.19	13.88
37A	70.12	7.74	1.45	4.24	0.63	.394	1.23	1.21	10.99
37B	74.59	5.52	14.55	3.45	0.15	.175	2.32	0.76	-1.52
37C	67.22	9.87	10.50	3.92	1.12	.220	2.57	0.74	3.84
37D	71.18	8.46	11.48	3.90	0.64	.260	1.52	0.92	1.34
39	65.37	10.68	1.08	5.20	0.76	.428	0.65	0.99	14.84
40	62.78	10.18	1.78	4.00	1.18	.409	3.65	0.90	15.12
41A	64.54	12.33	2.00	3.69	0.86	.429	1.15	0.94	14.06
41B	60.86	10.83	1.90	4.11	1.30	.466	2.43	0.74	17.36

Reference Section 3 Shale Chemistry

#	SiO_2	Al_2O_3	CaO	K_2O	MgO	TiO_2	Fe_2O_3	Na_2O	DIFF
1	68.56	8.38	1.06	3.94	1.07	.503	1.70	0.70	14.09
3	68.10	8.74	0.99	4.11	0.87	.544	2.15	0.85	13.65
5	65.73	9.41	1.92	4.19	0.73	.458	3.07	1.15	13.34
7	65.47	10.17	2.53	3.22	1.33	.477	2.71	1.14	12.95

Reference Section 4 Shale Chemistry

#	SiO_2	Al_2O_3	CaO	K_2O	MgO	TiO_2	Fe_2O_3	Na_2O	DIFF
1	66.45	9.40	5.89	4.88	0.80	.364	2.44	0.76	9.02
2	66.32	9.84	5.98	4.98	0.78	.358	2.31	0.71	8.72
4	64.59	10.09	1.28	4.63	1.11	.473	2.72	0.74	14.37
11	68.28	8.63	8.59	4.88	0.69	.288	2.61	0.59	5.44
12	66.96	9.30	8.57	4.79	0.85	.315	2.83	0.66	5.73
13	66.27	8.71	2.06	4.74	0.87	.388	3.08	0.80	13.08
14	65.23	9.80	1.20	4.41	1.03	.449	3.07	0.78	14.03
17	65.25	9.53	2.27	5.00	0.81	.399	2.89	0.77	13.08
18	66.69	8.49	0.92	4.68	0.91	.381	3.02	0.71	14.20
19	65.78	8.99	1.09	4.68	0.80	.379	3.12	0.70	14.46
20	66.35	8.72	1.03	4.61	1.00	.387	2.95	0.73	14.22

Reference Section 1 Siltstone Chemistry

#	SiO2	Al2O3	CaO	K2O	MgO	TiO2	Fe2O3	Na2O	DIFF
1	62.94	10.49	1.45	4.17	1.10	.430	3.12	1.29	15.01
2	60.28	11.10	1.09	4.29	1.44	.468	4.01	1.34	15.98
3	66.95	10.37	13.06	3.68	0.72	.339	2.33	1.52	1.03
4	63.53	9.85	1.24	3.72	1.32	.456	3.34	1.68	14.86
12A	65.67	9.66	3.88	3.77	1.03	.418	3.13	1.15	11.29
16A	64.55	9.63	1.57	4.06	1.07	.440	3.05	1.33	14.30
16B	62.59	10.75	1.95	4.62	1.09	.475	2.95	1.47	14.11
19	60.76	11.66	1.46	3.92	1.24	.498	4.50	0.93	15.03
27A	61.49	11.58	1.71	4.10	1.23	.439	3.26	0.73	15.46
27B	62.19	11.24	1.57	4.58	1.14	.483	3.28	1.16	14.36
30B	62.16	13.27	2.64	2.89	1.38	.422	2.15	0.79	14.30
30D	65.61	10.36	1.49	3.96	1.10	.393	2.05	0.94	14.10
31	67.48	9.22	2.06	3.86	0.96	.423	2.14	0.96	12.90
32	67.06	9.12	1.24	3.93	1.02	.421	2.31	0.96	13.94
33	62.81	10.56	1.47	3.96	1.38	.474	3.11	0.89	15.35

Reference Section 2 Siltstone Chemistry

#	SiO2	Al2O3	CaO	K2O	MgO	TiO2	Fe2O3	Na2O	DIFF
4	54.95	14.67	3.14	2.84	2.70	.471	3.22	2.33	15.68
5	55.01	14.65	2.18	2.90	2.72	.488	3.51	2.55	15.99
26	68.05	8.98	1.24	4.60	0.70	.445	1.56	1.42	13.01
27	61.02	10.43	1.20	3.05	1.71	.445	5.10	1.19	15.86
29	64.93	11.06	2.08	3.38	0.94	.388	2.38	1.19	13.65
35	66.38	9.50	1.35	3.84	0.96	.431	1.82	1.02	14.87
43	63.57	10.82	1.39	4.81	0.87	.449	3.27	0.96	13.86

Reference Section 3 Siltstone Chemistry

#	SiO2	Al2O3	CaO	K2O	MgO	TiO2	Fe2O3	Na2O	DIFF
8	69.01	8.47	7.16	4.60	0.71	.313	1.87	0.67	7.20

Reference Section 4 Siltstone Chemistry

#	SiO2	Al2O3	CaO	K2O	MgO	TiO2	Fe2O3	Na2O	DIFF
5	63.44	10.30	1.97	5.26	1.05	.402	2.90	0.64	14.04
6	64.26	9.85	1.18	4.27	1.09	.465	3.19	0.78	14.92
8	65.54	9.87	0.97	4.72	0.96	.451	2.06	0.77	14.66
9	63.64	10.74	0.92	4.63	1.04	.459	2.79	0.76	15.02
15	63.83	10.47	1.59	4.84	1.01	.416	3.01	0.70	14.13
16	68.62	7.98	5.19	4.60	0.84	.317	2.36	0.58	9.50

Reference Section 1 Tuff Chemistry

#	SiO_2	Al_2O_3	CaO	K_2O	MgO	TiO_2	Fe_2O_3	Na_2O	
12B	63.14	14.70	1.50	2.46	1.96	.294	2.34	1.57	1
12C	66.40	8.83	1.18	3.18	1.21	.356	2.79	2.16	1
21	62.33	12.07	2.51	2.95	1.52	.441	2.38	0.65	1
28A	67.36	11.41	3.02	2.41	0.82	.125	0.80	0.56	1
28B	65.01	11.55	2.62	2.66	1.07	.200	2.45	0.59	1

Reference Section 2 Tuff Chemistry

#	SiO_2	Al_2O_3	CaO	K_2O	MgO	TiO_2	Fe_2O_3	Na_2O	
17	72.37	10.05	1.29	3.82	0.67	.344	2.54	1.34	[illegible]
37T	70.96	12.24	1.07	4.78	0.97	.374	1.44	1.51	[illegible]

Reference Section 4 Chemistry

#	SiO_2	Al_2O_3	CaO	K_2O	MgO	TiO_2	Fe_2O_3	Na_2O	
3	62.79	10.88	1.23	5.22	1.05	.473	2.56	0.70	15
7	64.19	10.84	0.97	4.55	0.96	.492	2.52	0.81	14
10	65.41	10.88	0.90	4.63	0.98	.448	1.08	0.76	14

APPENDIX V

Reference Section 1 Clinoptilolite

SiO_2 vs MgO

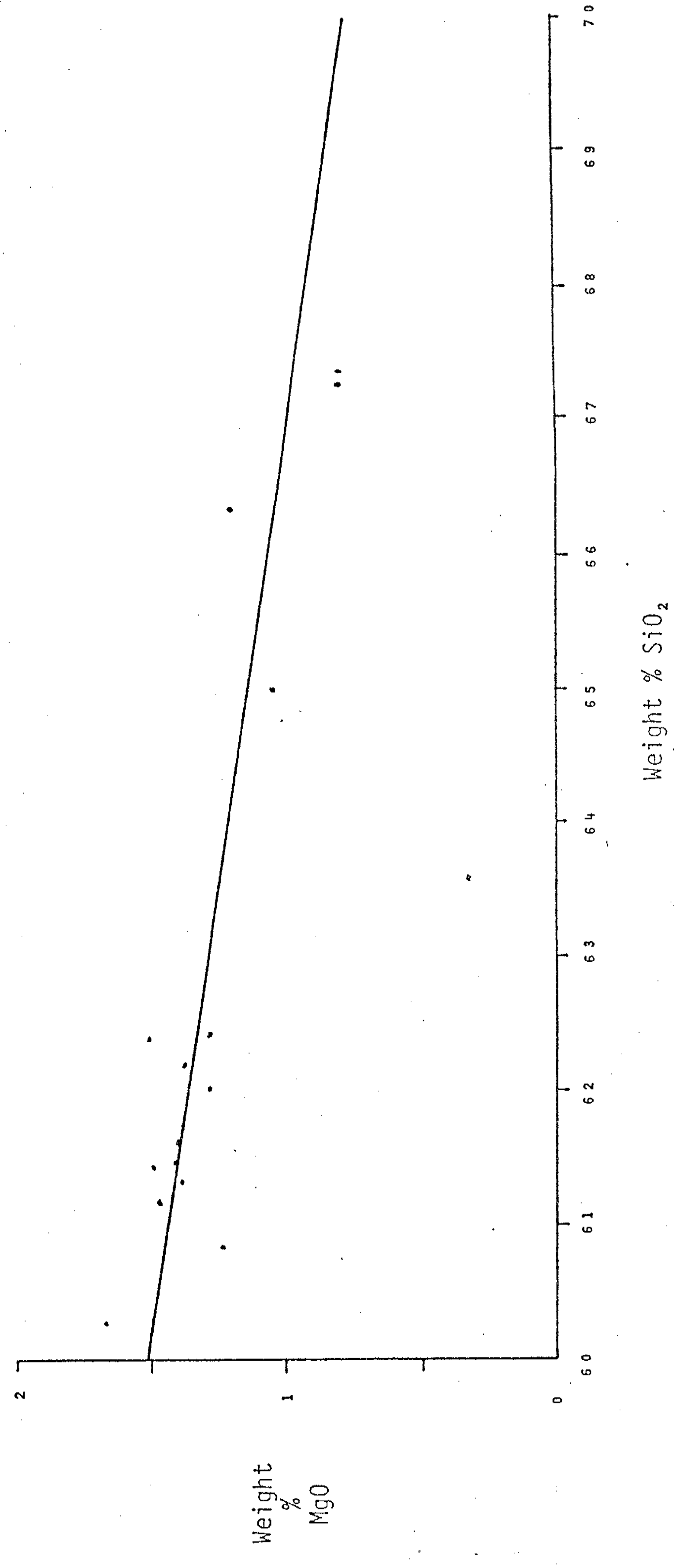

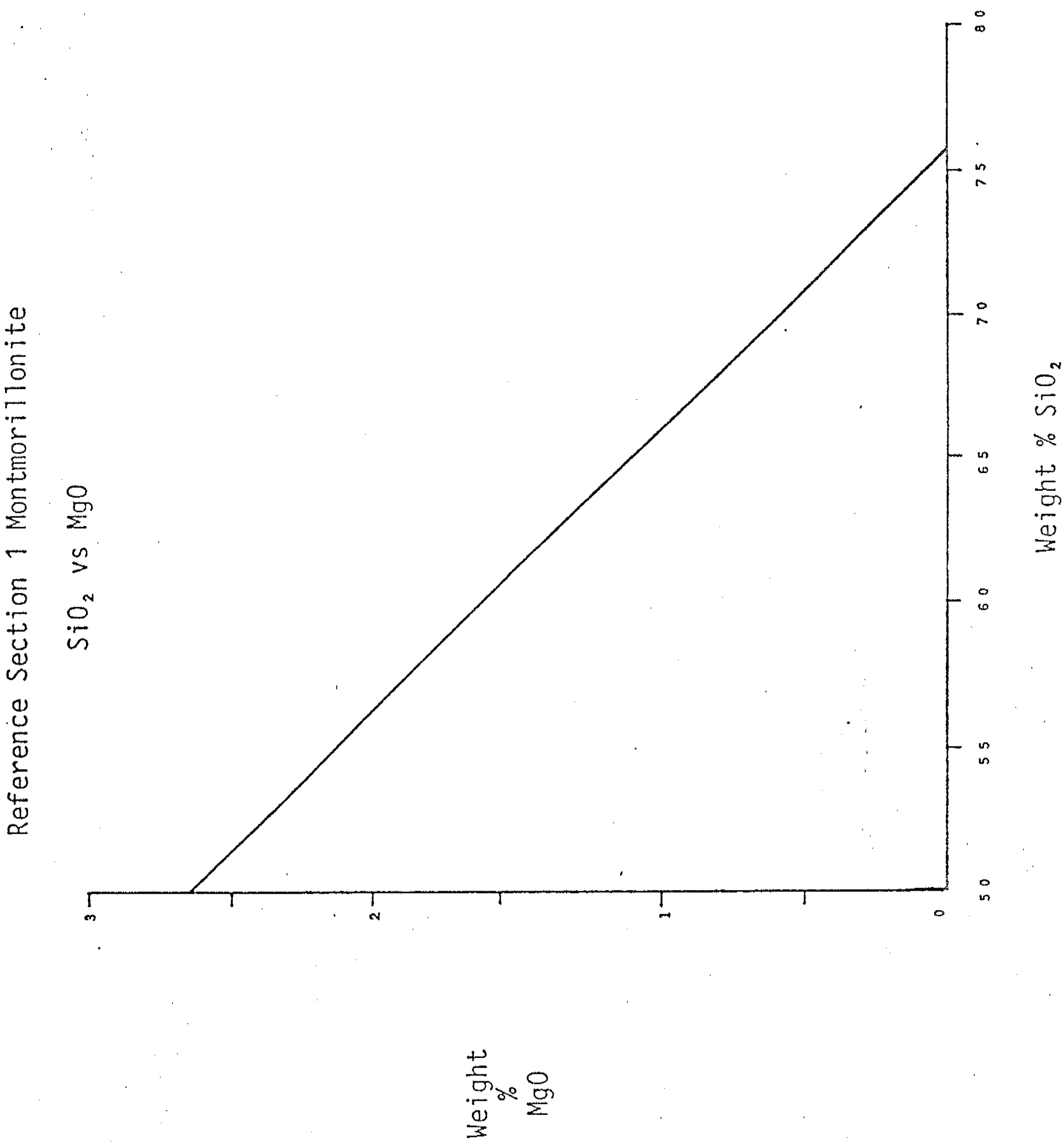
Reference Section 1 Montmorillonite
SiO₂ vs MgO
Weight % MgO
3
2
1
0
50
55
60
65
70
75
80
Weight % SiO₂

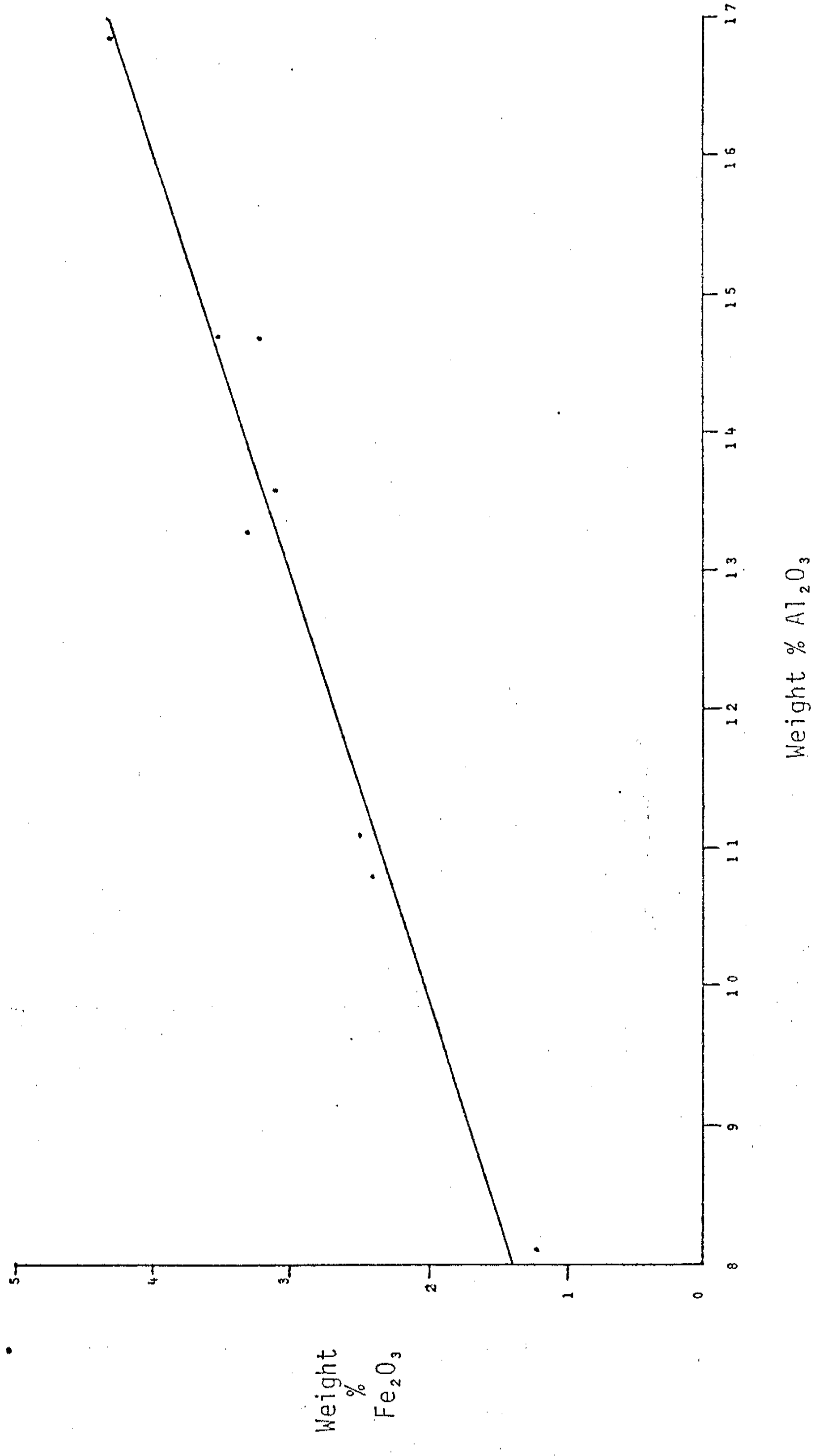

Reference Section 2 Montmorillonite

Al_2O_3 vs Fe_2O_3

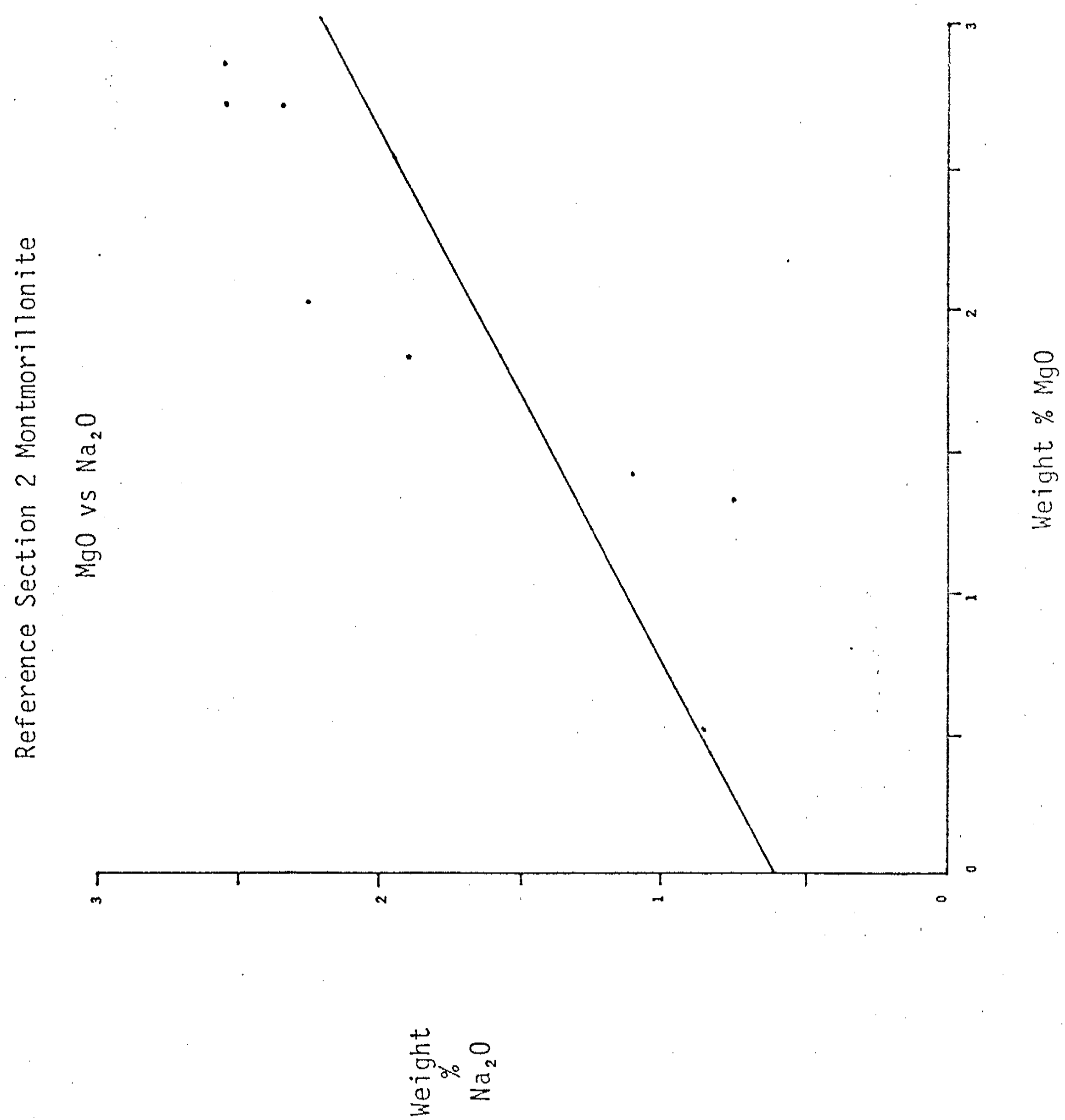
Reference Section 2 Montmorillonite
MgO vs Na$_2$O
Weight % Na$_2$O
Weight % MgO
0
1
2
3
0
1
2
3

Reference Section 2 Clinoptilolite

SiO_2 vs Al_2O_3, K_2O, MgO

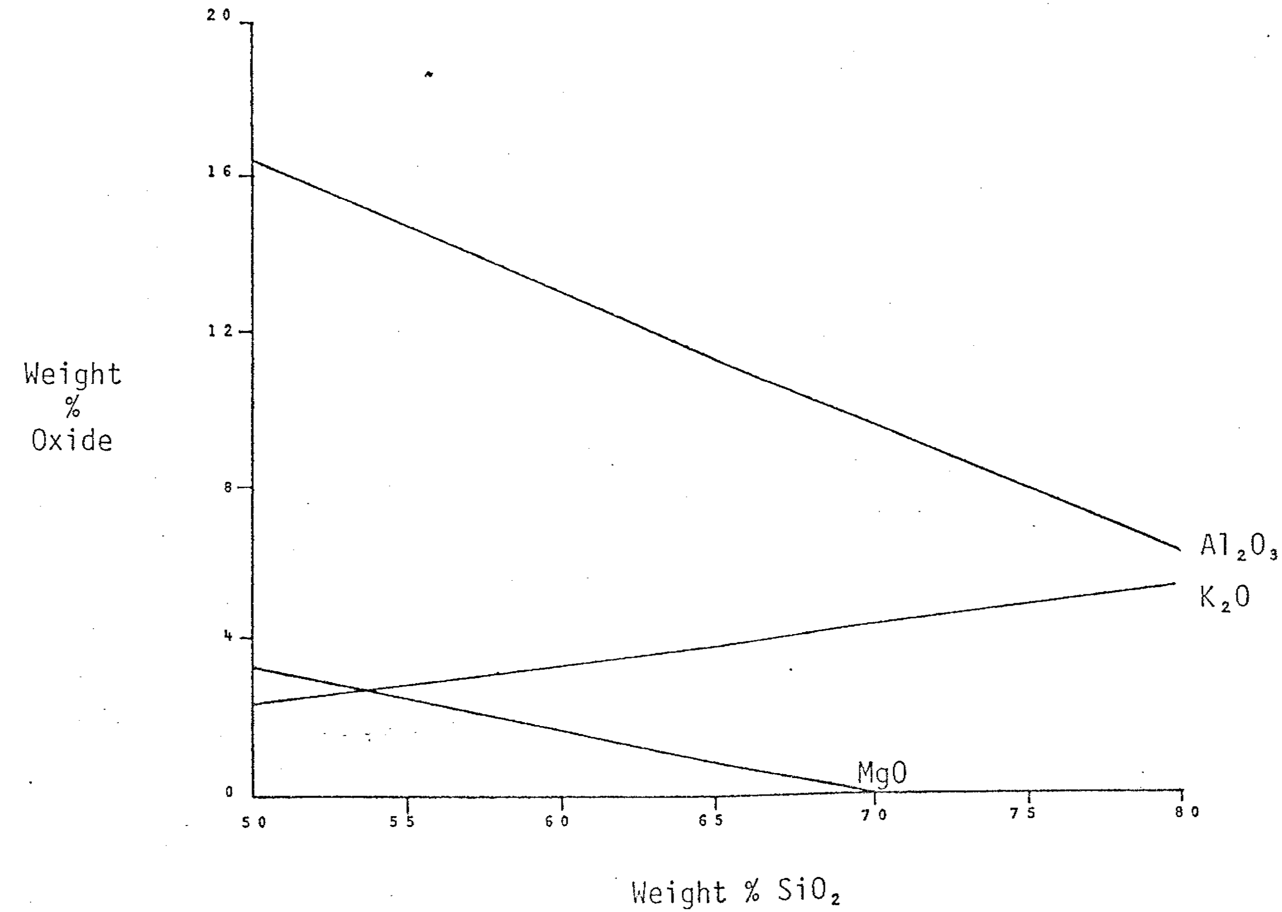

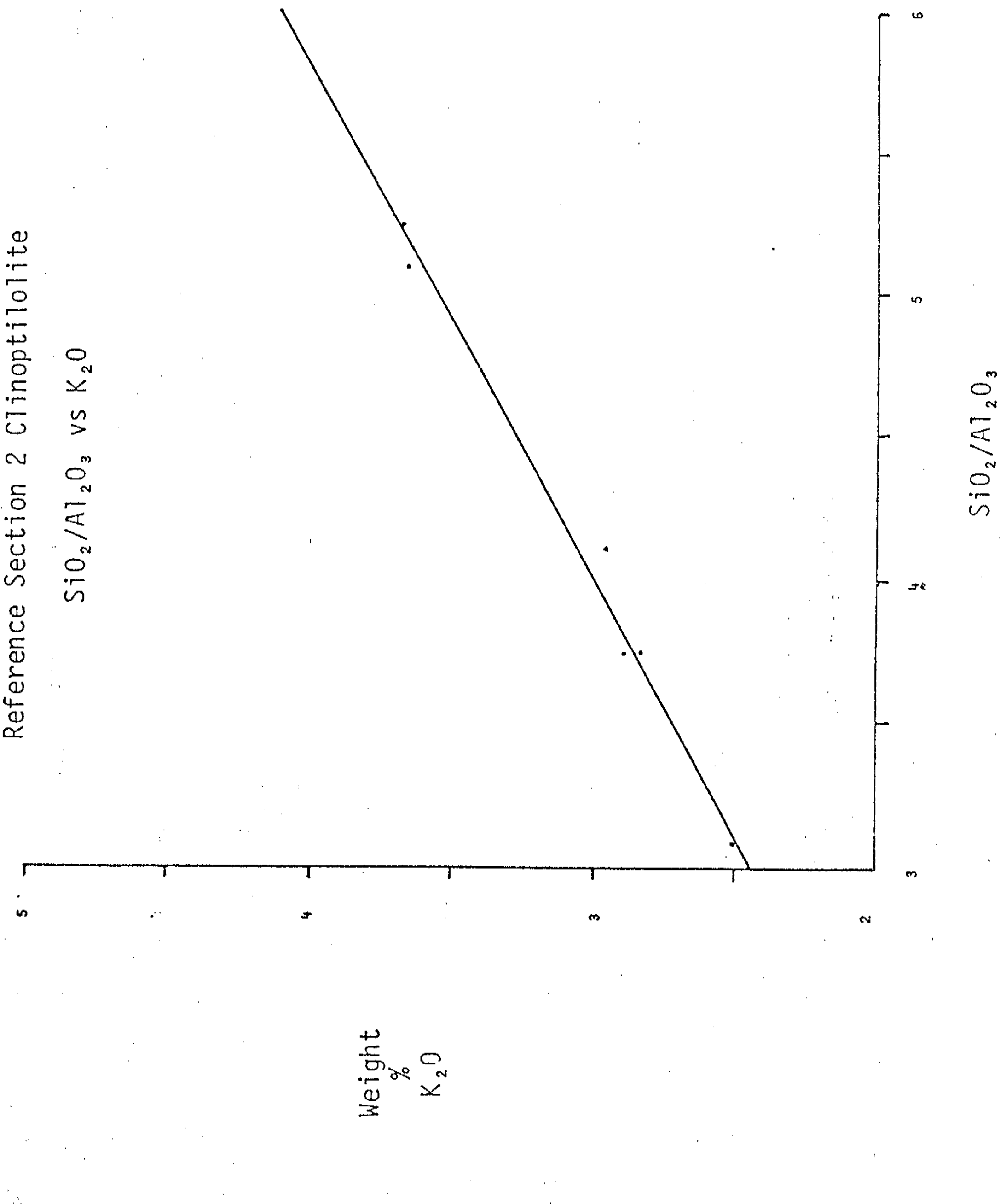

Reference Section 2 Clinoptilolite

SiO_2/Al_2O_3 vs K_2O

Reference Section 2 Montmorillonite

SiO_2 vs Al_2O_3, Fe_2O_3, MgO

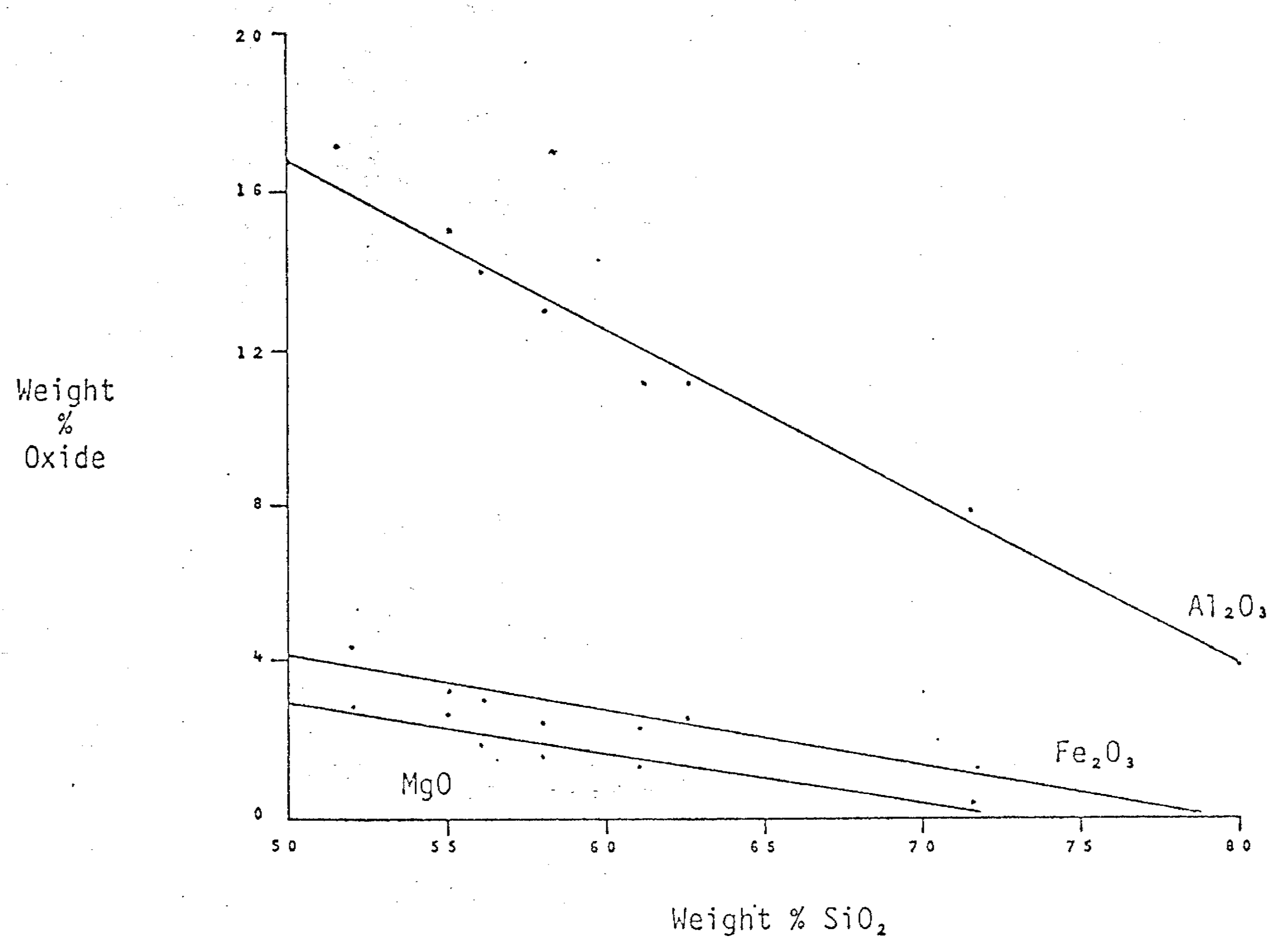

REFERENCES CITED

Alietti, A. (1972) Polymorphism and crystal chemisty of heulendites and clinoptilolite. Am. Min. 57, p. 1448-1462.

Bethke, P.M., and R.O. Rye (1979) Environment of ore deposition in the Creede Mining District, San Juan Mountains, Colorado: Part IV. Sources of fluids for oxygen, hydrogen and carbon isotope studies. Econ. Geol., V.74, p. 1832-1851.

Boles, J.R. (1972) Composition, optical properties, cell dimensions, and thermal stability of some heulandite group zeolites. Am. Min. 57, p. 1463-1493.

Carroll, Dorothy (1970) Clay Minerals: A guide to their X-ray identification. G.S.A. Spec. Paper 126, 80 pp.

Emmons, W.H. and E.S. Larson (1923) Geology and ore deposits of the Creede District, Colorado. U.S.G.S. Bull. 718, p. 1-73.

Hay, R.L. (1965) Pattern of silicate authigenesis in the Green River Formation of Wyoming. G.S.A. Spec. Paper 82, p. 88.

Hay, R.L. (1966) Zeolites and zeolitic reactions in sedimentary rocks. G.S.A. Spec. Paper 82, p. 88.

Hyndman, D.W. (1972) Petrology of igneous and metamorphic rocks. McGraw-Hill, Inc. p. 330-402.

Knowlton, R.H. (1923) Fossil plants from the Tertiary lake beds of southcentral Colorado. U.S.G.S. Prof. Paper 131, p. 183-198.

Krauskopf, K.B. (1967) Introduction to geochemistry. McGraw-Hill, Inc., p. 79-94.

Larsen, Jr., E.S. and W. Cross (1956) Geology and petrology of the San Juan region, southwestern Colorado. U.S.G.S. Prof. Paper 258, 303pp.

Lipman, P.W., B.R. Doe, C.E. Hedge, and T.A. Steven (1978) Petrologic evolution of the San Juan volcanic field, southewestern Colorado: Pb and Sr isotope evidence. G.S.A. Bull. 49, p. 59-82.

Lipman, P.W., T.A. Steven, and H.H. Mehnert (1970) Volcanic history of the San Juan Mountain, Colorado, as indicated by potasium-argon dating. G.S.A. Bull. 81, p. 2329-2352.

Love, D. and J.W. Hawley (1981) Personal communication.

MacGinitie, H.D. (1953) Fossil plants of the florissant beds, Colorado. Carnegie Inst. Washington, Pub. 599, 198 pp.

Mariner, R.H. and R.C. Surdam (1970) Alkalinity and formation of zeolites in saline, alkaline lakes. Science, V. 170, p. 977-979.

Pirsson, L.V. (1890) On mordenite. Am. Jour. Sci., 3rd serial, V. 40, p. 232-237.

Ratte, J.C. and T.A. Steven (1967) Ash flows and related volcanic rocks associated with the Creede Caldera, San Juan Mountains, Colorado. U.S.G.S. Prof. Paper 524-H, 58pp.

Saha, P. (1959) Geochemical and X-ray investigation of natural and synthetic analcites. Am. Min., V. 44, p. 300-313.

Sheppard, R.A. and A.J. Gude (1968) Distribution and genesis of authigenic silicate minerals in tuffs of Pleistocene Lake Tecopa, Inys County, California. U.S.G.S. Prof. Paper 597, 38 pp.

__________ (1969) Diagenesis of tuffs in the Barstow Formation, Mud Hills, San Bernardino County, Calif. U.S.G.S. Prof. Paper 634, 35 pp.

__________ (1973) Zeolites and associated authigenic silicate minerals in tuffaceous rocks of the Big Sandy Formation, Mohave County, Arizona. U.S.G.S. Spec. Paper 830, 36 pp.

Steven, T.A. and C.P. Eaton (1975) Environment of ore deposition in the Creede mining district, San Juan Mountains, Colorado: I. Geologic, hydrologic, and geophysical setting. Econ. Geol., V.70, p. 1023-1037.

Steven, T.A. and I. Friedman (1968) The source of travertine in the Creede Formation,San Juan Mountains, Colorado. U.S.G.S. Prof. Paper 600-B, p. 1329-1336.

Steven, T.A., H.H. Mehnert, and J.D. Obradovich (1967) Age of volcanic activity in the San Juan Mountains, Colorado. U.S.G.S. Prof. Paper 575-D, p. D47-D55.

Steven, T.A. and J.C. Ratte (1959) Caldera subsidence in the Creede area, San Juan Mountains, Colorado. G.S.A. Bull. 70, no. 12, pt. 2, p. 1788-1789.

_______ (1964) Revised Tertiary volcanic sequence in the central San Juan Mountains, Colorado. U.S.G.S. Prof. Paper 475-D, p. D54-D63.

_______ (1965) Geology and stuctural control of ore depostion in the Creede district, San Juan Mountains, Colorado. U.S.G.S. Prof. Paper 487, 90 pp.

Steven, T.A. and R.E. van Loenen (1971) Clinoptilolite bearing tuff beds in the Creede Formation, San Juan Mountains, Colorado. U.S.G.S. Prof. Paper 750-C, p. C98-C103.

Surdam, R.C. (1977) Mineralogy and geology of natural zeolites. M.S.A., Reviews in mineralogy, V. 4, p. 65-91.

Surdam, R.C. and R. B. Parker (1972) Authigenic aluminosilicate minerals in tuffaceous rocks of the Green River Formation, Wyoming. G.S.A. Bull. 83, p. 689-700.

This dissertation is accepted on behalf of the faculty of the Institute by the following committee:

Marc W. Bodine, Jr.
Adviser

R Wayne Ohline

David J. Norman

____

____

18 December 1981
Date